

THÈSE / UNIVERSITÉ DE BRETAGNE OCCIDENTALE

sous le sceau de l'Université Bretagne Loire

pour obtenir le titre de

DOCTEUR DE L'UNIVERSITÉ DE BRETAGNE OCCIDENTALE

Mention : Sciences et Technologies de l'Information et de la Communication

École Doctorale SICMA

présentée par

Abbass NASSER

Préparée au Lab-STICC UMR CNRS 6285
à l'UBO & Ensta-Bretagne

Spectrum Sensing for Half and Full-Duplex Interweave Cognitive Radio Systems

Thèse soutenue le 17 janvier 2017
devant le jury composé de :

M. Christian Jutten
Professeur, Université Joseph Fourier, Examinateur

M. Gilles Burel
Professeur, Université de Bretagne Occidentale, Examinateur

M. Karim Abed Meraim
Professor, Université d'Orléans, Rapporteur

M. Yannick Deville
Professeur, Université Paul Sabatier Toulouse 3, Rapporteur

M. Koffi-Clément Yao,
Maitre de Conférence, Université de Bretagne Occidentale, Encadrant

M. Ali Mansour,
Professeur, Ensta-Bretagne, Directeur de thèse

M. H. Charara,
Maitre de Conférence, Université Libanaise, Membre invité

To my kids Zahraa & Nour . . .

Abstract

Due to the increasing demand of wireless communication services and the limitation in the spectrum resources, Cognitive Radio (CR) has been initially proposed in order to solve the spectrum scarcity. CR divides the communication transceiver into two categories: the Primary (PU) or the Secondary (SU) Users. PU has the legal right to use the spectrum bandwidth, while SU is an opportunistic user that can transmit on that bandwidth whenever it is vacant in order to avoid any interference with the signal of PU. Hence the detection of PU becomes a main priority for CR systems. The Spectrum Sensing is the part of the CR system, which monitors the PU activities.

Spectrum Sensing plays an essential role in the mechanism of the CR functioning. It provides CR with the available channel in order to access them, and on the other hand, it protects occupied channels from the interference of the SU transmission. In fact, Spectrum Sensing has gained a lot of attention in the last decade, and numerous algorithms are proposed to perform it. Concerning the reliability of the performance, several challenges have been addressed, such as the low Signal to Noise Ratio (SNR), the Noise Uncertainty (NU), the Spectrum Sensing duration, *etc.*

This dissertation addresses the Spectrum Sensing challenges and some solutions are proposed. New detectors based on Cyclo-Stationary Features detection and the Power Spectral Density (PSD) of the PU are presented. Canonical Correlation Significance Test (CCST) algorithm is proposed to perform cyclo-stationary detection. CCST can detect the presence of the common cyclic features among the delayed versions of the received signal. This test can reveal the presence of a cyclo-stationary signal in the received mixture signal. Another detection method based on the cumulative PSD is proposed. By assuming the witheness of the noise (its PSD is flat), the cumulative PSD approaches a straight line. This shape becomes non-linear when a telecommunication signal is present in the received mixture. Distinguishing the Cumulative PSD shape may lead to diagnose the channel status.

Full-Duplex Cognitive Radio (FD-CR) has been also studied in this manuscript, where several challenges are analysed by proposing new contributions. FD functioning permits CR to avoid the silence period during the Spectrum Sensing. In classical CR system, SU stops transmitting during the Spectrum Sensing in order to not affect the detection reliability. In FD-CR, SU can eliminate the reflection of its transmitted signal and at the same time achieving the Spectrum Sensing. Due to some limitations, the residual of the Self Interference cannot be completely cancelled, then the Spectrum Sensing credibility is highly affected. In order to reduce the residual power, a new SU receiver architecture is worked out to mitigate the hardware imperfections (such as the Phase Noise and the Non-Linear Distortion of the receiver Low-Noise Amplifier). The new architecture shows its robustness by ensuring a reliable detection and enhancing the throughput of SU.

Acknowledgements

I would like to express my special appreciation and thanks to my director M. Ali Mansour, Professor at Ensta-Bretagne, you have been a tremendous mentor for me. I would like to thank you for encouraging my research and for allowing me to grow as a research scientist. Your advice on both research as well as on my career have been priceless.

My sincere gratitude goes to my supervisor M. Koffi-Clément Yao, Maitre de Conférence at UBO, for the continuous support of my Ph.D study and related research and for their patience and motivation. Their guidance helped me in all the time of research and writing of this thesis. I could not have imagined having a better advisor for my Ph.D study.

I would also like to thank to my PhD advisors in Lebanon, M. Hussein Charara and M. Mohamad Chaitou for their technical and editorial advice was essential to the completion of this dissertation.

Besides my advisors, I would like to thank the rest of my thesis committee: M. Christian Jutten, Professor at INP-Grenoble, M. Gilles Burel, Professor at Université de Bretagne Occidentale, M. Karim Abed Meraim, Professor at Université d'Orléans and M. Yannick Deville, Professor at Université Paul Sabatier-Toulouse 3, for examining the work of this thesis and being members of the jury.

My great thanks go to Dr. Abdul Majid Abdul Ghani, the president of the American University of Culture and Education, for providing all means of success, which resulted in the successful culmination of this project/phd thesis.

For the Dean of the Faculty of Science at AUCE, Dr. Hani Abdallah, thank you for providing me the suitable environment to work.

My sincere thanks also goes to academic and administrative teams at UBO, Ensta-Bretagne and AUCE, who provided me an opportunity to join their team as intern, and who gave access to the laboratory and research facilities. Without they precious support it would not be possible to conduct this research.

A special thanks to my family. Words cannot express how grateful I am to my mother Set El-Ekhwa, and my father Kassem, for all of the sacrifices that they have made on my behalf. Your prayer for me was what sustained me thus far. I would also like to thank all of my brothers, sisters and friends who supported me in writing, and incented me to strive towards my goal.

Finally, I would like to thank my wife Zeinab. Her support, encouragement, quiet patience and unwavering love were undeniably the bedrock upon which the past three years of my life have been built. Her tolerance of my occasional vulgar moods is a testament in itself of her unyielding devotion and love.

Contents

Abstract iii

Acknowledgements v

List of Figures x

List of Tables xiii

Acronyms xiv

1 General Introduction on Cognitive Radio 1
- 1.1 Cognitive Radio Paradigms . . . 3
  - 1.1.1 Underlay Access . . . 4
  - 1.1.2 Overlay Access . . . 5
  - 1.1.3 Inter-weave Access . . . 6
- 1.2 Main parts of Cognitive Radio . . . 7
  - 1.2.1 Spectrum Sensing . . . 7
  - 1.2.2 Spectrum Decision . . . 8
  - 1.2.3 Spectrum Mobility . . . 8
  - 1.2.4 Spectrum Sharing . . . 9
- 1.3 Thesis Organization . . . 10

2 State of art in Spectrum Sensing 13
- 2.1 Spectrum Sensing Measurements . . . 17
  - 2.1.1 Detection Criteria . . . 18
  - 2.1.2 Detection Decisions . . . 19
- 2.2 Classic Spectrum Sensing Algorithms . . . 21
  - 2.2.1 Energy Detector . . . 21
  - 2.2.2 Autocorrelation Detector . . . 22
  - 2.2.3 Cyclostationary Detector . . . 25
    - Cyclic Autocorrelation Function (CAF) as a Test Statistic in Spectrum Sensing . . . 26
    - GLRT-based Cyclo-Stationary Detector . . . 27
  - 2.2.4 Other detection techniques . . . 28
    - Waveform Detector . . . 28
    - Eigenvalue-based Detector . . . 28
    - Goodness of Fit Detector . . . 30

Kurtosis Detector 30
2.3 Performance Evaluation 31
2.3.1 Receiver Operating Characteristic 31
2.3.2 Sensing Time 32
2.3.3 Computation Complexity 33
2.3.4 Noise Uncertainty Impact 34
2.4 Cooperative Spectrum Sensing 36
2.4.1 Hard Combining Scheme 36
2.4.2 Soft Combining Scheme 37
2.4.3 Performance testing of Cooperative Spectrum Sensing 37
2.5 Spectrum Sensing based on Distributed Antennas 38
2.6 Conclusion 39

3 Cyclic Correlation Significance Test (CCST) 40
3.1 System Model 41
3.2 Spectrum Sensing based on CCST 42
3.3 Proposed CCST for Single Antenna System (SAS) 44
3.4 Proposed CCST on Multi-Antenna System (MAS) 47
3.5 Performance Evaluation 48
3.5.1 Single-Antenna System 48
3.5.2 MAS 49
3.5.2.1 Spatially Uncorrelated Noise 51
3.5.2.2 Spatially correlated Noise 51
3.5.2.3 Spatially Uncorrelated but colored Noise 52
3.6 conclusion 52

4 Cumulative Power Spectral Density 54
4.1 System Model and Background 56
4.2 Power Spectral density 57
4.2.1 Estimation of the Power Spectral Density 57
4.3 Cumulative Power Spectral Density-based Detector 58
4.3.1 Proposed cooperative detectors 61
4.3.1.1 OR Detector 62
4.3.1.2 Averaging Detector 62
4.4 Statistical Analysis 64
4.4.1 False Alarm and Detection Probabilities of T_p 64
4.4.1.1 False Alarm Probability of T_p 65
4.4.1.2 Probability of Detection of T_p 66
4.4.2 Probabilities of T_{or} 68
4.4.3 Probabilities of T_{av} 68
4.5 Probability of detection over Rayleigh Fading Channel 69
4.6 Performance Evaluation 72
4.6.1 Performance analysis over Gaussian Channel 72
4.6.2 Performance analysis over Rayleigh Channel 72
4.6.3 Complexity Analysis 75
4.7 Robustness of our proposed detectors under Noise Uncertainty 78
Spectrum Sensing based on Self Normalized CPSD 78

4.8 Conclusion 80

5 Full-Duplex Cognitive Radio **83**
5.1 Introduction 85
5.2 System model and Receiver chain Imperfection Analysis 88
5.3 The RSI effect on the Spectrum Sensing 90
5.4 Phase Noise Analysis 92
5.4.1 Proposed Architecture for PN suppressing 94
5.4.2 Numerical Analysis 95
5.5 The Non-Linear Distortion of the Low Noise Amplifier 99
LSE estimation 100
5.6 Full-Duplex Cognitive Radio 104
5.7 Conclusion 108

6 General Conclusion and Future Works **109**
6.1 Contributions 109
6.2 Future Works 111

A Variance of T_p under H_0 **113**

B Variance of T_p under H_1 **115**

C Approximation of the Detection Probability **117**

D Probability of Detection and Probability of False Alarm under Full-Duplex mode **119**

Bibliography **121**

List of Figures

1.1 Spectrum Hole partitions 4
1.2 The PU and SU co-existence in the Spectrum according to the three access types: Underlay, Overlay and Interweave Access 6
1.3 The Cognitive Radio Cycle 10

2.1 CR activity under both HD and FD modes. (a) HD-CR: the SU should stop the transmission while it performs the sensing of the channel. (b) FD-CR: SU can continue transmitting while the Spectrum Sensing is established 15
2.2 General architecture of Spectrum Sensing in a CR receiver 17
2.3 Effect of the distance on the power of the received signal in FD-CR system 18
2.4 The distribution of a TS under noise-only ($f(TS|H_0)$) case and signal-plus-noise case ($f(TS|H_1)$) 20
2.5 ROC curves for ED, CSD and ACD 31
2.6 Block-Diagram of the Energy Detector 32
2.7 The minimum SNR required to reach $(p_{fa}; p_d) = (0.1; 09)$ in terms of the number of samples 33
2.8 The number of operations required to reach $(p_{fa}; p_d) = (0.1; 09)$ 34
2.9 ROC curve for ED, CSD and ACD for various values of the Noise Uncertainty (ρ) 35
2.10 The ROC curve of ED for different CSS strategies 38

3.1 ROC curves of GLRT and CCST-S for various values of the length of the lag vector 49
3.2 ROC curves of CCST-S for various values NU with a comparison with Energy Detector 50
3.3 Time Diversity effect on the performance of CCST-S for $p_{fa} = 0.1$ 50
3.4 The probability of missed detection, $p_{md} = 1 - p_d$, for various number of receiving antennas (M) under $p_{fa} = 0.1$ 51
3.5 The probability of missed detection, $p_{md} = 1 - p_d$, for various SNR under $p_{fa} = 0.05$ 52
3.6 The probability of missed detection, $p_{md} = 1 - p_d$, for various SNR under $p_{fa} = 0.05$ 53

4.1 The Noralized CPSD shapes for $N = 10000$ samples with respect to the Frequency Points and several values of N_s and SNR 60
4.2 The overall diagram of the CPSD-based detectors 63
4.3 Analytic results Vs Simulation results under Gaussian channel 69
4.4 Simulations result Vs. Analysis result over Rayleigh fading channel, $N_s =$ 3 sps 71

4.5 ROC curves of our proposed detectors comparing to ED and CSD for various N_s, SNR of $-12dB$ and $N = 1500$ samples. 73
4.6 Variation of the probability of detection in terms of SNR for $N = 1000$ samples, a constant $p_{fa} = 0.1$ and various values of N_s. 74
4.7 ROC curves over Rayleigh fading channel for $N_s = 4$ and 8 sps for N=1000 samples and average SNR = -5 dB. 75
4.8 (a): The number of samples needed by the detectors in order to reach $(p_{fa}; p_d) = (0.1; 0.9)$ for various SNR and (b): the number of required operations performed by each detectors corresponding to the number of samples given in (a) 77
4.9 Performance loss of p_d in terms of noise uncertainty for $p_{fa} = 0.1$ 79
4.10 Self normalized CPSD under H_0 and H_1 81
4.11 ROC curves of the proposed schemes under various values of NU, N=1000 samples and SNR=-10 dB 82

5.1 The model of SU in FD-CR 87
5.2 Classical FD OFDM receiver 88
5.3 The number of samples required to reach $p_d = 0.9$ and $p_{fa} = 0.1$ with respect to SNR (dB) 92
5.4 Evolution of γ_d with respect to the SNR γ_s, for various values of PDR δ, $(p_{fa}^H \ ; \ p_d^H) = (0.1 \ ; \ 0.9)$ 93
5.5 Receiver architecture for a FD OFDM to reduce Phase Noise [86] 95
5.6 Proposed FD OFDM receiver architecture to suppress the Phase Noise effect, the conjugate of PN is estimated at AC, then it is multiplied by the output of the OC oscillator in order to suppress its effect. 96
5.7 Effect of the Non-LoS components power on the RSI power 97
5.8 PN power effect on the RSI power. PN offset is fixed to 10 KHz 97
5.9 Effect of the PN offset on the RSI power. PN power is fixed to -90 dBc/Hz 98
5.10 Effect of the Gaussian Noise on the RSI power 99
5.11 The variation of the RSI power in terms of the number of training symbols 99
5.12 FD architecture capable to eliminate the receiver PN and to reduce the NLD of the receiver LNA. When the switches are on (2), the NLD coefficients are estimated by avoiding the wireless channel. When the switches are on (1), the transceiver works in ordinary conditions, and the circuit associated to LNA alleviates the NLD at the output of LNA 101
5.13 The power of the residual NLD in terms of the number of training symbols. NLD power is fixed to -45 dBc (*i.e.* -85 dB for a 0 dB gain of the LNA) . 102
5.14 The effect of the GN power on the residual NLD power using LSE estimator 103
5.15 The power of the residual SIC power in terms of the NLD power 104
5.16 Activity period of SU under HD functioning is divide into Sensing sub-period (T_s) and Transmission sub-period (T_t). 104
5.17 Model of a Network where Secondary Transmitter and Secondary Receiver co-exists with a PU 106
5.18 Model of a Network where Secondary Transmitter and Secondary Receiver co-exists with a PU 106
5.19 Variation of p_d in terms of N_t 107
5.20 Variation of p_d in terms of N_t 107

C.1 (a): The probability of detection p_d^p and its approximation in terms of SNR for different p_{fa}, $N = 1500$ samples and $N_s = 4$ sps, (b): The probability of detection p_d^p and its approximation in terms of the number of samples N, for different p_{fa}, SNR=-10 dB samples and $N_s = 4$ sps 118

List of Tables

2.1 Comparison of different Spectrum Sensing Algorithms 36

5.1 Simulations Parameters 94
5.2 SNR and SNIR definitions 105

List of Acronyms

AC Auxiliary Chain

ACD Autocorrelation Detector

ADC Analogue to Digital Converter

AWGN Additive White Gaussian Noise

BSS Blind Source Separation

BW Band-Width

CAF Cyclic-Autocorrelation Function

CCT Canonical Correlation Theory

CCST Cyclic Correlation Significance Test

CDF Cumulative Distribution Function

CF Cyclic Frequency

CFAR Constant False Alarm Rate

CHT Channel Holding Time

CR Cognitive Radio

CSD Cyclo-Stationary Detector

CLT Central Limit Theorem

CSCGN Circular Symmetric Complex Gaussian Noise

CSS Cooperative Spectrum Sensing

CPSD Cumulative Power Spectral Density

DAC Digital to Analog Converter

DFT Discrete Fourier Transform

DSA Dynamic Spectrum Allocation

ED Energy Detector

EME Energy with Minimum Eigenvalue

EVD Eigenvalues-based Detector

FC Fusion Center

FCC Federal Communication Commission

FD Full-Duplex

FD-CR Full-Duplex Cognitive Radio

FFT Fast Fourier Transform

GN Gaussian Noise

GLRT Generalized Likelihood Ratio Test

GoF Goodness of Fit

HD Half-Duplex

HD-CR Half-Duplex Cognitive Radio

HCS Hard Combining Scheme

HD Half-Duplex

HD-CR Half-Duplex Cognitive Radio

HIM Hardware Imperfections Mitigation

IoT Internet of Things

KD Kurtosis Detector

LLR Likelihood ratio

LNA Low-Noise Amplifier

LSE Least-Square Error

MAS Multi-Antenna System

MME Maximum-Minimum Eigenvalue

NLD Non-Linear Distortion

NU Noise Uncertainty

OC Ordinary Chain

OFDM Orthogonal Frequency Division Multiplex

PDF Probability Distribution Function

PDR Probability of Detection Ratio

PN Phase Noise

PSD Power Spectral Density

PU Primary User

QoS Quality of Service

RF Radio Frequency

ROC Receiving Operating Characteristics

RSI Residual Self Interference

SAS Single-Antenna System

SCS Soft Combining Scheme

SDR Soft-Defined Radio

SI Self Interference

SIR Signal to Interference Ratio

SIC Self Interference Cancellation

SNIR Signal to Noise and Interference Ratio

SNR Signal-to-Noise Ratio

SOAO Shared Oscillator between Auxiliary and Ordinary Chains

SoI Signal of Interest

SU Secondary User

TS Test Statistic

UWB Ultra Wide Band

WFD Wave-Form Detector

WOC Wireless Optical Communication

Chapter 1

General Introduction on Cognitive Radio

List of Acronyms

CCT Canonical Correlation Theory

CCST Cyclic Correlation Significance Test

CHT Channel Holding Time

CR Cognitive Radio

CSS Cooperative Spectrum Sensing

CPSD Cumulative Power Spectral Density

DSA Dynamic Spectrum Allocation

FC Fusion Center

FCC Federal Communication Commission

FD Full-Duplex

FD-CR Full-Duplex Cognitive Radio

HD Half-Duplex

HD-CR Half-Duplex Cognitive Radio

HCS Hard Combining Scheme

HD Half-Duplex

HD-CR Half-Duplex Cognitive Radio

IoT Internet of Things

LNA Low-Noise Amplifier

NLD Non-Linear Distortion

MAS Multi-Antenna System

PN Phase Noise

PSD Power Spectral Density

PU Primary User

QoS Quality of Service

RF Radio Frequency

RSI Residual Self Interference

SAS Single-Antenna System

SCS Soft Combining Scheme

SDR Soft-Defined Radio

SI Self Interference

SIR Signal to Interference Ratio

SIC Self Interference Cancellation

SNR Signal-to-Noise Ratio

SoI Signal of Interest

SU Secondary User

UWB Ultra Wide Band

OWC Wireless Optical Communication

Due to the recent achievement toward the 5G service and the high advancement in the Internet of Thing (IoT), and numerous recent wireless applications, the wireless communication community is facing an enormous problem of how adapting the limited frequency resources to the increasing demand on the wireless communication services [1]. This ever growing increase of the wireless communication and multimedia services has led to congestion in the used Radio Frequency (RF) spectrum and arises a need to explore new frequency resources.

One of the proposed solutions toward the spectrum scarcity is the going to the Optical Wireless Communication (OWC). In fact, instead of using Radio Frequency (RF) carrier, OWC uses optical carrier to communicate between two points. OWC offers high data-rate with low power consumption [2, 3]. On the other hand, many limitations are facing OWC such as the short transmission distance (up to $\sim$ 2 Km) and a high sensitivity to the environment factors such as the rain, snow, fog, aerosol gases, *etc.* [4].
In parallel with the OWC, which gained huge research works, Dynamic Spectrum Allocation (DSA) in Radio Frequency (RF) spectrum became an attractive proposed technique to solve the Spectrum Scarcity [5]. Actually, most communication systems use static communication parameters and operate on static frequency allocation, so that they are designed to operate on a pre-selected frequency band. This static allocation results in low spectrum utilisation efficiency based on the recent statistics that show that the usage of the allocated frequency bands is lower than 15 % [6]. This low efficiency pushes the wireless communication community to invent the Dynamic Spectrum Allocation (DSA) as a solution to achieve wise and efficiently use of the spectrum [7, 8], which leads to getting more frequency resources. In this context, Cognitive Radio (CR) has been introduced as a candidate to perform DSA by exploiting the free frequency bands that are called "Spectrum Holes" or "white spaces" [9].

1.1 Cognitive Radio Paradigms

Initially, Mitola has proposed the Soft-Defined Radio (SDR) [10]. SDR is a reconfigurable and flexible system that is responsive to the user demands by adapting automatically the communication parameters such as modulation, channel coding, frequency band *etc.* CR is mainly based on SDR, with the major difference that CR is aware and adaptable to its radio environment to optimize the use of the available frequency bands while protecting the occupied ones from the harmful interference.
Being capable to identify its spectral opportunities, CR classifies the users into two types: Licensed which are the Primary Users (PUs) and unlicensed which are the Secondary

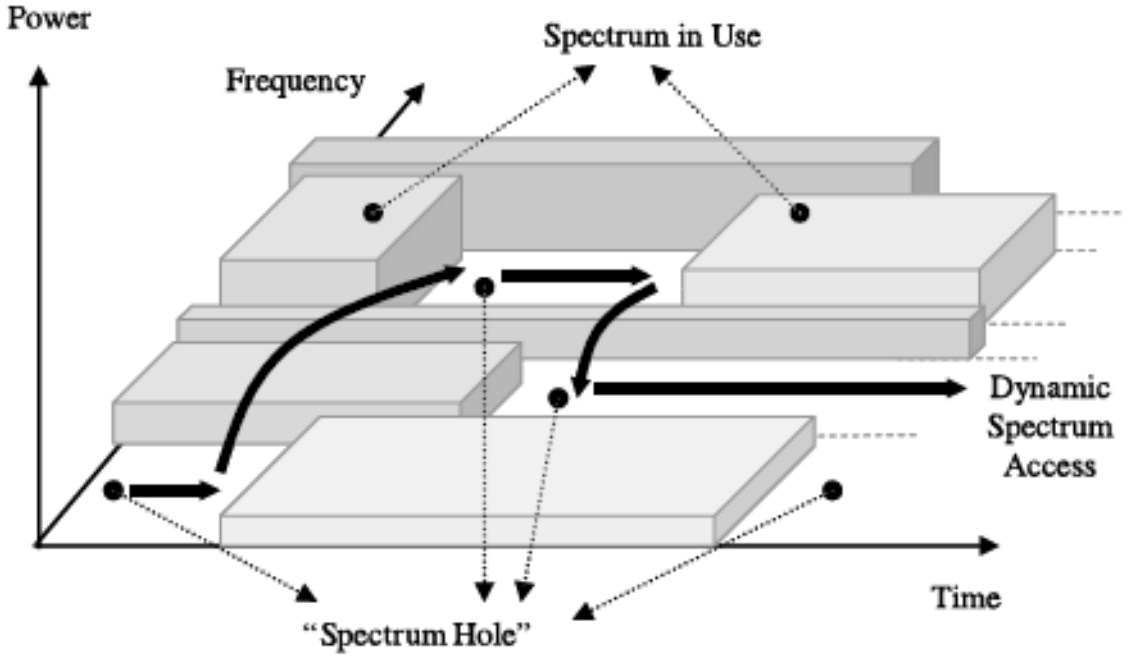


FIGURE 1.1: Spectrum Hole partitions

Users (SUs). The spectrum sharing between PU and SU is based on the fact that SU should respect the PU's Quality of Service (QoS). Any harmful interference coming from SU to PU transmission is prohibited. For that reason, three paradigms of CR based on the spectrum access can be distinguished according to the possibility of co-existence of SU and PU transmissions in the same channel, and, if this co-existence is possible, the permitted transmitted power of SU and the cooperation between SU and PU. The three spectrum access are listed as follows:

1. Underlay Access
2. Overlay Access
3. Interweave Access

1.1.1 Underlay Access

In Underlay Access [8, 11], SU can operate on the band allocated to PU even if PU is active. This can be done by respecting a power limit not to be exceeded in order to do not affect PU by a harmful interference. Federal Communication Commission (FCC) has set an interference limit called *interference temperature* [12], which is the amount of interference the PU receiver can tolerate. In order to respect this power constraint, SU can spread its signal on a very wide frequency band in order to ensure

that the transmitted power is bellow the power of any PU transmission [5]. Ultra Wide Band (UWB) based transmission was proposed as candidate to perform Underlay Access [13, 14]. Such type of transmission can be used for short range communication due to the limited transmission power.
The main advantage of the Underlay Access paradigm is that SU transmits regardless the PU transmission status. However, the main challenge of Underlay Access paradigm is how to measure the interference power at the PU receiver [11, 14].

1.1.2 Overlay Access

This kind of access stands for the situation where both SU and PU transmit at maximum power simultaneously unlike underlay access which obligates SU to set a level of power not to be exceeded. The overlay DSA model is the more recent development of DSA type [14, 15]. Unlike Underlay Access, in Overlay Access the interference level is not the constraint that SU abides, but the QoS of the PU is the criteria to be respected while the SU is active. In other words, SU can continue transmitting whatever the PU's QoS is not affected. In fact, Overlay Access is based on high cooperation level between PU and SU. This can be done based on channel or networking coding.
In channel coding, the cooperation between SU and PU is based on data sequence (or the codebook of transmission) transmitted from PU and known for SU [16]. Such knowledge permits the SU to split the power of its transmitted signal into two parts: the first one is allocated to retransmitting the PU sequence to the PU receiver, this fact ensures a high Signal to Interference Ratio (SIR) at PU receiver. The second one is to transmit the SU message. Thus, SU plays an assisting role for PU while profiting from the PU band to transmit its data. Knowledge of the PU data sequence (or the codebook) allows SU receiver to cancel the interference coming from the PU transmission. Here, the SU transmitter can use the Dirty Paper Coding [17] to precode the SU packet in order to eliminate the known PU interference [14–16].
Another approach in overlay access is based on network coding, where SU becomes a relay node between two PU nodes. While relaying the PU nodes, SU can encode its own data sequence using network coding [18].
Consequently, Overlay Access presents an attractive solution for the DSA, in which both PU and SU are winner since SU ensures the establishment of a robust link between PU transmitter and PU receiver. For example, this can be useful when PU is at the cell frontier of a mobile network, where the SNR of PU is very low, in this case, SU can be a relay between the PU and the corresponding base station. However, Overlay Access should be done with a high need for the cooperation between PU and SU. This necessitates the synchronization between them in addition to the high encryption needed

for the PU data in order to keep this data private and secured while it is received and treated by SU [14].

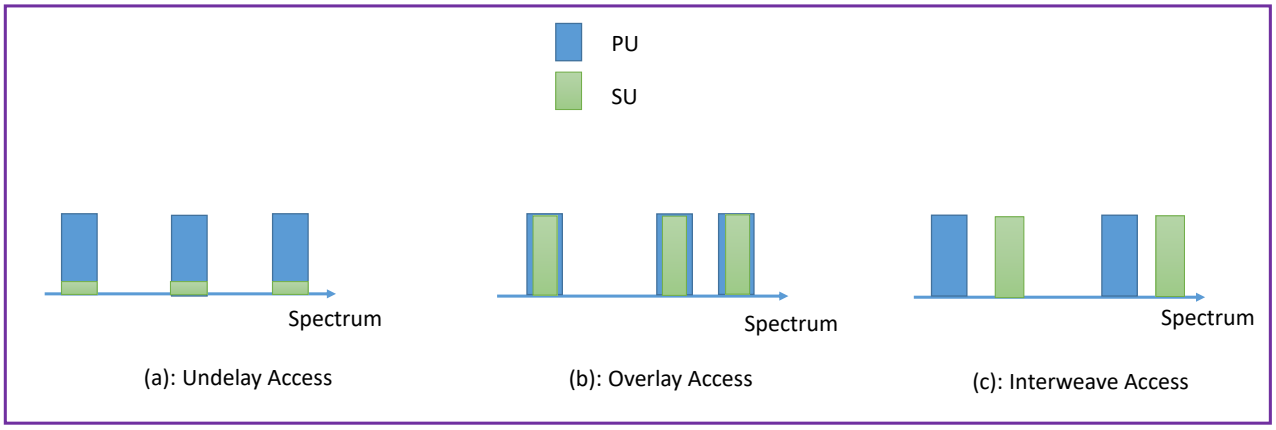


FIGURE 1.2: The PU and SU co-existence in the Spectrum according to the three access types: Underlay, Overlay and Interweave Access

1.1.3 Inter-weave Access

Such kind of access has been the most attractive in the last decade and this is the traditional CR system. This paradigm refers to the *Opportunistic Access* [8, 14, 19, 20], where CR aims at giving an access to the SU to operate on a band allocated to an inactive PU. SU should be continuously aware of any PUs' activity in order to avoid any interference. Thus, one of the main goals of the CR functionality is to protect PU from the impact of the SU interference. If CR discovers a PU activity in an operating channel, in this case SU should immediately stop transmitting in and find another vacant channel. Such access ensures a transmission with maximum power thanks to the mobility of SU from a band to another unlike Underlay Access [14, 15]. The main drawback of this CR is the time loss during the PU discovering, since SU should stop his transmission during this period (silence period) in order to not affect the decision on the PU status by the Self-Interference [19]. Such a type of CR system refers to as Half-Duplex CR due to the silence period. Based on the recent advances of the Self-Interference Cancellation (SIC) [21, 22], Full-Duplex CR has been proposed in order to keep SU active while CR diagnoses transmission band status [23–26]. This needs an efficient SIC with high gain in order to keep robust performance [27].

Figure 1.2 shows the three access types for a CR system. In Overlay or Underlay Accesses SU can use the same frequency band with an active PU, whereas in Interweave Access SU operates on the Spectrum Holes (PU is absent). For Underlay and Overlay Accesses, channel status examination is not required as in Interweave Access. For that reason, in Underlay and Overlay Accesses, SU can be active continuously regardless of the PU status at the cost of low power transmission in Underlay Access and high cooperation between PU and SU in Overlay Access. In contrast, in Interweave Access, although SU should stop transmitting during the channel status examination which affects the data rate, the transmission power is maximal whenever the PU is absent and without any need for cooperation. When PU returns active, SU moves to another available band.

Whatever the type of access and in order to detect, manage and switch among available bands, several parts of CR have to be cooperating in order to increase the efficiency of CR. These parts can be listed as follows [8]:

1. Spectrum Sensing
2. Spectrum Decision
3. Spectrum Mobility
4. Spectrum Sharing

1.2 Main parts of Cognitive Radio

The Cognitive Radio System can manage the communication activities of several SUs in a radio environment where several bands are available. First, CR should diagnose available bands, then choose the best one. In addition, CR should manage the transmission priority of the SUs, and the mobility of the SUs among available bands.

1.2.1 Spectrum Sensing

Spectrum Sensing is a key function of Interweave Access CR. Spectrum Sensing provides CR with the status of the channels (occupied or vacant); based on that, CR makes a decision and sets the transmission parameters of SU [19].
Robust Spectrum Sensing allows CR to efficiently profit from the spectrum opportunities. However, If the Spectrum Sensing decides wrongly that a channel is vacant, in this case SU starts to operate on that channel and affects the PU communications. On the other hand, if the Spectrum Sensing detects an occupied channel while it is really vacant, we can

miss the opportunity to access that available band. In other words, unqualified Spectrum Sensing can lead to either, harmful interference or inefficient use of the spectrum.
Spectrum Sensing can be performed locally or cooperatively [19, 20]. In local Spectrum Sensing, SU makes individually a decision on its radio environment. This decision is vulnerable to be wrong due to hidden PU phenomenon [19] (that happen due to fading, shadowing and other issues). To solve this problem, Cooperative Spectrum Sensing (CSS) has been proposed [28–30]. In CSS, several SUs are cooperating to make a decision on frequency band by exploiting their spatial diversity. A significant enhancement is achieved by using CSS comparing to local Spectrum Sensing.

1.2.2 Spectrum Decision

CR serves to meet the Quality of Service requirement of the SUs (QoS-SU). After sensing the channels, Spectrum Decision in CR selects and allocates the best available channel to a SU [11, 31]. In this context, in [31, 32] the authors show that the decision model which is based only on the channel capacity using the SNR is not the optimal one. In fact, in addition to that channel capacity, several parameters have to be identified and examined to satisfy the QoS-SU. Channel Holding Time (CHT) is an essential parameter which deals with idle PU duration [33, 34] predicted based on a provided Data-Base by PU or by a historical monitoring [11]. A long CHT ensures better QoS-SU. Other parameters such as spectrum switching delay [35–37], channel interference [38, 39], and others have to be taken in account [11, 31].

1.2.3 Spectrum Mobility

The Spectrum Mobility objective is to ensure a seamless switchover while SU changes the operating frequency band [40]. The main aim of Spectrum Mobility is the Spectrum Handoff, which means the mobility from an operating band to another one. This can be done by cooperating with Spectrum Sensing and Spectrum Decision. When SU discovers a PU activity, it should vacate this channel and transfers its ongoing transmission to another available channel. The new channel is selected by the Spectrum Decision. Thus, Spectrum Mobility functionality is related to both Spectrum Sensing and Spectrum Decision. The Spectrum Handoff should be performed as fast as possible in order to decrease as possible the degradation of SU data rate.
One can distinguish two strategies of Spectrum Handoff [40, 41]: the reactive and the proactive handoff. In reactive handoff, SU should sense available spectrum after the knowledge of a Spectrum Handoff trigger. The advantage of this strategy is the accurate decision of the channel availability as the Spectrum Sensing is performed in the most

relevant spectrum environment. In contrast, this strategy increases the SU delay before restarting the transmission.
For proactive handoff [42], SU performs Spectrum Sensing to detect available channels before Spectrum Handoff triggering occurs. This helps PU to avoid long delay before returning active. For that strategy, SU uses a historical tracking of PUs activities to predict the future ones. This fact allows SU to prevent multiple Spectrum Handoffs by selecting an appropriate channel before evacuating the actual channel. Even though this strategy is efficient, the poor prediction may deteriorate the Spectrum Mobility.
In contrast, some SU do not perform a Spectrum Handoff [40]. In fact, in some situations, when PU activity is detected by Spectrum Sensing, SU remains inactive and waits till the end of the PU's activity, then it can return active on the same channel. In such situation, Spectrum Mobility is not required. This fact leads to inflexible CR with a degradation on the SU data rate.

1.2.4 Spectrum Sharing

When multiple SUs are looking to access a limited number of frequency bands, a balanced rule should be maintained by taking into account the QoS of the SUs transmission and their priorities [1, 15]. This can be done by considering a policy rule providing a fair schedule to share available bands. In addition to policy fairness, the policy should take into account the collision of SUs and the interference amount caused by SUs to PU receiver [5]. That policy can be set based on a cooperation among the SUs. This refers to the CR network topology: Centralized or Distributed Network. In centralized network, the SUs send their informations to the network entity, which defines the most suitable policy to share available bands among the SUs. In distributed network, SUs exchange their informations, then each SU makes an individual decision on accessing the channel. Although the distributed cooperation leads to non fair Spectrum Sharing, it is preferred in a situation where users can make their own decisions on the spectrum access based mainly on local information.

Figure 1.3 shows the CR cycle. Spectrum Sensing informs Spectrum Decision on the available bands to choose best ones based on the SU transmission requirement. Later on, Spectrum Sharing assigns a channel to a SU. The allocated channels can be changed according to Spectrum Mobility, which is updated by the Spectrum Sensing decisions on the available channels.
In our manuscript, we are focusing on the Spectrum Sensing function, which plays the

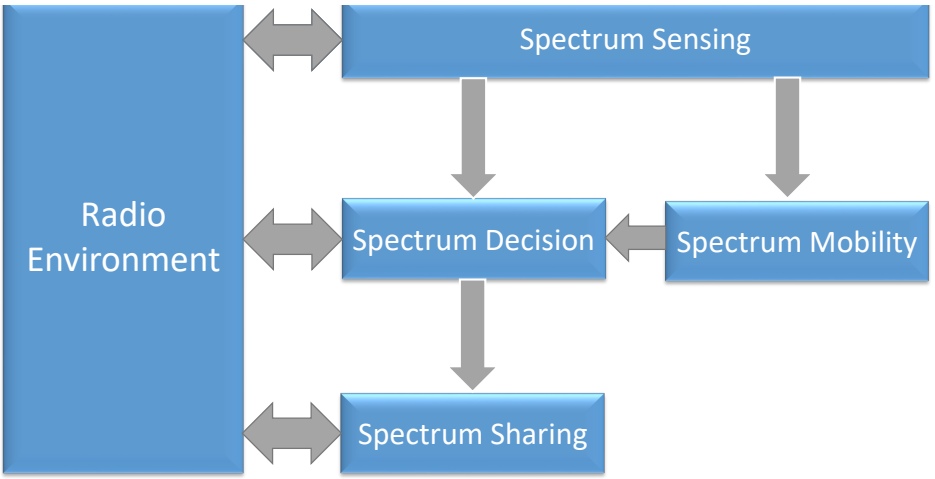


FIGURE 1.3: The Cognitive Radio Cycle

most important role in Interweave CR system, since the CR cycle is based on the decision of the Spectrum Sensing. When Spectrum Sensing truly provides this cycles with the available channels, the efficiency of CR is enhanced. Contrariwise, if the Spectrum Sensing is malfunctioned, both, the spectrum use efficiency or the PU QoS will be affected.

1.3 Thesis Organization

In this manuscript, we are focusing on the Interweave Access Cognitive Radio [1], especially on the Spectrum Sensing part. The important role of the Spectrum Sensing comes from that CR transmission is opportunistic, so that its operations are mainly based on the status of the frequency bands. In fact, many algorithms were presented in the literature to perform the Spectrum Sensing. Each of those algorithms has strong and weak points based on many criteria such as the robustness of detection, the blindness with respect to the PU signal, the vulnerability to the noise variance, the complexity, the oversampling effect, *etc*.
In our work, we are aiming at adapting and/or inventing new Spectrum Sensing algorithms for Half Duplex Cognitive Radio by taking into account the criteria listed above. Besides that, Full Duplex Cognitive Radio is also considered, where our main goal in such a system is the elimination of the hardware imperfections which affect greatly the Spectrum Sensing.

Our manuscript is organized as follows:

[1] Throughout the rest of the manuscript, Cognitive Radio means that uses the Interweave Access

Chapter 2 presents a state of the art on Spectrum Sensing. This chapter analyses popular algorithms according to several criteria, and focusing on their limitations and drawbacks of these algorithms. Different Spectrum Sensing strategies are also discussed in this chapter.

Chapter 3 will explain the application Canonical Correlation Theory (CCT) in Spectrum Sensing. CCT was applied on such domain to be candidate to test the cyclostationary of the received signals on Multi-Antenna System (MAS), in this case spatial diversity is exploited to discover the cyclostationarity of the PU signal. In this chapter, we extend CCST to Single-Antenna System (SAS), where a new algorithm is proposed based on the time diversity of the received signal. Exploiting the time diversity make CCST applicable on SAS. Moreover, this new proposed algorithm is then extended to MAS, where both time and spatial diversities are exploited. Several simulations are carried out in order to show the effectiveness of the proposed detector.

New Spectrum Sensing algorithms are proposed in chapter 4. In this chapter, new detection criterion based mainly on the cumulative sum of the Power Spectral Density (PSD) of the received signal is proposed. When assuming the whiteness of the noise samples, the noise's PSD becomes flat. This aspect does not exist for the PU signal, which is assumed to be oversampled. Therefore its PSD is no longer flat. If the PU is absent, the cumulative sum of the received signal PSD has a close shape to a straight line. Whereas a curved shape is obtained when PU exists.
Several algorithms will be proposed based on the PSD of the received signal, with a detailed analytic study. In this context, the False Alarm and Detection probabilities are evaluated analytically under Gaussian and Rayleigh fading channels. Our proposed algorithms are compared with other well known state-of-the-art ones, where they present a robust performance even at a low oversampling rate, where some detectors such as the autocorrelation and cyclostationary detectors provide a poor performance relatively to the energy detector. Furthermore, our detectors are less sensitive to the Noise Uncertainty problem than the energy detector. In particular, we demonstrate that the detectors we present can be made independent from noise variance.

Chapter 5 addresses the Full-Duplex Cognitive Radio (FD-CR), where the Secondary User (SU) can transmit and perform the Spectrum Sensing simultaneously unlike Half-Duplex Cognitive Radio (HD-CR) which stops the transmission during the sensing period. The main challenge in Full-Duplex (FD) consists in minimizing the Residual Self Interference (RSI) which represents the error of the Self Interference Cancellation (SIC)

and the receiver impairments mitigation such as the oscillator Phase Noise (PN), the Non-Linear Distortion (NLD) of the receiver Low-Noise Amplifier (LNA), the Analog to Digital Converter (ADC) noise *etc.* In Cognitive Network, SU should be aware of the Primary User (PU) activity; Hence, the RSI represents an important challenge for the SU to make a decision on the presence of PU. To mitigate the PN and the NLD of LNA, a new receiver model of the FD system is proposed.
At first, an analytic relationship is derived to show the effect of the RSI on the Spectrum Sensing performance in FD-CR comparing to HD-CR. After that, an auxiliary chain is presented to help the receiver avoid the PN effect. Further, the new receiver architecture is proposed in order to estimate the NLD coefficients. This estimation is followed by a re-generation and a subtraction of the NLD from the received signal. Such proposed model shows its efficiency by both enhancing the channel estimation and reducing the RSI power. A performance analysis of the proposed receiver model on FD-CR with all Full-Duplex receiver impairments is presented. Obtained ROC curve shows an important enhancement in the detection rate relative to the classical Self-Interference Canceller, this fact impacts positively the CR throughput gain as corroborated by intensive numerical results.

Chapter 6 stands for a general conclusion of our work by opening a new horizon in this domain.

Chapter 2

State of art in Spectrum Sensing

List of Acronyms

ACD Autocorrelation Detector

AWGN Additive White Gaussian Noise

BSS Blind Source Separation

CAF Cyclic-Autocorrelation Function

CDF Cumulative Density Function

CF Cyclic Frequency

CFAR Constant False Alarm Rate

CR Cognitive Radio

CSD Cyclo-Stationary Detector

CLT Central Limit Theorem

CSCGN Circular Symmetric Complex Gaussian Noise

CSS Cooperative Spectrum Sensing

ED Energy Detector

EME Energy with Minimum Eigenvalue

EVD Eigenvalues-based Detector

FC Fusion Center

FD Full-Duplex

FD-CR Full-Duplex Cognitive Radio

GLRT Generalized Likelihood Ratio Test

GoF Goodness of Fit

HD Half-Duplex

HD-CR Half-Duplex Cognitive Radio

HCS Hard Combining Scheme

HD Half-Duplex

HD-CR Half-Duplex Cognitive Radio

HIM Hardware Imperfections Mitigation

IoT Internet of Things

KD Kurtosis Detector

LLR Likelihood Ratio

LNA Low-Noise Amplifier

MAS Multi-Antenna System

MME Maximum-Minimum Eigenvalue

NU Noise Uncertainty

OFDM Orthogonal Frequency Division Multiplex

PDF Probability Density Function

PU Primary User

ROC Receiving Operating Characteristics

SCS Soft Combining Scheme

SU Secondary User

TS Test Statistic

WFD Wave-Form Detector

In the Cognitive Radio (CR) operation cycle, distinguishing the Primary User (PU) status is the first step to access (or not) a frequency band by a Secondary User (SU). To achieve an accurate decision, SU should stop the transmission during the Spectrum Sensing, which is performed periodically. This fact refers to the so-called Half-Duplex CR (HD-CR) system which divides its activity time into two periodic time slots: the first one stands for the Spectrum Sensing (SU is in silence period), while the second one is devoted for the transmission. To overcome this limitation, Full-Duplex CR (FD-CR) system has recently been proposed [26, 43]. FD-CR concerns mainly the Spectrum Sensing part in CR, where it aims at making SU active even when the Spectrum Sensing is under progress. This can be done by the Self-Interference Cancellation (SIC) of the SU signal (Self-Interference) at the SU receiving antenna.

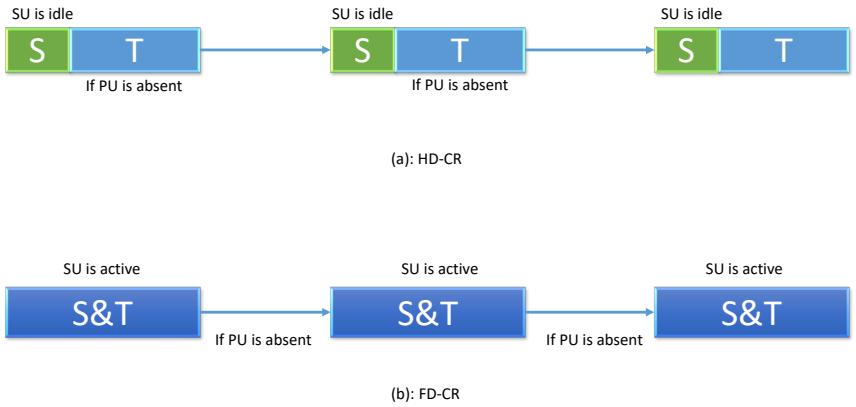


FIGURE 2.1: CR activity under both HD and FD modes. (a) HD-CR: the SU should stop the transmission while it performs the sensing of the channel. (b) FD-CR: SU can continue transmitting while the Spectrum Sensing is established

Figure (2.1) shows the time allocation of CR for HD and FD modes. In HD-CR, there is a time slot where SU is inactive, while in FD-CR, SU remains active continuously. This fact leads to data rate enhancement.

Traditionally, Spectrum Sensing algorithms are designed to deal with HD-CR. Spectrum Sensing is based on the basic but fundamental binary Bayesian detection problem: Under the hypothesis H_0, the PU is absent, whereas under the alternate hypothesis H_1 PU exists. The received signal $y(n)$ at the CR antenna in HD mode can be modelled under both hypotheses as follows:

$$\begin{cases} H_0 : y(n) = w(n) \\ H_1 : y(n) = hs(n) + w(n) \end{cases} \tag{2.1}$$

where h stands for the complex channel effect on the PU signal $s(n)$. $w(n) = w_p(n) + iw_q(n)$, is assumed to be an $i.i.d$ zero mean circular symmetric complex Gaussian noise (CSCGN), $i.e.$ $E[w(n)] = 0 = E[w^2(n)]$, where $E[.]$ stands for the mathematical expectation. The real part, $w_p(n)$, and the imaginary part, $w_q(n)$, of $w(n)$ are independent with the same variance.

$$E[w_p^2(n)] = E[w_q^2(n)] = \frac{\sigma_w^2}{2} \tag{2.2}$$

where $\sigma_w^2 = E[|w(n)|^2]$. Without loss of generality, we can assume that $s(n)$ is power normalized. In this case, the Signal to Noise Ratio (SNR), γ, is defined as follows:

$$\gamma = \frac{|h|^2}{\sigma_w^2} \tag{2.3}$$

Regarding Full-Duplex mode, received signal becomes under both hypotheses of presence/absence of PU as follows:

$$\begin{cases} H_0 : y(n) = x_g(n) + w(n) \\ H_1 : y(n) = hs(n) + x_g(n) + w(n) \end{cases} \tag{2.4}$$

$x_g(n)$ is the image of the SU signal $x(n)$ received by the CR receiving antenna (R_X) where $x(n)$ is the transmitted signal by SU at the transmitting antenna (T_X). $x_g(n)$ holds the channel effect between T_X and R_X and the receiver imperfections.
The existence of the SU signal at R_X makes the major difference between equations (2.1) and (2.4). When CR detects a PU activity, SU should immediately vacate the channel of PU. By estimating the channel coefficients and the circuit imperfections, CR regenerates an estimate, $\hat{x}_g(n)$, of $x_g(n)$ and subtracts it from $y(n)$ to obtain $\hat{y}(n)$. The Spectrum Sensing is then performed on $\hat{y}(n)$.

$$\hat{y}(n) = y(n) - \hat{x}_g(n) \tag{2.5}$$

For an ideal SIC ($i.e.$ $\hat{x}_g(n) = x_g(n)$), $\hat{y}(n) = y(n)$, the equation (2.4) corresponding to FD mode becomes the same as that of HD mode (equation (2.1)). (More details about FD-CR will be given in Chapter 5).

2.1 Spectrum Sensing Measurements

Generally, in order to perform the Spectrum Sensing, the received signal is down-converted to the baseband, on which a Test Statistic (TS) is applied to diagnose the channel status: PU exists or PU is absent.

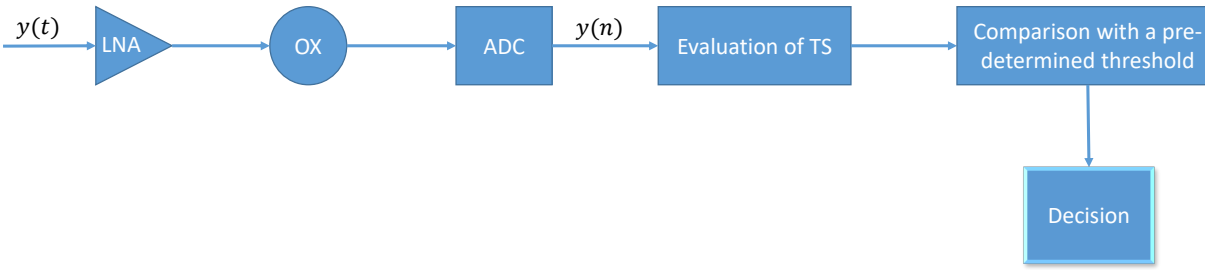


FIGURE 2.2: General architecture of Spectrum Sensing in a CR receiver

Figure (2.2) shows the CR receiver capable to evaluate the TS. The received RF analogue signal $y(t)$ should be amplified using a Low-Noise Amplifier (LNA) and converted to baseband signal using the oscillator (OX). Using Analog to Digital Converter (ADC) one can generate the equivalent digital signal $y(n)$, on which TS is applied and compared to a predetermined threshold to make a decision on the channel status. It is worth mentioning that LNA normally introduces a distortion in the amplified signal due to its non-linearity. In addition, the oscillator results in multiplicative noise due to noise phase error plus the ADC additive quantization uniform noise [21, 27]. In HD mode, the circuit imperfections (such as the LNA distortion, the ADC noise and the oscillator noise) are not taken into account since their appearance is related to the PU signal existence, in other words, these imperfections are presented only when PU signal is received and they are of negligible power compared to the PU signal. In contrast, in FD mode, these imperfections should be taken into account since the Self-Interference to be cancelled is coming with a very high power compared to PU signal, due to the short distance between SU's T_X and SU's R_X (see figure 2.3).

For that reason, the hardware imperfections and other noises should be considered in order to not affect TS, and consequently the Spectrum Sensing performance. More details on the effect of the receiver imperfections are given in chapter 5.

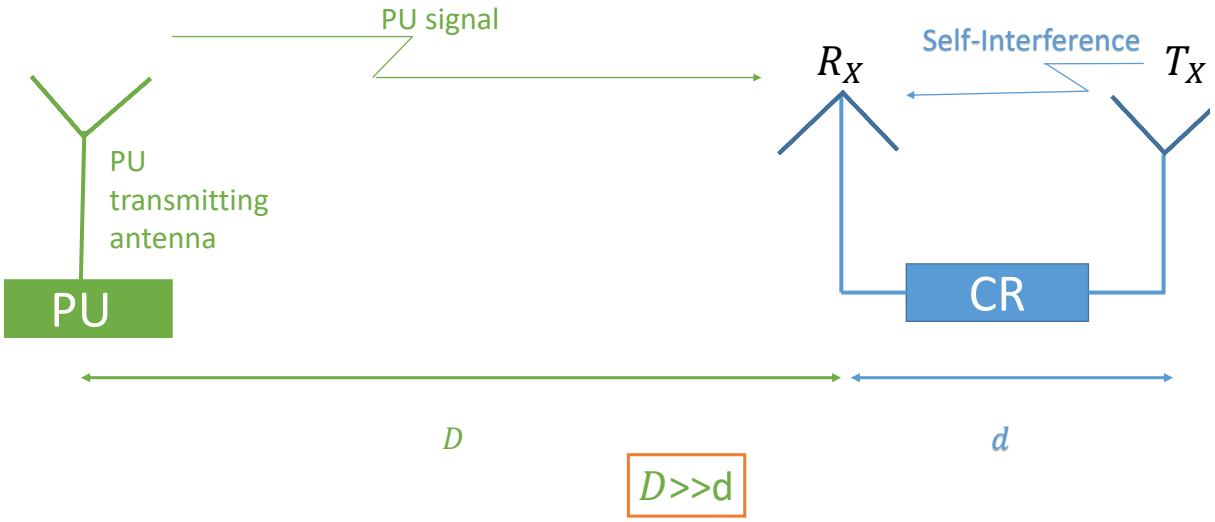


FIGURE 2.3: Effect of the distance on the power of the received signal in FD-CR system

2.1.1 Detection Criteria

In order to detect the PU signal, TS is generally evaluated based on one or many criteria such as:

1. Incremental Energy

   When PU starts to transmit, the energy of the received signal should be incremented compared to the noise-only case. By estimating previously the power of the stationary noise, and by comparing the energy of the received signal to a pre-defined threshold depending on the noise power, CR decides if the channel is occupied by a PU signal or not. This type of detection is used for the Energy Detector in both time and frequency domains.

2. PU signal pattern

   Many features (such as the modulation process, the sine-wave carrier, the periodic pilot, the cyclic-prefix (for OFDM signal), *etc*) make telecommunication signals distinguishable from the noise. A major characteristic of the modulated signals is the cyclo-stationarity property [44–46].
   Other aspects can also be employed by CR (such as the oversampling of the base-band PU signal, the periodic pilot sent by PU, the cyclic-prefix (for OFDM signal) *etc*) to detect the PU. Several detectors such as Auto-Correlation Detector (ACD) [47] and Eigenvalue-based Detector (EVD) [48] exploit the correlation presented in the PU signal due to aspects listed above.

Moreover, some detectors, such as Goodness of Fit test [49, 50] and Kurtosis detectors [51], compare the distribution of the received signal to the distribution of the noise-only-case.

3. PU signal's waveform: In some circumstances, CR has an image of the PU signal shape. Waveform and Matched filter detectors correlate the received signal with the PU signal shape in order to test the channel opportunity [52, 53].

2.1.2 Detection Decisions

Whatever the used criterion to detect the PU activity, the corresponding TS should be compared to a predefined threshold λ in order to make a decision:

$$\begin{cases} H_0 : \ TS < \lambda : \quad PU \ is \ idle \\ H_1 : TS \geq \lambda : \quad PU \ is \ transmitting \end{cases} \tag{2.6}$$

That comparison leads to one of the four following cases:

1. Reject

   SU decides correctly that PU is absent. Such decision helps CR to efficiently exploit the spectrum holes. Thus, the Reject probability p_{re} can be presented as:

   $$p_{re} = Pr\Big(TS < \lambda | H_0\Big) \tag{2.7}$$

2. False Alarm

   This case happens when CR decides that an absent PU is active. This wrong decision leads to miss the opportunity of available bands. The probability of False Alarm p_{fa} is evaluated by:

   $$p_{fa} = Pr\Big(TS \geq \lambda | H_0\Big) \tag{2.8}$$

3. Detection

   When CR truly detect an active PU. That decision protects PU against the interference of SU which should be idle in such case. Accordingly, the probability of Detection p_d is found as follows:

   $$p_d = Pr\Big(TS \geq \lambda | H_1\Big) \tag{2.9}$$

4. Missed Detection

   CR cannot detect an active PU. This decision leads to an interference on the PU's signal since that decision gives the permission to SU to transmit on the same band of an active PU. Therefore, the Probability of Missed Detection p_{md} is defined as follows:

$$p_{md} = Pr\Big(TS < \lambda | H_1\Big) \tag{2.10}$$

We should emphasize that:

$$p_{re} + p_{fa} = 1 \tag{2.11}$$

$$p_d + p_{md} = 1 \tag{2.12}$$

To analytically find the above probabilities, one should derive the Probability Density Function (PDF) of TS under H_0 and H_1. The importance of finding the PDF under H_0 is to set an appropriate threshold in order to satisfy both: protecting the PU from the interference and get a maximum profit of the channel opportunities. According to the IEEE.802 WRAN regulation [54], $p_{fa} = 0.1$ and $p_d = 0.9$ should be satisfied by the Spectrum Sensing at a limit SNR of -20 dB in the CR system. However, when p_{fa} is set, a suitable threshold can be found based on other parameters such as the noise variance and the number of used samples.

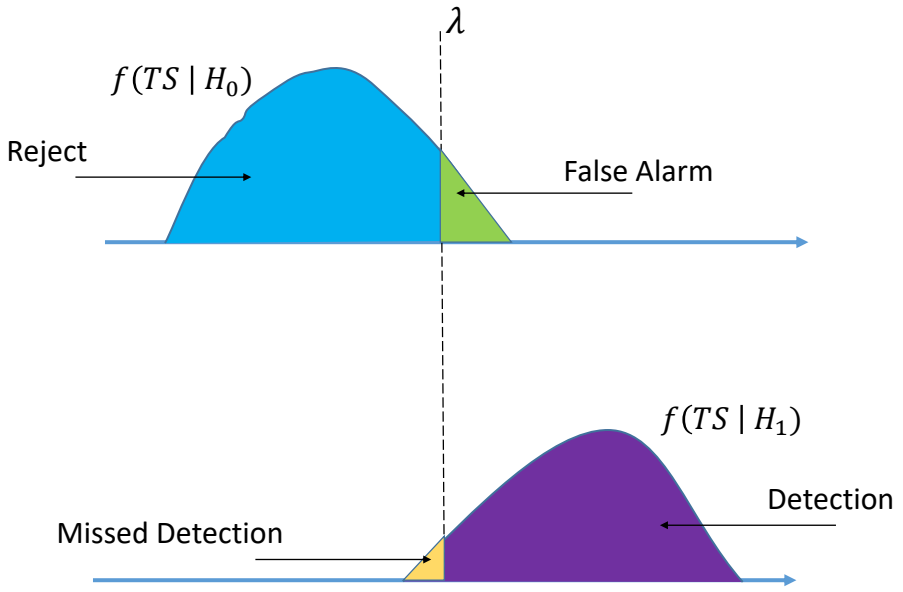


FIGURE 2.4: The distribution of a TS under noise-only ($f(TS|H_0)$) case and signal-plus-noise case ($f(TS|H_1)$)

Figure (2.4) shows the distribution of a given TS under the noise-only and the noise-plus-signal cases. The nature of the decision area is related to the chosen threshold, which is set to satisfy the CR detection requirement. Note that minimizing the area of overlapping between the distribution of TS under H_0 and H_1 leads to enhance the detection performance. This can be done by increasing the observation time of the received signal.
A wrong decision on the channel status (False Alarm or Missed Detection) can affect either the PU transmission or the efficient use of the channel. In fact, a missed detection can cause a harmful interference due to the transmission of the SU in the same band with the PU. A false alarm, however, decreases the profit of the channel. Therefore, the probability of detection (p_d) should be increased as much as possible, by keeping a small the probability of false alarm (p_{fa}). .

2.2 Classic Spectrum Sensing Algorithms

2.2.1 Energy Detector

The Energy Detector (ED) is a simple and blind detector who does not require any information about the PU signal. ED consists in evaluating its TS, T_{ED}, in the band of interest over N received samples and comparing it to a predefined threshold λ [55–57].

$$T_{ED} = \frac{1}{N}\sum_{n=1}^{N}|y(n)|^2 \tag{2.13}$$

The threshold λ is set according to a target p_{fa}, and using the distribution of the test statistic under H_0 to meet the detection requirement. When a target p_{fa} is fixed, the detector sets the required number of samples in order to reach that probability.
It has been proved that the distribution of T_{ED} under H_0 tends toward a central χ^2 distribution with $2N$ degrees of freedom [55, 57]. Under a low SNR, the number of samples required to perform the Spectrum Sensing increases largely. In this case, the distribution of T_{ED} tends toward a Normal Distribution according to the Central Limit Theorem (CLT):

$$T_{ED} \overset{H_0}{\sim} \mathcal{N}(\mu_0^{ED}, V_0^{ED}) \tag{2.14}$$

where $\overset{H_i}{\sim}$ stands for the asymptotic distribution under H_i, $i \in \{0,1\}$, and $\mathcal{N}(\mu, V)$ represents a Normal distribution of a mean μ and a variance V.

Under H_1, the distribution of T_{ED} depends on the ones of $s(n)$ and $w(n)$. Some researchers suggest to use the Gaussian distribution as generic model when $s(n)$ is unknown [57]. Such suggestion leads to obtain a Normal Distribution of T_{ED} under H_1 for a large number of samples according to CLT.

$$T_{ED} \overset{H_1}{\sim} \mathcal{N}(\mu_1^{ED}, V_1^{ED}) \tag{2.15}$$

PU's signal is assumed in some cases to be deterministic with unknown value, in order to derive the analytic distribution of the test statistic [45, 46, 57]. When no assumption is considered on the distribution of the PU signal, the distribution of the test statistic becomes non-derivable [57].
The probabilities of False Alarm and Detection of ED for a large N and the Gaussian assumption of the PU signal, can be derived as follows [57]:

$$p_{fa}^{ED} = Q\left(\frac{\lambda - \sigma_w^2}{\frac{1}{\sqrt{N}}\sigma_w^2}\right) \tag{2.16}$$

$$p_d^{ED} = Q\left(\frac{\lambda - (\sigma_w^2 + \sigma_s^2)}{\frac{1}{\sqrt{N}}(\sigma_w^2 + \sigma_w^2)}\right) \tag{2.17}$$

Where $Q(x)$ is the Q-function which is defined as follows [58]:

$$Q(x) = \frac{1}{\sqrt{2\pi}} \int_x^{+\infty} e^{-u^2} du \tag{2.18}$$

According to equation (2.16), the threshold λ can be expressed as follows:

$$\lambda = \frac{1}{\sqrt{N}} Q^{-1}(p_{fa})\sigma_w^2 + \sigma_w^2 \tag{2.19}$$

Equation (2.19) shows the dependency of λ to the noise variance, which should be estimated by the SU prior to perform the Spectrum Sensing. Any error in the noise variance estimation may lead to so-called Noise Uncertainty (NU) problem, which degrades harmfully the performance of ED as it is shown in section 2.3.4.

2.2.2 Autocorrelation Detector

A linearly modulated PU signal can be modelled in a base-band form as follows:

$$s(n) = \sum_{k} b_k g(n - kN_s) \tag{2.20}$$

b_k are the transmitted independent symbols and $g(n)$ is the shaping window, and $N_s \geq 1$ stands for the number of Samples per Symbols (sps).

In such model, the autocorrelation $r_{ss}(m)$ of $s(n)$ for some non-zero lags, m, becomes non zero:

$$r_{ss}(m) = E[s(n)s^*(n-m)] \neq 0 \tag{2.21}$$

For the linearly modulated signals (such as BPSK, M-QAM, ASK, *etc*), $r_{ss}(m)$ can be evaluated as follows[59]:

$$r_{ss}(m) = \begin{cases} \sigma_s^2 \left(1 - \dfrac{|m|}{N_s}\right); \ |m| \leq N_s \\ 0; |m| > N_s \end{cases} \tag{2.22}$$

where $\sigma_s^2 = E[|s(n)|^2]$.

The autocotrrelation $r_{yy}(m)$ of the received signal $y(n)$ can be found as follows [60–62]

$$\begin{aligned} r_{yy}(m) &= E[y(n)y^*(n-m)] \\ &= E\left[(hs(n) + w(n))(hs(n-m) + w(n-m))^*\right] \\ &= E\left[|h|^2 s(n)s^*(n-m)\right] + E\left[w(n)w^*(n-m)\right] \\ &\quad + E\left[h^* w(n)s^*(n-m)\right] + E\left[hw^*(n-m)s(n)\right] \end{aligned} \tag{2.23}$$

Since $w(n)$ is a white noise then

$$E[w(n)w^*(n-m)] = \sigma_w^2 \delta(m) \tag{2.24}$$

where $\delta(m)$ stands for Dirac distribution:

$$\delta(m) = \begin{cases} 1 \ if \ m \ = 0 \\ 0 \ elsewhere \end{cases} \tag{2.25}$$

By assuming that $s(n)$ and $w(n)$ are zero mean independent signals, then $E[h^*w(n)s^*(n-m)] + E[hw^*(n-m)s(n)] = 0$. Equation (2.23) becomes as follows:

$$\begin{aligned} r_{yy}(m) &= E\left[|h|^2 s(n)s^*(n-m)\right] + E[w(n)w^*(n-m)] \\ &= |h|^2 r_{ss}(m) + \sigma_w^2 \delta(m) \end{aligned} \tag{2.26}$$

As shown in Equation (2.26), $r_{yy}(m)$ vanishes when the PU signal is absent for any $m \neq 0$, and it is non zero for only the case when an oversampled PU signal exists and $1 \leq m \leq N_s$. Based on the above discussion, the autocorrelation for $1 \leq m \leq N_s$ becomes a candidate for the sensing of the spectrum:

$$r_{yy}(m) = \begin{cases} 0 \ under \ H_0 \\ \neq 0 \ under \ H_1 \end{cases} \tag{2.27}$$

In [47], the proposed Auto-correlation Detector (ACD) algorithm tests a linear combination of $\{r_{yy}(m)\}$ where $m \in [1; N_s - 1]$. The test statistic to be derived, T_{ACD}, is presented as follows [47]:

$$T_{ACD} = \frac{1}{\hat{r}_{yy}(0)} \sum_{m=1}^{N_s-1} c_m Re\{\hat{r}_{yy}(m)\} \tag{2.28}$$

Where $Re\{.\}$ stands for the real part, $\hat{r}_{yy}(m) = \frac{1}{N}\sum_{n=1}^{N} y(n)y^*(n-m)$ is an estimator of the autocorrelation function $r_{yy}(m)$ and c_m is a set of weighting coefficients. $\hat{r}_{yy}(0)$ is the power of the received signal.

The division operation by $\hat{r}_{yy}(0)$ avoids the vulnerability of ACD to NU, since ACD becomes independent of the noise variance under H_0 [47]. This operation makes ACD a Constant False Alarm Rate (CFAR) detector, so that the threshold of comparison is only depending on the number of samples used in the detection process.

According to [47], the False Alarm and Detection probabilities of ACD are expressed as follows:

$$p_{fa}^{ACD} = Q\left(\lambda\sqrt{\frac{N}{\lambda^2 + \varphi}}\right) \tag{2.29}$$

$$p_d^{ACD} = Q\left(\frac{\lambda - \frac{\beta\gamma}{\gamma+1}}{\sqrt{V_{ACD}}}\right) \tag{2.30}$$

Where $\varphi = \frac{1}{2}\sum_{l=1}^{N_s-1} c_l^2$, $\beta = \sum_{l=1}^{N_s-1} c_l \frac{r_{ss}(l)}{r_{ss}(0)}$, $V_{ACD} = \frac{(1+\gamma)\lambda^2 - 4\beta\gamma\lambda + \Sigma + \eta\gamma}{N(\gamma+1)^2}$, $\eta = \sum_{l=1}^{N_s-1}\sum_{k=1;l\neq k}^{N_s-1} c_l c_k \frac{r_{ss}(l-k) + r_{ss}(l+k)}{r_{ss}(0)}$ and γ is the SNR as mentioned above.

2.2.3 Cyclostationary Detector

The Cyclo-Stationary Detection (CSD) is widely used in the Spectrum Sensing context due to its robustness under low SNR and its capacity to distinguish between modulated signals and noise, based on the fact that almost of telecommunications signals are cyclo-stationary due to the modulation process, the sine-wave carrier, the periodic pilots, *etc.* These existing cyclo-stationary features present in telecommunication signals are not present in the noise.

The signal $s(n)$ is said to be Cyclo-Stationary if its autocorrelation function is periodic with a period T_α [63].

$$r_{ss}(n,m) = E[s(n)s^*(n-m)] = r_{ss}(n+T_\alpha, m) \tag{2.31}$$

Since $r_{ss}(n,m)$ is periodic with respect to n, then it can be expanded using Fourier Series as follows [63, 64]:

$$r_{ss}(n,m) = \sum_{p=-\infty}^{\infty} R_{ss}\left(\frac{p}{T_\alpha}, m\right) \exp\left(j2\pi\frac{p}{T_\alpha}n\right) \tag{2.32}$$

Where the Fourier Coefficient $R_{ss}(\frac{p}{T_\alpha}, m)$ are referred to be the Cyclic-Autocorrelation Function (CAF), and $\{\frac{p}{T_\alpha}\}$ is the set of Cyclic-Frequencies.

Accordingly, $R_{ss}(\alpha, m)$ can be evaluated by:

$$R_{ss}(\alpha, m) = \lim_{N\longrightarrow+\infty} \frac{1}{N} \sum_{n=-\frac{N}{2}}^{\frac{N}{2}} s(n)s^*(n-m))\exp\left(-j2\pi\alpha n\right) \tag{2.33}$$

$R_{ss}(\alpha, m) \neq 0$ if $\alpha \in \{\frac{p}{T_\alpha}\}$, in this case α is a cyclic-frequency [44]. If $\alpha = 0$, $R(0,m)$ refers to the classical autocorrelation. When $m = 0$ and $\alpha = 0$, $R_{ss}(0,0)$ stands for the energy of $s(n)$.

Cyclic Autocorrelation Function (CAF) as a Test Statistic in Spectrum Sensing :

Due to the cyclo-stationary features of the PU signal, it is sufficient to examine the cyclo-stationarity of the received signal to analyse the channel status. According to model (2.1), the CAF $R_{yy}(\alpha, m)$ of the received signal can be derived as follows:

$$\begin{aligned} R_{yy}(\alpha,m) &= \lim_{N\longrightarrow\infty} \sum_{n=-\frac{N}{2}}^{\frac{N}{2}} y(n)y^*(n-m)\exp\left(-j2\pi\alpha n\right) \\ &= \lim_{N\longrightarrow\infty} \sum_{n=-\frac{N}{2}}^{\frac{N}{2}} \Big(hs(n)+w(n)\Big)\Big(h^*s^*(n-m)+w^*(n-m)\Big)\exp\left(-j2\pi\alpha n\right) \\ &= \lim_{N\longrightarrow\infty} \sum_{n=-\frac{N}{2}}^{\frac{N_i}{2}} \Big(|h|^2 s(n)s^*(n-m)+w(n)w^*(n-m)+s(n)w^*(n-m) \\ &\quad + w(n)s^*(n-m)\Big)\exp\left(-j2\pi\alpha n\right) \\ &= R_{ss}(\alpha,m)+R_{ww}(\alpha,m)+R_{sw}(\alpha,m)+R_{ws}(\alpha,m) \end{aligned} \tag{2.34}$$

Since the noise $w(n)$ does not exhibit any cyclo-stationarity then $R_{ww}(\alpha, m) = 0, \forall\alpha \neq 0$. $R_{ws}(\alpha, m) = R_{sw}(\alpha, m) = 0$ since there is no common cyclic-frequency between $s(n)$ and $w(n)$.
Consequently, the CAF of the received signal becomes that of the PU signal.

$$R_{yy}(\alpha,m) = R_{ss}(\alpha,m) \tag{2.35}$$

Applying CAF necessitates the pre-knowledge (or estimation) of the cyclic-frequency. Due to the limitation in the observation time, then $R_{yy}(\alpha, m)$ is estimated by $\hat{R}_{yy}(\alpha, m)$:

$$\hat{R}_{yy}(\alpha,m) \simeq \frac{1}{N}\sum_{n=-\frac{N}{2}}^{\frac{N}{2}-1} y(n)y^*(n-m)\exp\left(-j2\pi\alpha n\right) \tag{2.36}$$

To examine the channel opportunity, the test statistic T_{CAF} is found as the modulus of $\hat{R}_{yy}(\alpha, m)$ [63, 65]

$$T_{CAF} = |\hat{R}_{yy}(\alpha,m)|^2 \tag{2.37}$$

T_{CAF} is compared to a predefined threshold in order to made a decision on the activity of the PU.

GLRT-based Cyclo-Stationary Detector :

In fact, several algorithms have been proposed to perform the cyclo-stationary detection [44, 45, 66]. In [44], the authors proposed the well known Generalized Likelihood Ratio Test (GLRT)-based cyclostationary features detector. The test statistic considered in GLRT is the following [44].:

$$T_{CSD} = N\hat{r}_y \mathbf{K} \hat{r}_y^T \tag{2.38}$$

Where the upper script T stands for the transpose operation, and $\hat{r}_y$ is defined as follows:

$$\begin{aligned}\hat{r}_y = \Big[& Re\{\hat{R}_{yy}(\alpha, m_1)\}, Re\{\hat{R}_{yy}(\alpha, m_2)\} ..., Re\{\hat{R}_{yy}(\alpha, m_M)\}, \\ & Im\{\hat{R}_{yy}(\alpha, m_1)\}, Im\{\hat{R}_{yy}(\alpha, m_2)\} ..., Im\{\hat{R}_{yy}(\alpha, m_M)\}\Big]\end{aligned} \tag{2.39}$$

where $Re\{.\}$ and $Im\{.\}$ stand for the real and imaginary parts respectively and M is the number of the time lags used in the detection process. $\mathbf{K}$ stands for the covariance matrix:

$$\mathbf{K} = \frac{1}{2} \begin{bmatrix} Re\{\mathcal{P} + \mathcal{U}\} & Im\{\mathcal{U} - \mathcal{P}\} \\ Im\{\mathcal{P} + \mathcal{U}\} & Re\{\mathcal{P} - \mathcal{U}\} \end{bmatrix}^{-1} \tag{2.40}$$

Where $\mathcal{P} = \left(P_{pq}\right)$ and $\mathcal{U} = \left(U_{pq}\right)$ are found as follows:

$$\begin{aligned} P_{p,q} &= \sum_{l=\frac{1-L}{2}}^{\frac{L-1}{2}} f(l) \hat{R}_{yy}\left(\alpha + \frac{2\pi l}{N}, m_p\right) \hat{R}^*_{yy}\left(\alpha + \frac{2\pi l}{N}, m_q\right) \\ U_{p,q} &= \sum_{l=\frac{1-L}{2}}^{\frac{L-1}{2}} f(l) \hat{R}_{yy}\left(\alpha + \frac{2\pi l}{N}, m_p\right) \hat{R}_{yy}\left(\alpha - \frac{2\pi m}{N}, m_q\right) \end{aligned} \tag{2.41}$$

L is the length of the normalized weighting window $f(l)$, so that $\sum_{l=1}^{L} f(l) = 1$. The distributions of T_{CSD} under both H_0 and H_1 follow the χ^2 law with $2M$ degrees of freedom, with the difference that under H_0 χ^2 is centred whereas it is non-centred under H_1 with a non-centrality parameter of $N\hat{r}_y \mathbf{K} \hat{r}_y^T$.

$$\begin{cases} T_{CSD} \overset{H_1}{\sim} \chi^2_{2M} \\ T_{CSD} \overset{H_1}{\sim} \chi^2_{2M}\left(N\hat{r}_x \mathbf{K} \hat{r}_x^T\right) \end{cases} \tag{2.42}$$

The probabilities of false alarm (p_{fa}) and detection (p_d) are given based on the distributions under H_0 and H_1 respectively:

$$p_{fa}^{CSD} = \Gamma(\lambda/2, M) \tag{2.43}$$

$$p_d^{CSD} = Q_M\left(\sqrt{\lambda}, \sqrt{N\hat{r}_x \mathbf{K} \hat{r}_x^T}\right) \tag{2.44}$$

where $\Gamma(a, b)$ is the upper incomplete gamma function and $Q_M(a, b)$ is the generalized Marcum Q-function, and they are defined as follow respectively [58]:

$$\Gamma(a, b) = \int_0^b t^{a-1} \exp(-t) dt \tag{2.45}$$

$$Q_M(a, b) = \frac{1}{a^{M-1}} \int_b^{+\infty} t^M \exp\left(-\frac{t^2 + a^2}{2}\right) I_{M-1}(at) dt \tag{2.46}$$

Where $I_M(t)$ is the Bessel function of the first kind of order M.

2.2.4 Other detection techniques

Even though, ED, ACD and CSD are well known in the Spectrum Sensing Context, other algorithms are used, such as Waveform Detector (WFD), Eigenvalue-based Detector (EVD), Goodness of Fit Detector (GFD), Kurtosis Detector (KD) *etc.*

Waveform Detector :
WFD is an optimal method [19, 52, 53] in terms of detection performance. WFD keeps good performance even at a very low SNR. Hence, the SU should know the waveform of PU signal or pilot [19, 28, 53], and correlate it with the received signal. The pilot is a simple signal transmitted by the PU as a signature signal. The optimal performance of WFD is reached with the perfect synchronization in time and frequency between SU and PU.
However, the application of WFD in a general or blind CR context is very limited since CR would deal with a great variety of signals in its radio environment.

Eigenvalue-based Detector :
Unlike WFD, Eigenvalue-based Detector (EVD) do not require any prior knowledge on the PU signal. Contrary to ED, EVD does not need an estimation of the noise variance. This fact makes EVD non vulnerable to the NU. EVD is based on finding a

set $\{\beta_i\}_{i=1,\ldots,m}$; $(m \leq N_s)$ of Eigenvalues of the $m \times m$ samples Covariance C_{yy} matrix of the received signal.

$$C_{yy} = \begin{bmatrix} E[y(n)y^*(n)] & E[y(n)y^*(n-1)] & \ldots & E[y(n)y^*(n-m)] \\ E[y(n-1)y^*(n)] & E[y(n-1)y^*(n-1)] & \ldots & E[y(n-1)y^*(n)] \\ \vdots & \vdots & \ldots & \vdots \\ E[y(n-m)y^*(n)]\ldots & E[y(n-)y^*(n-1)] & \ldots & E[y(n-m)y^*(n-m)] \end{bmatrix} \tag{2.47}$$

For the case of white noise, C_{yy} will result in diagonal matrix under H_0. Then, the eigenvalues C_{yy} are equal to noise variance [48]

$$\beta_1 = \beta_2 = ... = \beta_m = \sigma_w^2 \tag{2.48}$$

Under H_1, and thanks to the independence between $s(n)$ and $w(n)$, C_{yy} becomes the sum of C_{ss} and C_{ww}, the covariance matrices of $s(n)$ and $w(n)$ respectively.

$$\begin{aligned} \beta_1 &= \beta_1^s + \sigma_w^2 \\ \beta_2 &= \beta_2^s + \sigma_w^2 \\ &\cdot \\ &\cdot \\ &\cdot \\ \beta_m &= \beta_m^s + \sigma_w^2 \end{aligned} \tag{2.49}$$

where $\beta_1^s \geq \beta_2^s ... \geq \beta_m^s$. Using equation (2.49), many EVD algorithms have been proposed. Herein, we present the two well known EVD detectors:

1. Maximum-Minimum Eigenvalue (MME): This algorithm finds the Maximum β_{max} and the minimum β_{min} of the Eigenvalues of C_{yy}, and then compares the ratio β_{max}/β_{min} to a threshold to made a decision on the PU status.

2. Energy with Minimum Eigenvalue (EME): Here the Spectrum Sensing is performed by comparing the ratio, T_{ED}/β_{min}, of the energy of the received signal (equation (2.13)) over the minimum eigenvalue β_{min} to a threshold.

Note that other Eigenvalues-based Spectrum Sensing algorithms are proposed based on the distribution of the eigenvalues of C_{yy}. On the other hand, EVD algorithms can be applied on a multi-antenna system, where the spatial covariance matrix is evaluated instead of time covariance matrix. MME and EME can be applied on such scenario if the noise is spatially white.

Goodness of Fit Detector :

The detection can be done based on comparing the Cumulative Density Function (CDF) of the received signal's samples to (known or a priori estimated) CDF of the noise [49]. The test statistic of the Goodness of Fit (GoF) detector is the sum of the differences between the two curves of the two CDFs or the maximum of these differences.

For AWGN complex and circular noise $w(n)$, the modulus $||w(n)||^2$ follows a χ^2 distribution. In [50], a Likelihood Ratio (LLR) GoF test based on χ^2 (LLR χ^2) is proposed. The associated Test Statistic to be found T_{GoF} [49] can be derived by.

$$T_{GoF} = -\sum_{n=1}^{N} \left(\frac{ln(F_0(y(n)))}{N-n+1/2} + \frac{ln(1-F_0(y(n)))}{n-1/2} \right) \tag{2.50}$$

where F_0 is the CDF of the χ^2 distribution. If T_{GoF} is greater than the predefined threshold then a non-Gaussian signal is detected.

This algorithm faces a problem when the noise's CDF and the PU signal's CDF have the same nature, or when they are similar. However, this type of detection has gained a lot of attention due to its blindness since it does not require any prior information on the PU signal.

Kurtosis Detector :

Kurtosis Detector (KD) is sensitive to the Gaussian aspect of the noise. In fact, the kurtosis of the Gaussian signals is zero [67]. Applying the kurtosis metric on the received signal will result in non zero value only if a non Gaussian signal such as PU's signal exists [51]. Note that if the PU signal is also Gaussian, KD becomes inapplicable. Such scenario can occur when the PU signal is an OFDM due to the FFT operation that performs the sum of independent samples which leads to a distribution closed to Gaussian according to CLT.

2.3 Performance Evaluation

2.3.1 Receiver Operating Characteristic

Receiver Operating Characteristic (ROC) presents the variation of the probability of Detection p_d with respect to the probability of False Alarm p_{fa}. It is worth mentioning that p_d reaches '1' as p_{fa} increases as well to '1' [58]. The main challenge of any detection technique is to reach a high p_d by keeping p_{fa} low. This can be achieved by setting a reliable threshold that satisfies the detection requirement (target p_d and p_{fa}) in terms of the number of received samples (observation time) and the SNR. ROC curves can be considered as an essential criterion to evaluate the Spectrum Sensing performance in detection sense.

A comparison of various algorithms is presented based on the ROC curves. ED, CSD and ACD will be compared, when they are applied on 16-QAM modulated signal, oversampled by $N_s = 4$ samples per symbol (sps). The noise is assumed to be Additive Complex Circular Symmetric Gaussian Noise (CCSGN). As shown in figure 2.5, ACD presents

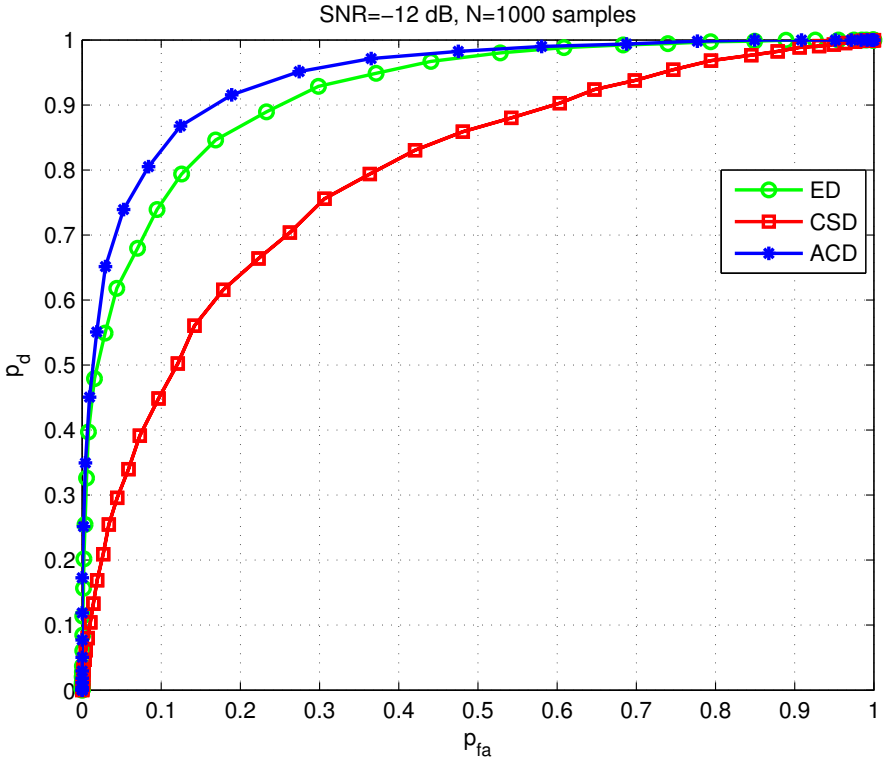


FIGURE 2.5: ROC curves for ED, CSD and ACD

the more reliable performance with higher ROC curve comparing to the other detectors. In figure (2.6), p_d is evaluated in terms of SNR for $p_{fa} = 0.1$, $N_s = 8$ sps and $N = 1000$ samples. ACD outperforms ED and CSD since it reaches higher value of p_d for a fixed value of p_{fa}. Note that the performance of ACD increases with N_s [68]. In addition, the

performance of ED is presented here for a perfect estimation of the noise variance, so that Noise Uncertainty is not taken into account (see section (2.3.4)).

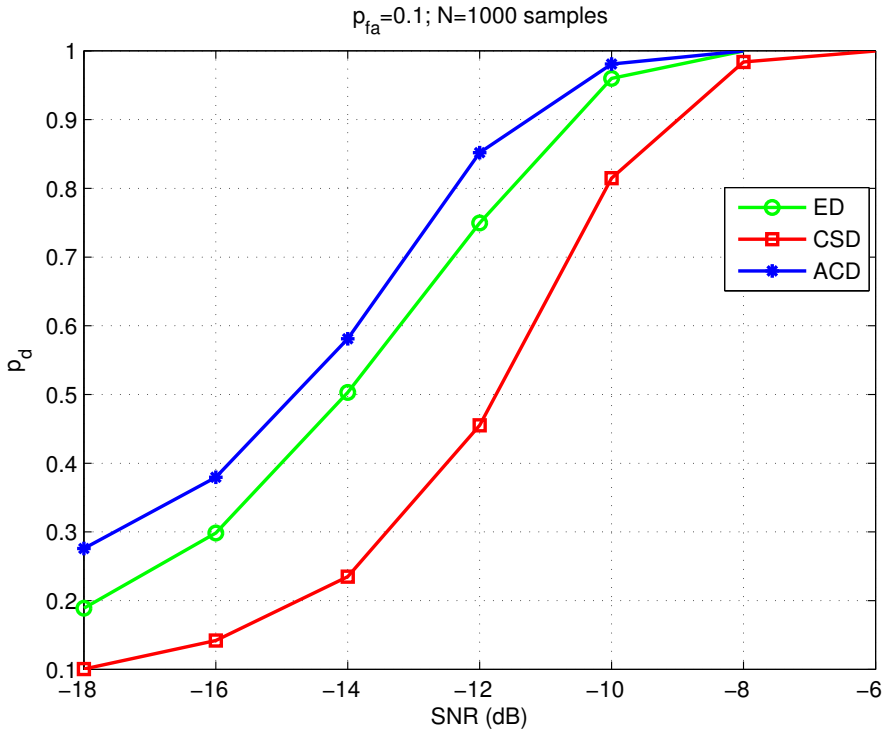


FIGURE 2.6: Block-Diagram of the Energy Detector

2.3.2 Sensing Time

To reach the detection requirement (*i.e.* target (p_d, p_{fa})), the number of received samples (Sensing time) is considered as a main challenge. Using a long sensing time affects the data rate of SU which should stop transmitting during the Spectrum Sensing. On the other hand, an algorithm with a short sensing time is acceptable only if it is robust with respect to low SNR. In general, the performance of the detectors is enhanced with the increasing N. A good detector should present an efficient performance with a short observation time. For a fixed target $(p_{fa} = 0.1, p_d = 0.9)$, figure (2.7) presents the variation of the SNR in terms of the number of samples. The PU signal is 16-QAM with $N_s = 3$ sps. The SNR decreases with the increasing of N for all the tested algorithms. On the other hand, ED shows the best performance with the lower SNR.

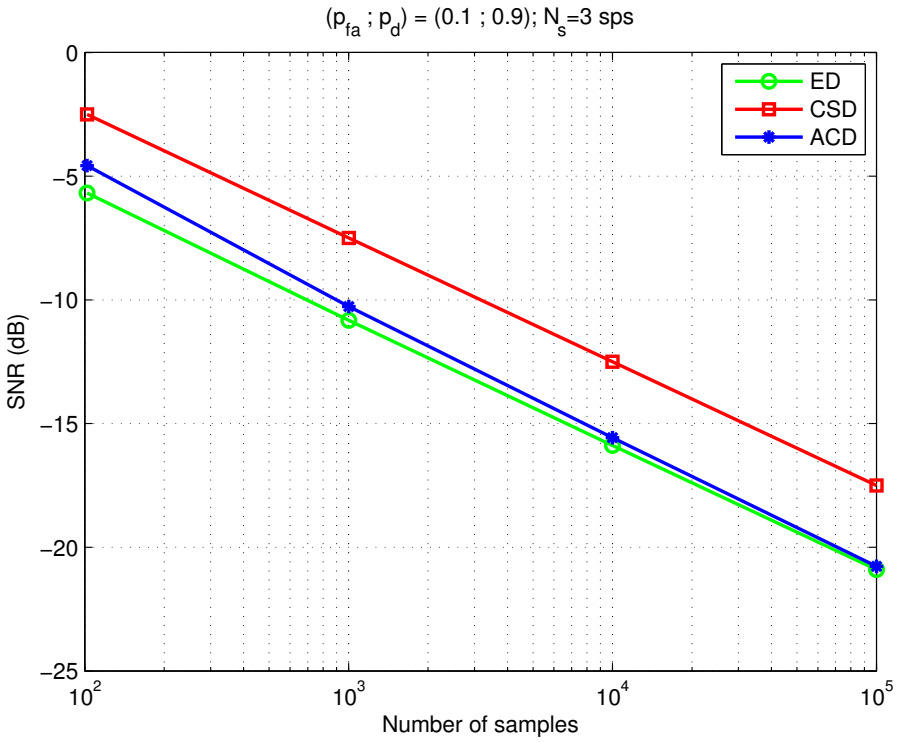


FIGURE 2.7: The minimum SNR required to reach $(p_{fa}; p_d) = (0.1; 09)$ in terms of the number of samples

2.3.3 Computation Complexity

The computational complexity plays an essential role in the selection of a suitable Spectrum Sensing algorithm. High complexity requires high power consumption and complicated hardware circuitry, which makes the Spectrum Sensing process expensive for a CR.

The computational complexity of ED (C_{ED}) can be measured according to equation (2.13): N multiplication operations are required to evaluate $|y(n)|^2$ and $N-1$ addition operations are required to perform the sum of N terms of $|y(n)|^2$. Totally, $2N-1$ computational operations are required to perform the energy detection.

$$C_{ED} = 2N - 1 \tag{2.51}$$

The complexity of CSD is given in [69]:

$$C_{CSD} = (N_s-1)N(L+1) + 4(N_s-1)L^2 + 8(N_s-1)^3 + 6(N_s-1)^2 + 2(N_s-1)) \tag{2.52}$$

According to equation (2.28), for a unit weighting function ($c_m = 1$), ACD performs for each lag $2N-1$ computational operations similarly to ED. This process is repeated for each lag before doing the summation operation of $\hat{r}_{yy}(m)$. For a linearly modulated

signal, with an oversampling factor N_s, the number of the useful lags is $N_s - 1$ ($m = 1, ..., N_s - 1$), the complexity of ACD becomes as follows:

$$\begin{aligned} C_{ACD} &= (N_s - 1)(2N - 1) + N_s - 2 \\ &= 2(N_s - 1)N - 1 \end{aligned} \tag{2.53}$$

The number of the required samples is related to the detection requirement as shown in figure (2.7). This number of samples is changed from one algorithm to another. Accordingly, the computational complexity of ED, CSD and ACD is measured in terms of the number of samples required to reach ($p_{fa} = 0.1; p_d = 0.9$). The results shown in figure (2.8) are found according to the results shown in figure (2.7). ED is still the simplest algorithm, whereas CSD is the most complicated one.

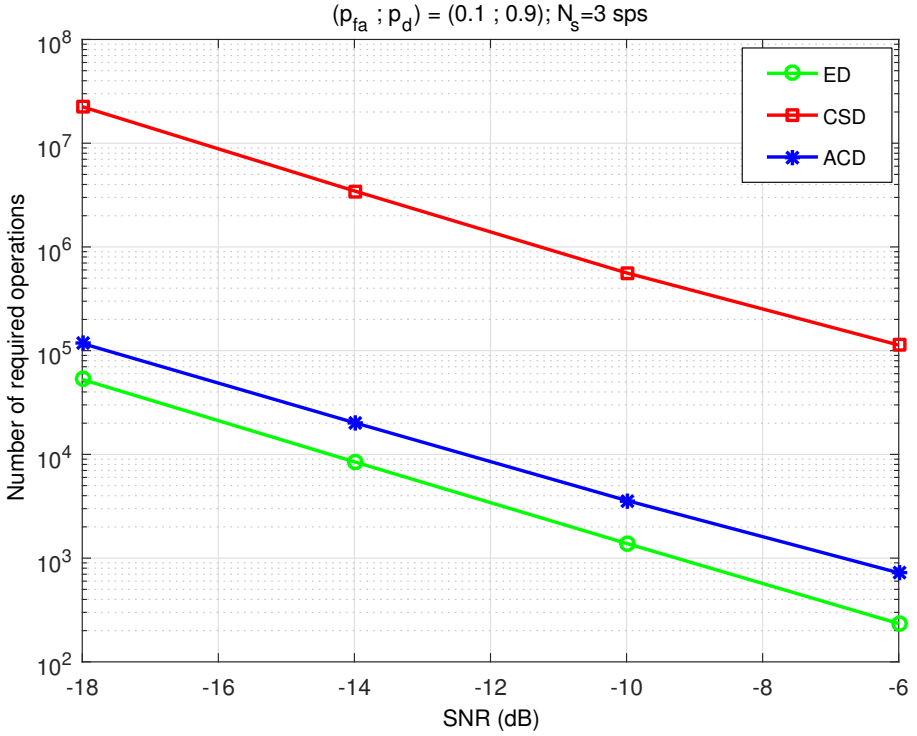


FIGURE 2.8: The number of operations required to reach $(p_{fa}; p_d) = (0.1; 09)$

2.3.4 Noise Uncertainty Impact

A major problem affecting the Spectrum Sensing algorithms is the Noise Uncertainty. Because of several limitations (such as thermal noise, ambient interference, receivers non-linearity, *etc*), the noise variance cannot be perfectly estimated [70]. This fact leads to the so-called SNR-wall phenomenon, where an accurate decision on the channel status cannot be reached even if the observation time becomes very large [70].

The estimated noise variance $\hat{\sigma}_w^2$ can be expressed as being bounded as follows:

$$\hat{\sigma}_w^2 \in \left[\frac{1}{\kappa}\sigma_w^2; \kappa\sigma_w^2\right] \tag{2.54}$$

σ_w^2 is the nominal value of the noise variance and κ stands for the NU factor with $\kappa \geq 1$. The distribution of $\hat{\sigma}_w^2$, $f_{\hat{\sigma}_w^2}(\hat{\sigma_w^2})$, is assumed to be uniform in a logarithmic scale [66].

$$f_{\hat{\varepsilon}}(\hat{\varepsilon}) = \begin{cases} \frac{1}{2\rho}, & \varepsilon - \rho \leq \hat{\varepsilon} \leq \varepsilon + \rho \\ 0, & elsewhere \end{cases} \tag{2.55}$$

Where $\varepsilon = 10\log_{10}(\sigma_w^2)$, $\hat{\varepsilon} = 10\log_{10}(\hat{\sigma}_w^2)$ and $\rho = 10\log_{10}(\kappa)$.

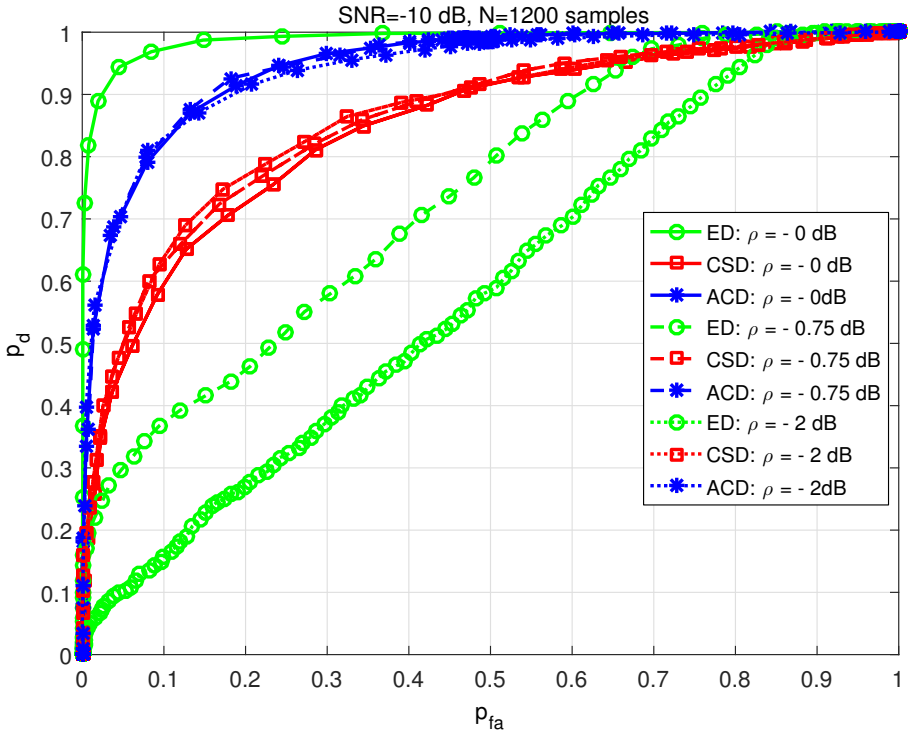


FIGURE 2.9: ROC curve for ED, CSD and ACD for various values of the Noise Uncertainty (ρ)

For the studied detectors in this manuscript, ED is affected by NU since its p_{fa} depends on the noise variance. It was shown in [70] that the number of samples required to meet a target ($p_{fa} < 0.5; p_d > 0.5$) approaches infinity as the SNR approaches ($\kappa - 1/\kappa$) which is called SNR-Wall. According to figure (2.9), the performance of ED is highly degraded when NU increases, while CSD and ACD keep the same performance for the different values of NU. In this simulation, PU signal is assumed to be 16-QAM with $N_s = 2$ sps. It is worth mentioning that for $\rho = 0$ dB, ED outperforms ACD unlike figure (2.5) when N_s was 4 sps. This is because ACD is highly affected by the oversampling rate.

TABLE 2.1: Comparison of different Spectrum Sensing Algorithms

Algorithm	PU signal requirement	Limitations	Complexity
ED	Blind	Sensitive to Noise Uncertainty	Low $(2N-1)$
ACD	Blind	Poor performance for low oversampling rate	Low $(2(N_s-1)N)$
CSD	Cyclic Frequency	Long Sensing time	High $\Big((N_s-1)N(L+1)+4(N_s-1)L^2+8(N_s-1)^3+6(N_s-1)^2+2(N_s-1)\Big)$

Table (2.1) shows a briefed comparison among ED, CSD and ACD. This comparison is done with respect to the pre-requirement, the limitation and the complexity. ED suffers from the NU problem, whereas ACD is only applicable on oversampled signal and requires a white noise in order to distinguish between signal-plus-noise case and noise-only case. CSD overcomes that two problems (NU and oversampling aspect), but it needs the knowledge of the cyclic frequency of the PU signal and it suffers from the computational complexity (for GLRT algorithm [44]).

2.4 Cooperative Spectrum Sensing

Many factors (such as channel fading, shadowing, *etc*) can lead to the hidden PU phenomenon, which means that the SU becomes incapable to discover the PU activity. Using Multi-Antenna System (MAS) and spatial diversity, Cooperative Spectrum Sensing (CSS) has been proposed in order to solve this problem [19, 20]. In CSS, a Fusion Center (FC) combines the data of the cooperating antennas (Which can be SUs). Two strategies are admitted to make the final decision on the PU status [20].

2.4.1 Hard Combining Scheme

Hard Combining Scheme (HCS) is the strategy of combining the decisions of the cooperative SUs. Each SU makes a decision based on comparing its measured Test Statistic

to a pre-defined threshold. All the decisions of the SUs are sent to the Fusion Center in order to reach a final decision based on a logic rule (such as Or, And or the majority rule).

1. OR-rule: the fusion center makes the decision by ORing the received decisions, so that it is enough that one SU decides that the PU is active to made a final decision that the channel is occupied. This fact leads to increase the detection rate but at cost of increasing the false alarm rate.

2. AND-rule: FC decides that the channel is occupied if all the received decisions are '1'. This rule decreases the false alarm rate but by decreasing the detection rate.

3. Majority Rule: This rule is based on a voting process, where FC respects the decision of the majority of the cooperative SUs.

2.4.2 Soft Combining Scheme

Instead of sending their decisions on the channel opportunity, each cooperative SU sends its own measured TS in Soft Combining Scheme (SCS) to FC which performs a linear combination of all received test statistics and compares the result to a threshold. In SCS, the cooperative SU needs several bits to transmit their data to FC.

2.4.3 Performance testing of Cooperative Spectrum Sensing

To show the performance of Cooperative Spectrum Sensing, HCS and SCS are tested by simulation using ED. 16-QAM modulated signal is used, with $N = 1000$ samples and $N_a = 5$ antennas. The channel between the PU base-station and the SUs is assumed to be Rayleigh flat-fading. The majority rule results in "one" if 3 out of 5 decisions are "ones", else it decides "zero" (PU is absent).

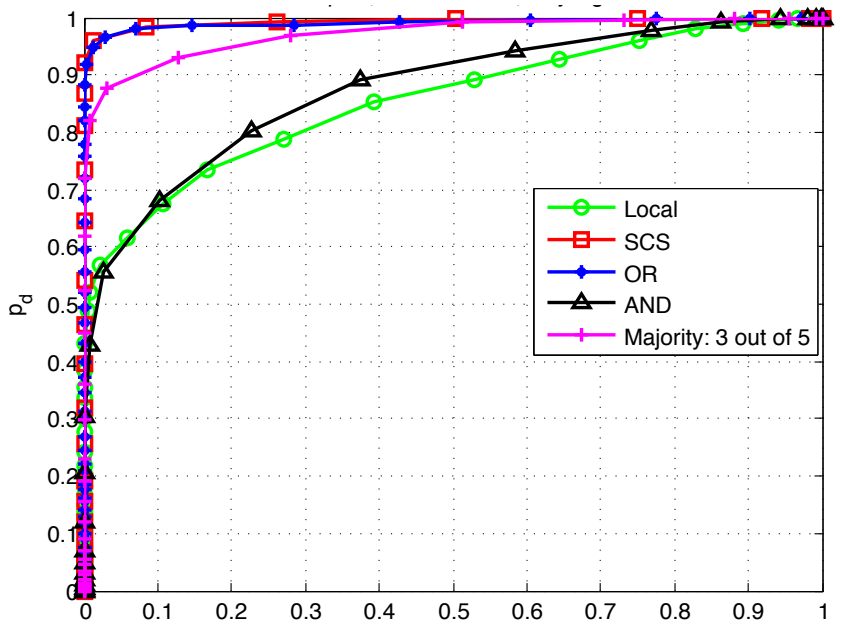


FIGURE 2.10: The ROC curve of ED for different CSS strategies

As shown in figure 2.10, CSS using different schemes and rules enhance the Spectrum Sensing performance. SCS outperforms HCS for its different rules. On the other hand, OR rule is better than AND and Majority rules.

2.5 Spectrum Sensing based on Distributed Antennas

Some detectors need Multi-Antenna System (MAS) in order to be applied. In [71, 72], a Spectrum Sensing technique based on Blind Source Separation has been proposed. The BSS techniques have been introduced in CR in order to avoid the silence period during the Spectrum Sensing [71–73] (make the CR Full-Duplex). BSS consists in the separation of N_{sig} independent sources basing on N_a observations (Generally $N_{sig} \leq N_a$) [74]. Once the separation is achieved, a test of kurtosis can be carried out on the separated signal in order to make a decision on the presence of PU [71, 72].

Other algorithm is proposed on the correlation of the received signal on MAS [75]. When the noise is assumed to be spatially uncorrelated and the antennas of MAS are synchronized, the correlation of the observed signals at the receiving antennas will be zero when the PU signal is absent. This correlation will be non zero when the PU signal exists. This fact leads to diagnose the channel status.

In addition, the Canonical Correlation Significance Test (CCST)-based Cyclo-stationary detector was proposed initially to deal with MAS [66, 76]. This algorithm tests the

common cyclo-staionarity of the received signals at the receiving antennas. When the PU signal is absent, there is no common cyclo-stationary features because the channel is only occupied by noise. On the other hand, common cyclo-stationary features will be found when PU is active, since on each receiving antenna a faded copy of the PU signal will be received. Note that we extend CCST to deal with a Single Antenna System, this study is presented and it was published in [77].

In [78], we proposed a new Spectrum Sensing strategy base on MAS, leading to enhance the performance. This model proposes the use of the Principal Component Analysis (PCA) as a pre-processing step of the received signals on MAS. Such strategy leads to enhance the SNR of the PU signal, and consequently to ameliorate the Spectrum Sensing performance comparing to SAS.

2.6 Conclusion

In this chapter, we present an overview on the main Spectrum Sensing algorithms used in the literature. Moreover, a comparison among the most frequently used ones (such as Energy Detector, Cyclo-stationary Detector and Autocorrelation Detector) is presented. In addition, we addressed the cooperative Spectrum Sensing with its various techniques. We can conclude that ED is simple blind detector, but it suffers from the Noise-Uncertainty problem caused by the dependency of ED to the noise variance. ACD is independent from the noise variance but it requires a white noise and an oversampled PU signal. ACD's performance increases with the sampling rate. Similarly to ACD, CSD is independent from the noise variance, but can be applied on non-white noise. However, CSD has a high computational complexity.

Chapter 3

Cyclic Correlation Significance Test (CCST)

List of Acronyms

AWGN Additive White Gaussian Noise

CAF Cyclic-Autocorrelation Function

CCT Canonical Correlation Theory

CCST Cyclic Correlation Significance Test

CR Cognitive Radio

CSD Cyclo-Stationary Detector

CLT Central Limit Theorem

ED Energy Detector

GLRT Generalized Likelihood Ratio Test

MAS Multi-Antenna System

NU Noise Uncertainty

PU Primary User

ROC Receiving Operating Characteristics

SAS Single-Antenna System

SU Secondary User

TS Test Statistic

Cyclo-Stationarity Detection (CSD) serves as a main research domain in Spectrum Sensing, since this kind of detection shows its robustness against the low SNR and its independence to the noise variance, so that no Noise Uncertainty (NU) problem is occurred. Several CSD algorithms are proposed in the literature. One of them is based on Canonical Correlation Theory (CCT) [79] and it was called Cyclic Correlation Significance Test (CCST), where a Multi-Antenna System (MAS) owing N_a receiving antennas, is used to perform the Spectrum Sensing, which shows its efficiency in MAS where the noise is spatially correlated or spatially colored. In the following, we present a brief review on the CCT and its application in signal detection, especially the application of CCST in Spectrum Sensing context, where a Cognitive Radio (CR) system of multi-antenna is required. The last condition makes the application of CCT in Spectrum Sensing limited only to CR of MAS. In order to overcome this limitation, we extend this CCST from MAS to Single-Antenna System (SAS), where the cyclic correlation existing in the PU signal is exploited. Moreover, our extended algorithm is applied in MAS where both Spatial and Time diversities are treated to diagnose the channel status.

3.1 System Model

The problem formulation on the presence/absence of the PU signal in CR of MAS is presented in a classic Bayesian detection problem as follows:

$$H_\eta : y_i(n) = \eta h_i s(n) + w_i(n) \tag{3.1}$$

Where $\eta \in \{0; 1\}$. H_0 stands for the case where PU is absent, whereas under H_1 PU is transmitting. $y_i(n)$ is a $1 \times N$ vector representing the observation at the ith SU receiving antenna, N stands for the total number of received samples, $s(n)$ is the PU signal, $w_i(n)$ is the noise at the ith SU receiving antenna and assumed to be stationary zero mean White Gaussian Noise (AWGN), with a variance $\sigma^2_{w_i}$ and the channel gain, h_i, between the PU base station and the ith SU receiving antenna is assumed to be constant during the Spectrum Sensing period.

3.2 Spectrum Sensing based on CCST

The Canonical Correlation Theory (CCT) aims at finding common factors between two sets of data, $\mathbf{y}(n)$ and $\mathbf{z}(n)$. The number of these common factors is equal to the rank of the following matrix [66, 76, 80]:

$$\mathbf{C} = \mathbf{C}_{\mathbf{yy}}^{-1}\mathbf{C}_{\mathbf{yz}}\mathbf{C}_{\mathbf{zz}}^{-1}\mathbf{C}_{\mathbf{zy}} \tag{3.2}$$

Where $\mathbf{C}_{\mathbf{yz}} = \mathrm{Cov}[\mathbf{y}(n), \mathbf{z}(n)]$ and can be estimated by $\hat{C}_{\mathbf{yz}}$

$$\hat{\mathbf{C}}_{\mathbf{yz}} = \frac{1}{N}\sum_{n=1}^{N}\mathbf{y}(n)\mathbf{z}^{H}(n) \tag{3.3}$$

Where $\mathbf{z}^{H}(n)$ is the Hermitian transpose of $\mathbf{z}(n)$.

In the signal detection context, the number of common factors is, in fact, the number of the common signals existing in the two data sets $\mathbf{y}(n)$ and $\mathbf{z}(n)$. In fact, data set are a vector of observations of the received signals at several receiving antennas [66, 80].

$$\mathbf{z}(n) = [z_1(n), z_2(n), ..., z_{N_{a_1}}(n)]^T \tag{3.4}$$

$$\mathbf{y}(n) = [y_1(n), y_2(n), ..., y_{N_{a_2}}(n)]^T \tag{3.5}$$

where $y_i(n)$ (resp. $z_i(n)$) is the signal received at the ith receiving antenna in a set of N_{a_1} (resp. N_{a_2}) antennas.
In [80], CCT is used to determine the number of signals existing in a Band of Interest. Being using MAS, the proposed algorithm divides the signals received from N_a antennas into two groups, N_{a_1} and N_{a_2}, on which CCT is applied to test the significance correlation between these two groups. This correlation leads to extract the number of signals.

In [66] and [76], CCT is applied on the received signals in MAS in order to extract the number of signals having common cyclic features. Instead of dividing the observations on N_a antennas into two subsets as in classical CCT, the algorithm proposed in [76] and [66] aims at identifying the common factors between $\mathbf{y}(n)$ and a shifted version of $\mathbf{y}(n)$ in time and frequency $\mathbf{z}(n, m, \alpha) = \mathbf{y}(n-m)\exp(j2\pi\alpha n)$, where α is a known cyclic frequency of $s(n)$ and the lag m is chosen off-line in order to maximize $\sum_{n=1}^{N} s(n)s^*(n-m)e^{-j2\pi\alpha n}$ at a non-zero cyclic frequency α, where $s^*(n)$ stands for the conjugate of $s(n)$. This algorithm was called *Cylic Correlation Significance Test* (CCST). It is worth mentioning that the number of common factors in this case is the number of signals having a cyclic

frequency α [76].
In this case, the cyclic-covariance matrix can be estimated by $\hat{\mathbf{R}}_{\mathbf{yz}}$ as follows:

$$\begin{aligned}\hat{\mathbf{R}}_{\mathbf{yz}} = \frac{1}{N}\sum_{n=1}^{N}\mathbf{y}(n)\mathbf{z}^H(n,m,\alpha)\\ \frac{1}{N}\sum_{n=1}^{N}\mathbf{y}(n)\mathbf{y}^H(n-m)\exp\left(-j2\pi\alpha n\right)\end{aligned} \tag{3.6}$$

For $\hat{\mathbf{R}}_{\mathbf{zy}}$, it is simple to show that it is equal to $\hat{\mathbf{R}}^H_{\mathbf{yz}}$. Regarding $\hat{\mathbf{R}}_{\mathbf{zz}}$, it is independent of α and it is equal to $\hat{\mathbf{R}}_{\mathbf{yy}}$ for a large N:

$$\begin{aligned}\hat{\mathbf{R}}_{\mathbf{zz}} &= \frac{1}{N}\sum_{n=1}^{N}\mathbf{y}(n-m)\exp\left(j2\pi\alpha n\right)\mathbf{y}^H(n-m)\exp\left(-j2\pi\alpha n\right)\\ &= \frac{1}{N}\sum_{n=1}^{N}\mathbf{y}(n-m)\mathbf{y}^H(n-m)\end{aligned} \tag{3.7}$$

Consequently, the CCST matrix $\hat{\mathbf{R}}$ is evaluated by:

$$\hat{\mathbf{R}} = \hat{\mathbf{R}}^{-1}_{\mathbf{yy}}\hat{\mathbf{R}}_{\mathbf{yz}}\hat{\mathbf{R}}^{-1}_{\mathbf{zz}}\hat{\mathbf{R}}^H_{\mathbf{yz}} \tag{3.8}$$

Note that when $N_a = 1$, $\hat{\mathbf{R}}_{\mathbf{yz}} = \frac{1}{N}\sum_{n=1}^{N} y_1(n)y_1^*(n-m)\exp\left(-j2\pi\alpha n\right) = \hat{R}_{y_1y_1}(\alpha,m)$, which is the Cyclic-Autocorrelation Function (CAF) of $y_1(n)$ (see equation (2.34)).
In addition, $\hat{\mathbf{R}}_{\mathbf{zz}} = \frac{1}{N}\sum_{n=1}^{N}|y_1(n-m)|^2 \simeq \hat{R}_{y_1y_1}(0,0)$ for a large N, where $\hat{R}_{y_1y_1}(0,0) = \frac{1}{N}\sum_{n=1}^{N}|y_1(n)|^2$ and it stands for the energy of $y_1(n)$ (similarly for $z_1(n) = y_1(n-m)\exp\left(j2\pi\alpha n\right)$). In this case, the CCST is found as follows:

$$\begin{aligned}\hat{\mathbf{R}} &= \hat{R}^{-1}_{y_1y_1}(0,0)\hat{R}_{y_1y_1}(\alpha,m)\hat{R}^{-1}_{y_1y_1}(0,0)\hat{R}^*_{y_1y_1}(\alpha,m))\\ &= \frac{1}{|\hat{R}_{y_1y_1}(0,0)|^2}|\hat{R}_{y_1y_1}(\alpha,m)|^2\end{aligned} \tag{3.9}$$

Equation (3.9) results in the classical test of cyclo-stationarity (see equation (2.37)).
However, for $N_a > 1$, $\hat{\mathbf{R}}_{\mathbf{yz}}$ is expressed by:

$$\hat{\mathbf{R}}_{\mathbf{yz}} = \begin{bmatrix} \hat{R}_{y_1y_1}(\alpha,m) & \hat{R}_{y_1y_2}(\alpha,m) & \dots & \hat{R}_{y_1y_{N_a}}(\alpha,m)\\ \hat{R}_{y_2y_1}(\alpha,m) & \hat{R}_{y_2y_2}(\alpha,m) & \dots & \hat{R}_{y_2y_{N_a}}(\alpha,m)\\ \vdots & \vdots & \dots & \vdots\\ \hat{R}_{y_{N_a}y_1}(\alpha,m)\dots & \hat{R}_{y_{N_a}y_2}(\alpha,m) & \dots & \hat{R}_{y_{N_a}y_{N_a}}(\alpha,m)\end{bmatrix} \tag{3.10}$$

In order to examine the presence of PU, CCST aims at finding the eigenvalues of the matrix $\hat{\mathbf{R}}$. The Test Statistic (TS) to be measured is evaluated as follows [66]

$$T_{CCST} = -N \log \left(\prod_{i=1}^{N_a} (1 - \beta_i) \right) \tag{3.11}$$

where $\{\beta_i\},\ 1 \leq i \leq N_a$ are the eigenvalues of $\hat{\mathbf{R}}$ and $1 \geq \beta_1 \geq \beta_2 \geq ...\beta_{N_a} \geq 0$. The eigenvalues are normalized ($i.e.\beta_i \leq 1$) due to existence of the inverse of the covariance matrices $\hat{\mathbf{R}}_{\mathbf{yy}}^{-1}$ and $\hat{\mathbf{R}}_{\mathbf{zz}}^{-1}$ in the expression of $\hat{\mathbf{R}}$.
Under H_0, where the received signals at the N_a antennas are only stationary noise, the matrix $\hat{\mathbf{R}}_{\mathbf{yz}} \simeq \mathbf{0}$ that result in $\beta_1 = \beta_2, ..., \beta_{N_a} = 0$. Consequently T_{CCST} becomes zero. In contrast, under H_1, $\hat{\mathbf{R}}_{\mathbf{yz}}$ is not a zero matrix due to the cyclic statistics of $s(n)$ leading T_{CCST} to have a non-zero value. Based on the above discussion, T_{CCST} stands for a distinguishing criterion to examine the channel availability. After calculating the eigenvalues of $\hat{\mathbf{R}}$ and evaluating T_{CCST}, the last one should be compared to a threshold in order to make a decision on the presence of PU signal.
The analytic study that presented in [66] proves the independence between detection threshold of CCST and the noise variance, this fact makes CCST non-vulnerable to NU problem.
However, according to the discussion above, the application of the CCST is limited to MAS to ensure the vector $\mathbf{y}(n)$. This issue makes CR less flexible when CCST is used for a local Spectrum Sensing, where SU should make its decision on the channel status individually. In our work, in order to keep CCST applicable even if CR of SAS is used, we develop it under a situation where only one receiving antenna is used.

3.3 Proposed CCST for Single Antenna System (SAS)

In our Spectrum Sensing context, under H_0 the received signal is a stationary noise that does not exhibit any cyclostationarity; whereas under H_1, we should have only one PU *Cyclo-stationary* signal. Our developed algorithm is based on the time cyclic-correlation of the single received signal, instead of the spatial cyclic-correlation. In other terms, we apply CCST to discover the cyclo-stationarity based on time diversity instead of spatial diversity. Later on, MAS is used to exploit both spatial and time diversities. The received signal in SAS under H_0 and H_1 is presented as follows:

$$\begin{cases} H_0 : y_1(n) = w_1(n) \\ H_1 : y_1(n) = h_1 s(n) + w_1(n) \end{cases} \tag{3.12}$$

Let us define the vector V containing the lag values:

$$V = [m_1, m_2, ..., m_P] \tag{3.13}$$

Where P stands for number of used lags, which are chosen off-line in such a way $\sum_{n=1}^{N} s(n-m_p)s^*(n-m_k)e^{-j2\pi\alpha n} \neq 0, \forall\ m_p, m_k \in V$.
A vector of shifted signals, $\mathbf{r}_1(n, [m_1; m_k])$, is defined as follows:

$$\mathbf{r}_1(n, [m_1; m_{k_1}]) = \Big[y_1(n-m_1),\ y_1(n-m_2),\ \ldots\ y_1(n-m_{k_1})\Big]^T \tag{3.14}$$

Where $1 < k_1 \leq P$. The CCST will be estimated based on $\mathbf{r}_1(n, [m_1; m_{k_1}])$ and $\mathbf{q}_1(n, [m_1; m_{k_2}], \alpha)$ where

$$\mathbf{q}_1(n, [m_1; m_{k_2}], \alpha) = \mathbf{r}_1(n, [m_1; m_{k_2}]) \exp(j2\pi\alpha n),\ \forall\ k_1, k_2 \in [1; P] \tag{3.15}$$

with [80]:

$$\min(k_1; k_2) > l \tag{3.16}$$

where l is the number of signals to be detected. In the rest of this chapter, we assume that $k_1 \geq k_2 > 1$.
The new proposed contribution serves at detecting the common factors (signals) having the common cyclic features between $\mathbf{r}_1(n, [m_1; m_{k_1}])$ and $\mathbf{q}_1(n, [m_1; m_{k_2}], \alpha)$ using CCST. When $y_1(n)$ not exhibit any cyclo-stationary features, then its shifted versions do not have any common cyclic factors. In contrast, when $y(n)$ is cyclo-stationary, CCST should confirm the presence of the existing common factors by means of the matrix $\hat{R}_{SAS}$:

$$\hat{\mathbf{R}}_{SAS} = \hat{\mathbf{R}}^{-1}_{\mathbf{r}_1\mathbf{r}_1} \hat{\mathbf{R}}_{\mathbf{r}_1\mathbf{q}_1} \hat{\mathbf{R}}^{-1}_{\mathbf{q}_1\mathbf{q}_1} \hat{\mathbf{R}}_{\mathbf{q}_1\mathbf{r}_1} \tag{3.17}$$

where $\hat{\mathbf{R}}_{\mathbf{r}_1\mathbf{q}_1}$, $\hat{\mathbf{R}}_{\mathbf{q}_1\mathbf{r}_1}$, $\hat{\mathbf{R}}_{\mathbf{r}_1\mathbf{r}_1}$ and $\hat{\mathbf{R}}_{\mathbf{q}_1\mathbf{q}_1}$ are estimated as presented in (3.6). $\hat{\mathbf{R}}_{\mathbf{r}_1\mathbf{q}_1}$ and $\hat{\mathbf{R}}_{\mathbf{q}_1\mathbf{r}_1}$ represents the matrices that show the cyclostationarity based on time diversity since they evaluate the cyclostationarity between the received signal and its shifted versions.
Under H_0, the cyclic autocorrelation matrix, $\hat{\mathbf{R}}^0_{\mathbf{r}_1\mathbf{q}_1}$, of the shifted versions of the noise is obtained as follows:

$$\hat{\mathbf{R}}^0_{\mathbf{r}_1\mathbf{q}_1} = \begin{bmatrix} \hat{R}_{ww}(\alpha, [m_1; m_1]) & \hat{R}_{ww}(\alpha, [m_1; m_2]) & \ldots & \hat{R}_{ww}(\alpha, [m_1; m_{k_2}]) \\ \hat{R}_{ww}(\alpha, [m_2; m_1]) & \hat{R}_{ww}(\alpha, [m_2; m_2]) & \ldots & \hat{R}_{ww}(\alpha, [m_2; m_{k2}]) \\ \vdots & \vdots & \ldots & \vdots \\ \hat{R}_{ww}(\alpha, [m_{k_1}, m_1]) \ldots & \hat{R}_{ww}(\alpha, [m_{k_1}; m_2]) & \ldots & \hat{R}_{ww}(\alpha, [m_{k_1}; m_{k_2}]) \end{bmatrix} \tag{3.18}$$

where $\hat{R}_{ww}(\alpha, [m_i; m_j])$ is defined by:

$$\hat{R}_{ww}(\alpha, [m_i; m_j]) = \frac{1}{N} \sum_{n=1}^{N} w_1(n - m_i) w_1^*(n - m_j) e^{-j2\pi\alpha n} \tag{3.19}$$

Since $w_1(n)$ is purely stationary and does not exhibit any cyclic correlation for all $\alpha \neq 0$, then $\hat{\mathbf{R}}^0_{\mathbf{r}_1\mathbf{q}_1} \simeq \mathbf{0}$. Therefore, CCST test results in zero common factors between $\mathbf{r}_1(n, [m_1; m_{k_2}])$ and $\mathbf{q}_1(n, [m_1; m_{k_2}], \alpha)$.

Under H_1, the cyclic autocorrelation matrix, $\hat{\mathbf{R}}^1_{\mathbf{r}_1\mathbf{q}_1}$, is presented as follows:

$$\hat{\mathbf{R}}^1_{\mathbf{r}_1\mathbf{q}_1}(\alpha) = \hat{R}_{ss}(\alpha) + \hat{R}_{sw}(\alpha) + \hat{R}_{ws}(\alpha) + \hat{R}^0_{rq}(\alpha) \tag{3.20}$$

where $\hat{R}_{ws}(\alpha)$ and $\hat{R}_{sw}(\alpha)$ are the cyclic autocorrelation matrices between the noise and the PU signal, and they should be equal to zero, and $\hat{R}_{ss}(\alpha)$ is defined as follows:

$$\hat{R}_{ss}(\alpha) = |h|^2 \begin{bmatrix} \hat{R}_{ss}(\alpha, [m_1; m_1]) & \hat{R}_{ss}(\alpha, [, [m_1; m_2]) & \dots & \hat{R}_{ss}(\alpha, [m_1; m_{k_2}]) \\ \hat{R}_{ss}(\alpha, [m_2; m_1]) & \hat{R}_{ss}(\alpha, [m_2; m_2]) & \dots & \hat{R}_{ss}(\alpha, [m_2; m_{k2}]) \\ \vdots & \vdots & \dots & \vdots \\ \hat{R}_{ss}(\alpha, [m_{k_1}, m_1]) \dots & \hat{R}_{ss}(\alpha, [m_{k_1}; m_2]) & \dots & \hat{R}_{ss}(\alpha, [m_{k_1}; m_{k_2}]) \end{bmatrix} \tag{3.21}$$

Where $\hat{R}_{ss}(\alpha, [m_i; m_j])$ is the estimated cyclic autocorrelation of $s(n)$ at two lags m_i and m_j and it can be found similarly to equation (3.19). $R_{ss}(\alpha)$ is a non-zero matrix thanks to the cyclic autocorrelation of $s(n)$ at the cyclic frequency α.

The channel status can be examined using (3.17) by estimating the number of the signals having a cyclic frequency α. Since one PU signal can be existing in the channel, the challenge becomes to differentiate between two cases: noise-only case or signal-plus-noise case.

The test statistic, T_{SAS}, that leads to determine the vacancy of the channel is defined as follows [80]:

$$T_{SAS} = -N \log \prod_{i=1}^{k_1} (1 - \beta_i^s) \tag{3.22}$$

Where $\{\beta_i^s\}$, $i = 1, 2, ..., N_a$ and $1 \geq \beta_1^s \geq \beta_2^s \geq ... \geq \beta_{N_a}^s$. According to [80], it is enough to put only the l greatest eigenvalues in equation (3.22), where l is the number of signals to be detected. In Spectrum Sensing context, if only one PU signal exists, then

the channel is considered as occupied, so that there no need to capture the total number of the PU signals. Therefore $l = 1$ is enough in equation (3.22). Subsequently, T_{SAS} becomes as follows:

$$T_{SAS} = -N \log(1 - \beta_1^s) \tag{3.23}$$

T_{SAS} will be compared to a certain threshold, λ, in order to examine an existing vacancy of the bandwidth.

$$T_{SAS} \underset{H_0}{\overset{H_1}{\gtrless}} \lambda \tag{3.24}$$

The following algorithm summarizes the steps followed to calculate T_{SAS} and to make a decision on the channel status.

Algorithm 1 Spectrum Sensing using CCST

1. Estimate the matrix $\hat{R}_{SAS}$ using (3.17)
2. Calculate the greatest eigenvalue of $\hat{R}_{SAS}$
3. Evaluate the test statistic T_{SAS} according to (3.23).
4. Make a decision on the channel opportunity by comparing T_{SAS} to a threshold λ

3.4 Proposed CCST on Multi-Antenna System (MAS)

In this section, we develop the detector CCST-S in order to be applied in the Multi-Antenna System (MAS). Let us denote by $\mathbf{X}(n, m)$ and $\mathbf{Y}(n, p, \alpha)$ the two following vectors respectively:

$$\mathbf{X}(n, [m_1; m_{k_1}]) = [\mathbf{r}_1(n, [m_1; m_{k_1}]), \mathbf{r}_2(n, [m_1; m_{k_1}]), ..., \mathbf{r}_{N_a}(n, [m_1; m_{k_1}])]^T \tag{3.25}$$

$$\mathbf{Y}(n, [m_1; m_{k_2}], \alpha) = [\mathbf{q}_1(n, [m_1; m_{k_2}], \alpha), \mathbf{q}_2(n, [m_1; m_{k_2}], \alpha), ..., \mathbf{q}_{N_a}(n, [m_1; m_{k_2}], \alpha)]^T \tag{3.26}$$

Where $\mathbf{r}_i(n, [m_1; m_{k_2}])$, $1 \leq i \leq N_a$, is the vector containing the shifted versions of the signal received at the ith antenna, and is defined according to (3.14), and $\mathbf{q}_i(n, [m_1; m_{k_2}], \alpha) = \mathbf{r}_i(n, [m_1; m_{k_2}])e^{j2\pi\alpha n}$, $1 \leq i \leq N_a$.

In order to find the number of cyclostationary signals with a cyclic frequency α in the two data sets $\mathbf{X}(n, [m_1; m_{k_1}])$ and $\mathbf{Y}(n, [m_1; m_{k_2}], \alpha)$, the CCST is applied:

$$\hat{\mathbf{R}}_{MAS} = \hat{\mathbf{R}}_{\mathbf{XX}}^{-1} \hat{\mathbf{R}}_{\mathbf{XY}} \hat{\mathbf{R}}_{\mathbf{YY}}^{-1} \hat{\mathbf{R}}_{\mathbf{YX}} \tag{3.27}$$

The test statistic evaluated to examine the channel is presented as follows:

$$T_{MAS} = -N \log(1 - \beta_1^m) \tag{3.28}$$

Where β_1^m is the greatest eigenvalue of $\hat{\mathbf{R}}_{MAS}$.
The advantage of this proposed detector with respect to the original one proposed in [66] is exploitation of both spatial and temporal diversities, while the detector of [66] is only based on the spatial diversity as the CCST is done over $\mathbf{X}(n, [0; 0])$ and $\mathbf{Y}(n, [m_1; m_1], \alpha)$.

3.5 Performance Evaluation

In this section, we examine the performance of our proposed detectors. The performance of CCST-S is compared to the GLRT cyclostationary detector of [44]. To show the robustness of CCST-S to the Noise Uncertainty (NU), simulations for several NU values are presented. The performance of CCST-M is compared with the CCST detector of [66] that we refer to it by CCST-D. Throughout the simulations, the PU signal is assumed to be down-converted 16-QAM modulated signal. The symbol duration is $1\mu s$ and the sampling frequency, F_s, is 8 MHz (*i.e.* $F_s = 8B$ where B is the bandwidth of the PU signal). A square-root raised cosine shape is used with a roll-off factor of 0.5. the channel between the PU base station and the ith SU receiver is modeled as flat-fading Rayleigh. The lag vector used in this simulation is $V_{sim} = [0, T_s, 2T_s, 3T_s, 4T_s, 5T_s, 6T_s, 7T_s]$ is assigned, where $T_s = \frac{1}{F_s}$.
The presented curves in the following simulations are obtained using intensive Monte-Carlo simulations with few thousands of iterations.

3.5.1 Single-Antenna System

In figure (3.1), the number of samples is 2000 and the lag vector length of $\mathbf{r}_1(n, [m_1; m_{k_1}])$ is $k_1 = 8$, whereas various values are assigned for the lag vector length, k_2, of $\mathbf{q}_1(n, [m_1; m_{k_2}], \alpha)$. It is worth mentioning that GLRT algorithm exploits all the shifted versions of the received signal, *i.e.* its lag vector is the same as V_{sim}. This figure shows the ROC curve which is the variation of the probability of detection (p_d) with respect to the probability of false alarm (p_{fa}). Our proposed algorithm outperforms the GLRT algorithm of [44], and its performance is enhanced by increasing the number of lags k_2.

In order to illustrate the performance of CCST-S with respect to the NU, figure (3.2) shows the ROC curves of the proposed algorithm and the Energy Detector (ED). As

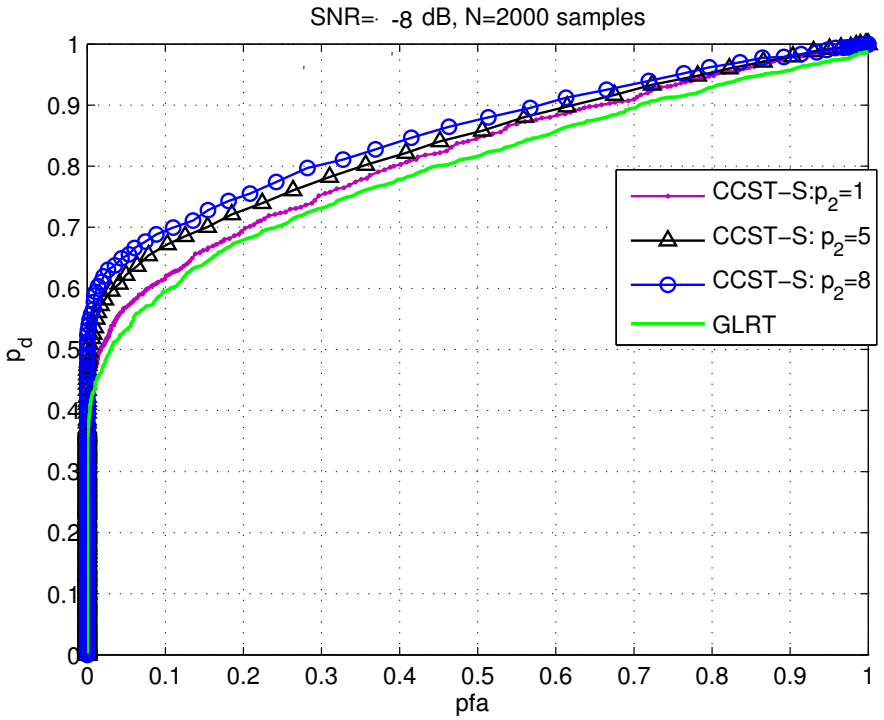


FIGURE 3.1: ROC curves of GLRT and CCST-S for various values of the length of the lag vector

shown in this figure, CCST-M is not affected by the NU for all the considered values, whereas ED exhibits an enormous performance loss with the increasing of NU. Note that for NU=0 dB ED outperforms CCST-T, this case refers to the ideal noise variance estimation. With NU=0.5 dB, CCST-M outperforms ED for low p_{fa} values, which are more interesting in real application At NU=1.5, the performance of ED is greatly deteriorated while CCST-M performance is not affected.

To show the time diversity effect on the performance of CCST-S, we examine this algorithm performance for various values of V_{sim}'s length of the two vectors $\mathbf{r}_1(n,[m_1;m_{k_1}])$ and $\mathbf{q}_1(n,[m_1;m_{k_2}],\alpha)$ which are assumed to have the same length (*i.e.* $k_1 = k_2 = p$). Our simulations are done under various SNR and a constant $p_{fa} = 0.1$. Figure (3.3) shows the interdependence between CCST-S and the time diversity, where p_d increases progressively when the length of the lag vector increases.

3.5.2 MAS

In this section we evaluate CCST-M for different types of noise: the spatially uncorrelated noise, the spatially correlated noise and the spatially colored but uncorrelated noise. Through the following simulations, $\mathbf{X}(n,[m_1;m_{k_1}])$ and $\mathbf{Y}(n,[m_1;m_{k_2}],\alpha)$ are assumed to have the same lag vector which is the same as V_{sim}.

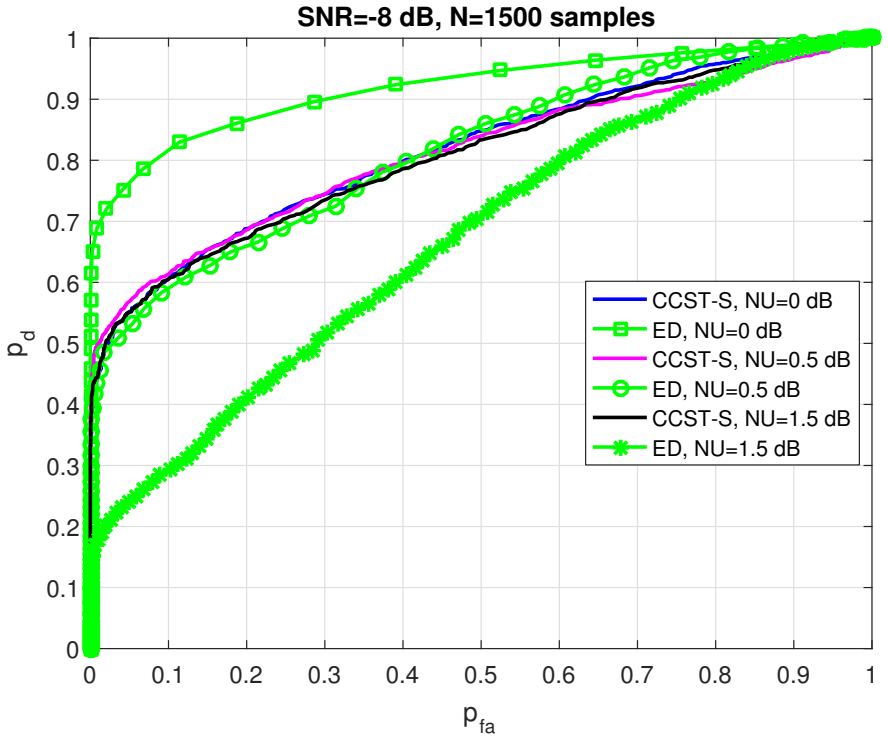


FIGURE 3.2: ROC curves of CCST-S for various values NU with a comparison with Energy Detector

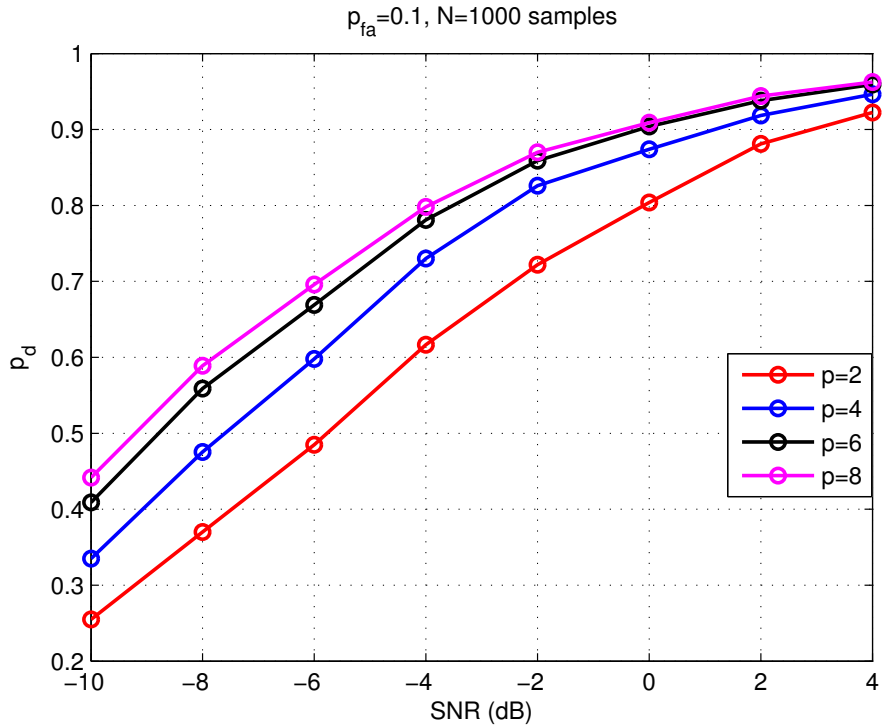


FIGURE 3.3: Time Diversity effect on the performance of CCST-S for $p_{fa} = 0.1$

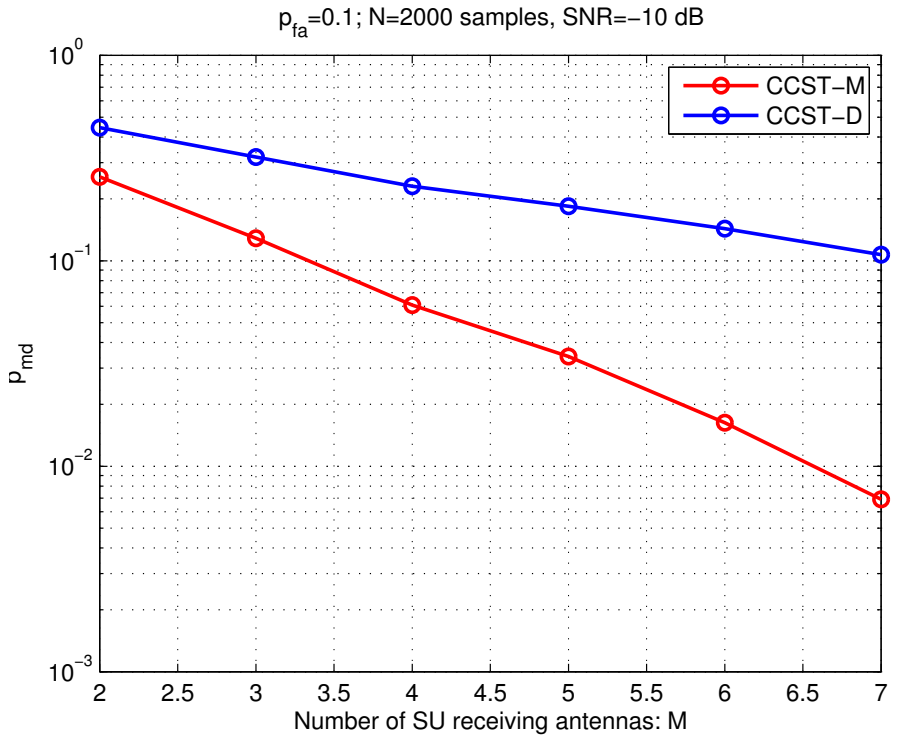


FIGURE 3.4: The probability of missed detection, $p_{md} = 1 - p_d$, for various number of receiving antennas (M) under $p_{fa} = 0.1$

3.5.2.1 Spatially Uncorrelated Noise

Figure (3.4) shows the probability of missed detection (p_{md}) for different number of receiving antennas, N_a. The number of received samples at each antenna is considered to be $N = 1000$ samples, the SNR is fixed to -10 dB and ($p_{fa} = 0.1$). For different different values of N_a, our algorithm achieves a lower p_{md} than the one of CCST-D. When N_a increases the gap between CCST-M and CCST-D becomes larger. For example, at $N_a = 5$ antennas, $p_{md} \simeq 0.2$ for CCST-D and $p_{md} \simeq 0.06$ for CCST-M. When $N_a = 7$, p_{md} becomes 0.1 approximatly for CCST-D while CCST-M reaches $p_{md} = 0.004$.

3.5.2.2 Spatially correlated Noise

Figure (3.5) shows the simulation results of CCST-M under spatially correlated noise. The correlation among the noise components at the SU receiving antennas is defined as follows:

$$E[w_i(n)w_j^*(n)] = \begin{cases} \sigma_w^2 & i = j \\ \sigma_w^2 \gamma^{|i-j|} & i \neq j \end{cases} \quad ; 1 \leq i, j \leq M; \tag{3.29}$$

Where γ is the correlation factor and $0 \leq \gamma \leq 1$.

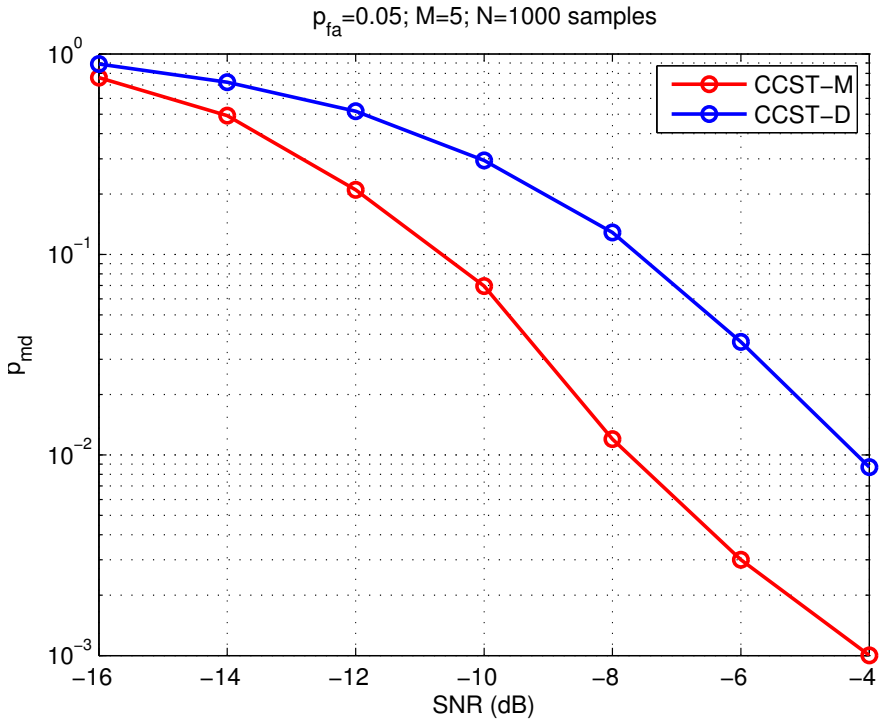


FIGURE 3.5: The probability of missed detection, $p_{md} = 1 - p_d$, for various SNR under $p_{fa} = 0.05$

In this simulation the number of SU receiving antennas is $N_a = 5$, the number of received samples at each antenna is $N = 1000$. According to figure (3.5), our algorithm considerably outperforms CCST-D by more than 2 dB. For example, our algorithm reaches $p_{md} = 0.5$ at SNR $= -14dB$, whereas CCST-D reaches this probability at SNR $= -12dB$.

3.5.2.3 Spatially Uncorrelated but colored Noise

In this simulation, we assume that the noise components on the N_a receiving antennas are spatially uncorrelated but colored. The average SNR is fixed to -12 dB, $N_a = 6$ antennas and $N = 2000$ samples. As shown in figure (3.6), CCST-M has a lower Complementary ROC curve than CCST-D. CCST-M achieve $p_{md} = 0.1$ for a $p_{fa} = 0.03$, whereas CCST-D achieve the same p_{md} for $p_{fa} = 0.5$.

3.6 conclusion

In this chapter, we presented a new algorithm based on the Cyclic Correlation Significance Test (CCST). The main objective of this work was to apply CCST for Single-Antenna System (SAS), instead of Multi-Antenna System (MAS) as previously proposed in the literature. To test the existence of the cyclostationarity, the time diversity of the

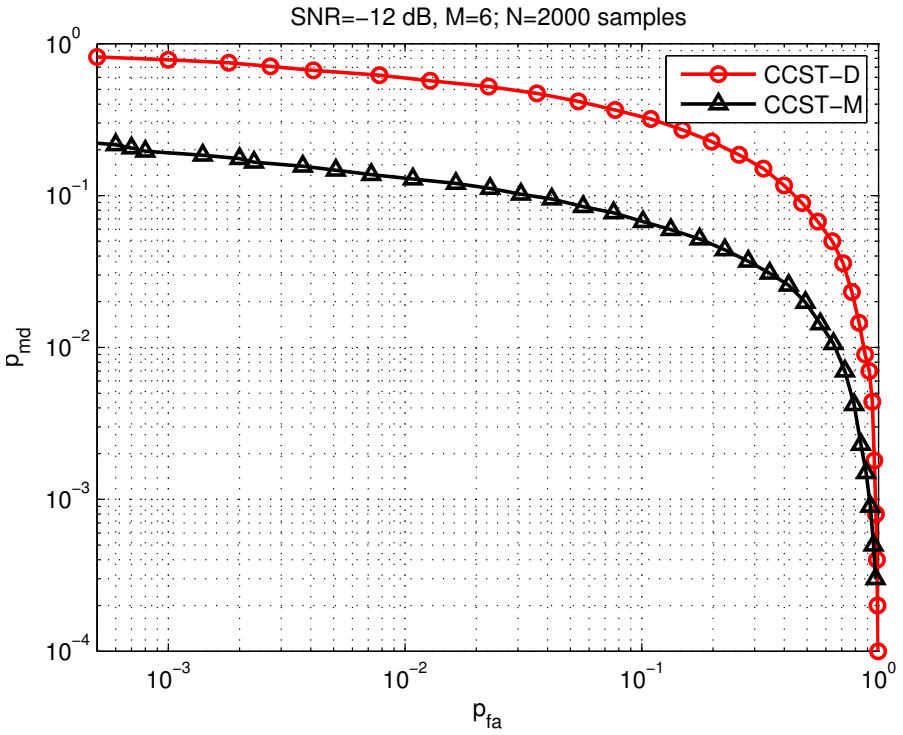


FIGURE 3.6: The probability of missed detection, $p_{md} = 1 - p_d$, for various SNR under $p_{fa} = 0.05$

received signal on a receiving antenna is manipulated. For Multi-Antenna System, both spatial and time diversities are exploited to detect the PU signal, this fact helped the Cognitive Radio to enhance the detection performance, which becomes more efficient than the case when only spatial or time diversity is manipulated. On the other hand, our simulations corroborate the effectiveness of our proposed algorithms which outperform other existing ones for various noise models under both SAS and MAS.

Chapter 4

Cumulative Power Spectral Density

List of Acronyms

ACD Autocorrelation Detector

CR Cognitive Radio

CSD Cyclo-Stationary Detector

CLT Central Limit Theorem

CPSD Cumulative Power Spectral Density

DFT Discrete Fourier Transform

ED Energy Detector

FFT Fast Fourier Transform

GLRT Generalized Likelihood Ratio Test

NLD Non-Linear Distortion

NU Noise Uncertainty

PSD Power Spectral Density

PU Primary User

ROC Receiving Operating Characteristics

SNR Signal-to-Noise Ratio

SU Secondary User

TS Test Statistic

In this chapter, new Spectrum Sensing algorithms based on the Cumulative Power Spectral Density (CPSD) is presented. The main idea is to diagnose the curved shape of the cumulative sum of the Power Spectral Density (PSD) of the received signal.
In fact, it is known that the PSD of a white noise is flat. However, PSD loses this property with an oversampled baseband PU signal (*i.e.* number of samples per symbol: $N_s \geq 2$). If the PU is absent, the cumulative sum of the received signal PSD should be close to a straight line. Whereas a curved shape is obtained when PU exists. Consequently, diagnosing the linearity of the Cumulative PSD (CPSD) leads to examine the channel status.
We propose here hard and soft cooperative schemes, where the spectrum is divided into two parts: At first, the negative frequency points are considered while the second part deals with the positive frequency points. Hence, two test statistics based on the Cumulative PSD of each part are calculated and combined according to the considered scheme. The False Alarm and Detection probabilities are evaluated analytically under Gaussian and Rayleigh fading channels. Our detectors are compared to the Energy Detector (ED) [55], Cyclostationary Detector (CSD) [47] and Autocorrellation Detector (ACD) [47]. Unlike ACD and CSD (especially Generalized Likelihood Ratio Test (GLRT)-based CSD based on the cyclostationarity that is being introduced by the oversampling [44]), our detectors present a better performance than ED, even with $N_s = 2$ samples per symbol (sps). We should notice that with $N_s = 2$ sps, ACD and CSD detectors provide a poor performance relatively to ED. Furthermore, our detectors are less sensitive than ED to the Noise Uncertainty. In particular, we demonstrate that our detectors can be independent from the noise variance. This case represents an important advantage in real applications.

This chapter is organized as follows. In section (4.1), the system model and the spectrum sensing hypothesis are presented. In section (4.2), PSD and its properties are given. Our proposed detectors based on the Cumulative sum of the PSD are discussed in section (4.3). Section (4.4) provides an analytic study on the statistical distributions of the test statistics as well as the calculus of the False Alarm and Detection probabilities. In section (4.5), the probability of detection over Rayleigh flat fading channel is provided. The numerical results of our detectors are presented in section (4.6). The effects of the noise uncertainty problem on our detectors are shown in section (4.7). To overcome the

Noise Uncertainty problem, this section presents modified versions of our detectors which are independent of the noise variance. At the end, a conclusion and perspective section of our work is provided[1][2].

4.1 System Model and Background

The base-band Primary User (PU) signal, $s(n)$ is assumed to be narrowband signal with a bandwidth B and a real even autocorrelation function. The considered model is a common as the one used in [45] and [46], where $s(n)$, is assumed to be complex-valued zero mean unknown deterministic signal. $s_p(n)$ and $s_q(n)$ are assumed to be independent with same autocorrelation function. In mathematical model, $s(n)$ is given by:

$$s(n) = \sum_k b_k g(n - k + N_s) = s_p(n) + j s_q(n) \tag{4.1}$$

b_k are the transmitted symbols, $g(n)$ is the shaping window, N_s satisfies the Nyquist criterion ($N_s = \frac{F_s}{B} \geq 2$ Samples per Symbol (sps), where F_s is the sampling frequency), and $s_p(n)$ and $s_q(n)$ are respectively the real and imaginary parts of $s(n)$.

As presented in Chapter 3, the presence/absence of PU can be presented as a binary hypothesis: Under H_0, the PU is absent; Whereas under H_1, PU exists.

$$\begin{cases} H_0 : y(n) = w(n) \\ H_1 : y(n) = hs(n) + w(n) \end{cases} \tag{4.2}$$

Where h is the complex channel gain. $w(n)$ is Gaussian with a mean 0 and a variance σ_w^2: $\mathcal{N}(0, \sigma_w^2)$. Further, $w(n) = w_p(n) + j w_q(n)$, is an $i.i.d$ complex circular symmetric random variable, $i.e.$ $E[w^2(n)] = 0$ and the real part, $w_p(n)$, and the imaginary part, $w_q(n)$, of $w(n)$ are independent Gaussian processes with equal variance.

$$E[w_p^2(n)] = E[w_q^2(n)] = \frac{\sigma_w^2}{2} \tag{4.3}$$

Where $\sigma_w^2 = E[|w(n)|^2]$ and $E[.]$ stands for the mathematical expectation. Without any loss of generality, we can assume that $s(n)$ is a unit power signal. In this case, the Signal to Noise Ratio (SNR), γ, is defined as follows:

$$\gamma = \frac{|h|^2}{\sigma_w^2} \tag{4.4}$$

[1] Part of this chapter was published in [81]

[2] The presented work of this chapter is under review [82]

4.2 Power Spectral density

The power spectral density (PSD) is the distribution of the signal on the frequency axis. The PSD $P_x(k)$, of a signal $x(n)$ is the Fourier Transform of its autocorrelation function $r_{xx}(m)$: [83]:

$$r_{xx}(m) = E[x(n)x^*(n-m)] \tag{4.5}$$

PSD can be estimated using the Discrete Fourier Transform (DFT) of the discrete time autocorrelation function:

$$P_x(k) = \lim_{N\to+\infty} \sum_{m=\frac{N}{2}-1}^{\frac{N}{2}} r_{xx}(m) \exp\left(-j2\pi k \frac{m}{N}\right) \tag{4.6}$$

For the white noise $w(n)$, the autocorrelation function of $w(n)$ becomes:

$$r_{ww}(m) = E[w(n)w^*(n-m)] = \sigma_w^2 \delta(m) \tag{4.7}$$

Where $\delta(m)$ is the Dirac Delta function. Based on equation (4.7), the PSD of the white noise, $P_w(k)$, becomes a real and constant ($= \sigma_w^2$). Therefore the cumulative sum of this PSD becomes a straight line, with a slope σ_w^2. In contrast, the over-sampling aspect of $s(n)$ produces correlated samples and a non constant PSD $P_s(k)$.
According to model (4.2), PSD of the received signal, $(y(n))$, becomes not constant when the PU signals exists. This fact leads us to distinguish the two channel status presented in equation (4.2).

4.2.1 Estimation of the Power Spectral Density

The PSD of a random signal $x(n)$ can be estimated as follows [83]:

$$\hat{P}_x(k) = \frac{1}{N}|X(k)|^2 \tag{4.8}$$

Where $X(k)$ is the Discrete Fourier Transform (DFT) of the signal $x(n)$ with N samples:

$$X(k) = \sum_{n=\frac{N}{2}-1}^{\frac{N}{2}} x(n) \exp\left(-j2\pi k \frac{n}{N}\right) \tag{4.9}$$

Therefore, the estimated PSD of a random signal is related to the modulus of its DFT.

Lemma 1: The DFT, $X(k)$, of a zero mean circular symmetric process $x(n) = x_p(n) + jx_q(n)$, becomes a zero mean circular symmetric process.

Proof. By definition, $X(k)$ is a circular symmetric if and only if (iff) $E[X^2(k)] = 0$ [84]. As $X(k)$ is the DFT of $x(n)$ and according to equation (4.9), we can derive the following equation:

$$\begin{aligned} E[X^2(k)] &= E\left[\sum_{m,n=-\frac{N}{2}-1}^{N} x(n)\exp\left(-j2\pi k\frac{n}{N}\right)x(m)\exp\left(-j2\pi k\frac{m}{N}\right)\right] \\ &= \underbrace{\sum_{m=n=-\frac{N}{2}-1}^{N} E[x^2(n)]\exp\left(-j2\pi k\frac{2n}{N}\right)}_{=0;\ \textit{using the circularity property of } x(n)} \\ &\quad + \underbrace{\sum_{m\neq n}^{N} E\left[x(n)x(m)\right]\exp\left(-j2\pi k\frac{n+m}{N}\right)}_{=\ 0\ \textit{as } x(n)\ \textit{is i.i.d. and zero mean}} \\ &= 0 \end{aligned} \tag{4.10}$$

□

Based on *Lemma* 1, the DFT $W(k)$, of $w(n)$, becomes a circular symmetric process.

4.3 Cumulative Power Spectral Density-based Detector

Let us define the Cumulative Power Spectral Density (CPSD), $CP_y(k)$, of the received signal $y(n)$, over a frequency interval as follows,

$$CP_y(k) = \sum_{u=v}^{k} \hat{P}_y(u), \quad ,\forall k \in [v; l], \tag{4.11}$$

Where $\hat{P}_y(u)$ is the estimated PSD of $y(n)$ using Equation (4.8). Let us define the Normalized CPSD, $\Psi(k)$, of $y(n)$ by:

$$\Psi(k) = \frac{CP_y(k)}{(l - v + 1)\sigma_w^2} \tag{4.12}$$

The term $(l-v+1)\sigma_w^2$ corresponds to the mean value of $CP_w(l)$, which is the last term of the CPSD of $w(n)$.

$$\begin{aligned}
E[CP_w(l)] &= \frac{1}{N}\sum_{k=v}^{l} E[|W(k)|^2] = \frac{1}{N}\sum_{k=v}^{l}\sum_{n,m=1}^{N} E\left[w(n)w^*(m)\exp\left(-j2\pi(n-m)\frac{k}{N}\right)\right] \\
&= \frac{1}{N}\sum_{k=v}^{l}\underbrace{\sum_{n=m=1}^{N} E[|w(n)|^2]}_{=E[|W(k)|^2]=N\sigma_w^2} \\
&\quad + \frac{1}{N}\sum_{k=v}^{l}\underbrace{\sum_{n\neq m}^{N} E\left[w(n)w^*(m)\right]\exp\left(-j2\pi(n-m)\frac{k}{N}\right)}_{=\,0 \text{ since } w(n) \text{ and } w(m) \text{ are independent and } E[w(n)]=0} \\
&= \frac{1}{N}(l-v+1)N\sigma_w^2 = (l-v+1)\sigma_w^2
\end{aligned} \tag{4.13}$$

Under H_0 and thanks to the flat PSD of $w(n)$, the shape of $\Psi(k)$ becomes close to a straight line $D(v,l;k)$.

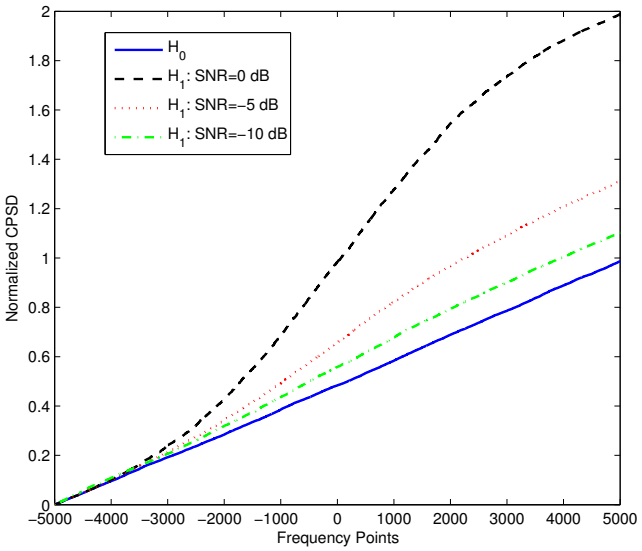
$$D(v,l;k) = \frac{k-v+1}{l-v+1} \tag{4.14}$$

Due to the presence of an oversampled signal $s(n)$ under H_1, the PSD of $y(n)$ becomes a non constant, and $\Psi(k)$ has higher values than the one obtained under H_0 because of the additional power of $s(n)$.
Figure (4.1) shows $\Psi(k)$ under H_0 and H_1, for various values of N_s and different SNR. The signal modulation is 16-QAM and the number of used samples is $N = 10^4$. As shown in figure (4.1), the gap between the Normalized CPSD shape under H_1 and that under H_0 increases with the SNR. In addition, the non-linearity of the CPSD shapes grows with N_s. Therefore, we define a test statistic T as the difference between $\Psi(k)$ and the reference straight line $D(v,l;k)$. Accordingly, we introduce two detectors:

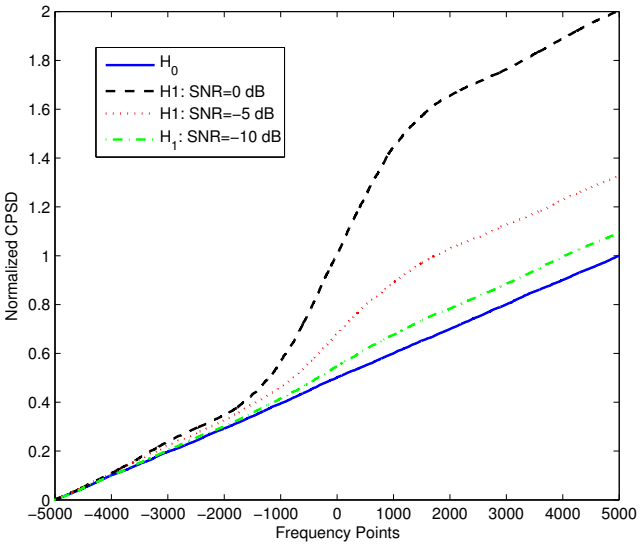
1. T_p: This detector is based on the CPSD, $\Psi_p(k)$, of $\hat{P}_y(k)$ for positive frequency points (*i.e.* $1 \leq k \leq \frac{N}{2}$):

$$\begin{aligned}
\Psi_p(k) &= \frac{2}{N\sigma_w^2}\sum_{u=1}^{k} P_y(u) \\
&= \frac{2}{N^2\sigma_w^2}\sum_{u=1}^{k}|Y(u)|^2
\end{aligned} \tag{4.15}$$

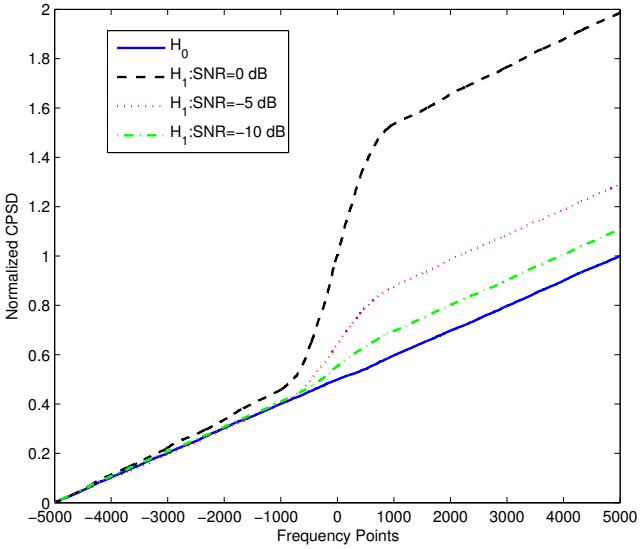
   T_p detector aims at finding the difference between $\Psi_p(k)$ and the corresponding reference shape $D(1,\frac{N}{2};k)$:



(a) $N_s = 2$ sps



(b) $N_s = 4$ sps



(c) $N_s = 8$ sps

FIGURE 4.1: The Noralized CPSD shapes for $N = 10000$ samples with respect to the Frequency Points and several values of N_s and SNR

$$T_p = \sum_{k=1}^{\frac{N}{2}} \left(\Psi_p(k) - D\left(1, \frac{N}{2}; k\right) \right)$$
$$T_p = \sum_{k=1}^{\frac{N}{2}} \left(\Psi_p(k) - \frac{2k}{N} \right)$$
$$= \sum_{k=1}^{\frac{N}{2}} \Psi_p(k) - \frac{N+2}{4} \tag{4.16}$$

2. T_a: This detector is based on the CPSD of all frequencies of $y(n)$ (i.e. $-\frac{N}{2}+1 \leq k \leq \frac{N}{2}$), similarly to T_p:

$$T_a = \sum_{k=-\frac{N}{2}+1}^{\frac{N}{2}} \left(\Psi_a(k) - D\left(-\frac{N}{2}+1, \frac{N}{2}; k\right) \right)$$
$$= \sum_{k=-\frac{N}{2}+1}^{\frac{N}{2}} \Psi_a(k) - \frac{N+1}{2} \tag{4.17}$$

Where $\Psi_a(k)$ can be found as follows:

$$\Psi_a(k) = \frac{1}{N^2\sigma_w^2} \sum_{u=-\frac{N}{2}+1}^{k} |Y(u)|^2 \tag{4.18}$$

4.3.1 Proposed cooperative detectors

In order to enhance the detection performance, two cooperative detectors are proposed. The cooperation is done between negative frequencies PSD ($P_y(k)$ $s.t.$ $\frac{N}{2}+1 \leq k \leq 0$) part and the positive frequency part ($P_y(k)$ $s.t.$ $1 \leq k \leq \frac{N}{2}$). The first proposed detector, T_{or}, aims to exploit all the frequency points of the signal $y(n)$, by applying two test statistics: 1) the first one tests the shape of the CPSD for positive frequency points (which is T_p). 2) T_n tests the CPSD shape of the CPSD of the **symmetric** of the negative frequencies PSD part. The detector, T_{or}, makes a decision by ORing the decisions of T_p and T_n.

The second proposed cooperative detector, T_{av}, performs the average, P_{av}, between the positive frequencies PSD and the **symmetric** of the negative frequency PSD. CPSD is

then performed on P_{av}. The averaging process smooth the PSD, since $P_s(k)$ is symmetric, and the components of $\hat{P}_w(k)$ are independent as shown in section (4.4).

4.3.1.1 OR Detector

Let T_n be the detector over negative frequencies. Similarly to T_p, T_n makes a decision by comparing its corresponding normalized CPSD shape to the reference straight line $D(1, \frac{N}{2}; k)$.

$$\begin{aligned} T_n &= \sum_{k=1}^{\frac{N}{2}} \left(\Psi_n(k) - D\left(1, \frac{N}{2}; k\right) \right) \\ &= \sum_{k=1}^{\frac{N}{2}} \Psi_n(k) - \frac{N+2}{4} \end{aligned} \tag{4.19}$$

Where $\Psi_n(u)$ in this case is given by:

$$\Psi_n(k) = \frac{2}{N^2 \sigma_w^2} \sum_{u=1}^{k} |Y(-u+1)|^2 \tag{4.20}$$

Due to the fact that $P_s(k)$ is symmetric and deterministic since $s(n)$ is deterministic and $W(k)$ is $i.i.d.$ (as it is shown in section 4.4.1.1), T_p and T_n become independent and have same mean and variance.
Once T_p and T_n make their own decisions, T_{or}, acting as a hard cooperative detector of the two decisions using an OR-rule.

$$T_{or} = OR(d_{T_p}, d_{T_n}) \tag{4.21}$$

Where d_{T_p} and d_{T_n} are the detection results of T_p and T_n respectively.
That cooperation between the positive and negative frequencies parts of the PSD leads to enhance the detection performance due to the fact that the noise is $i.i.d.$ In this case, T_{or} exploits the diversity of the parts of PSD using the decision of the two independent test statistics T_p and T_n.

4.3.1.2 Averaging Detector

The property of symmetry of $P_y(k)$ is exploited in this section by averaging $P_y(k)$ and $P_y(-k+1)$, $1 \leq k \leq \frac{N}{2}$, to obtain $P_y^{av}(k)$.

$$P_{av}(k) = \frac{\hat{P}_y(k) + \hat{P}_y(-k+1)}{2}; \qquad 1 \leq k \leq \frac{N}{2} \tag{4.22}$$

T_{av} can be considered as a soft combining detectors of T_p and T_n, to exploit the diversity of the two parts of PSD based on the *i.i.d.* property of the noise.

$$\begin{aligned} T_{av} &= \sum_{k=1}^{\frac{N}{2}} \Psi_{av}(k) - D\left(1, \frac{N}{2}; k\right) \\ &= \sum_{k=1}^{\frac{N}{2}} \Psi_{av}(k) - \frac{N+2}{4} \end{aligned} \tag{4.23}$$

Where

$$\Psi_{av}(k) = \frac{2}{N\sigma_w^2} \sum_{u=1}^{k} P_{av}(u) \tag{4.24}$$

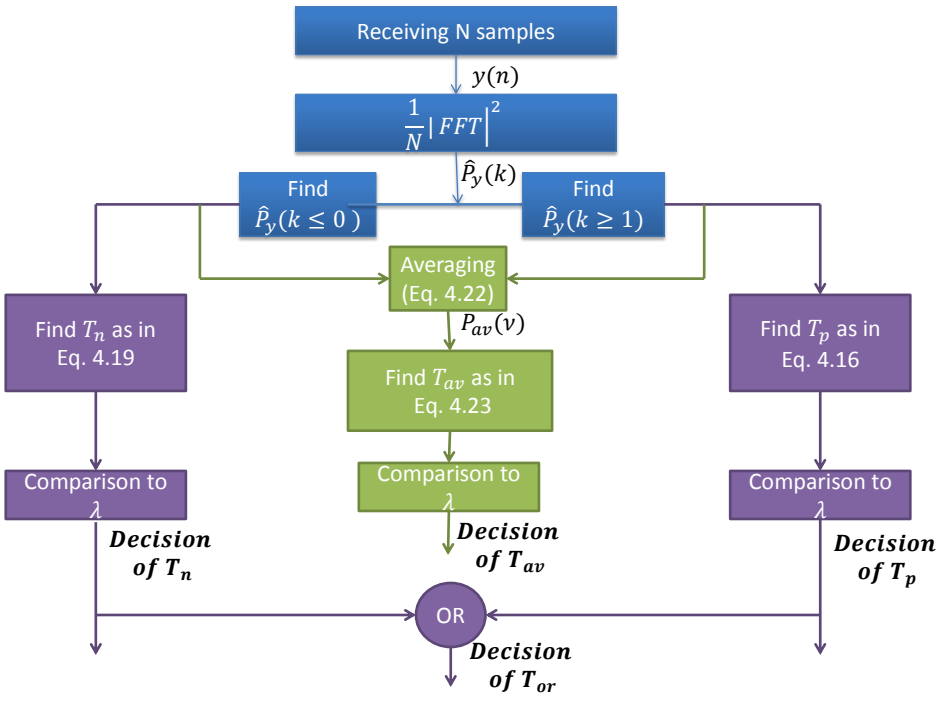


FIGURE 4.2: The overall diagram of the CPSD-based detectors

Figure 4.2 shows the diagram of the proposed detectors. The relation between T_p and T_n from one hand, and T_{or} and T_{av} on the other hand is clear. Concerning T_{or}, the relation

of cooperation is at the decision level, whereas this relation is at the test statistic level regarding T_{av}. Hereinafter, we present an analytic study for the proposed detectors, where the False Alarm, p_{fa}, and Detection, p_d, probabilities are derived under both Gaussian and Rayleigh channels.

4.4 Statistical Analysis

Deriving the analytic p_{fa} and p_d is essential for any detector in order to meet the detection requirement of the Spectrum Sensing. For a target p_{fa}, a threshold should be set by the help of the expression of p_{fa} by taking into account other parameters in some circumstances such as the number of the received samples and the noise variance. However, the distributions of test statistics are essential in order to find p_{fa} and p_d analytically. Regarding the proposed detectors in this chapter, T_p and T_a share the same statistical distribution since $W(k)$ is *i.i.d.* and $S(k)$ is deterministic as $s(n)$ is assumed to be deterministic. In the following, we develop the distribution of T_p under H_0 and H_1 over a Gaussian channel, where the channel effect h is assumed to be constant. Similarly, the distribution of T_a can be found. T_{or} makes a decision by applying the logical OR on the decisions of T_p and T_n.

4.4.1 False Alarm and Detection Probabilities of T_p

The distribution of T_p depends on $\sum_{k=1}^{\frac{N}{2}} \Psi_p(k)$ as presented in equation (4.16). A simplification of the term $\sum_{k=1}^{\frac{N}{2}} \Psi_p(k)$ can be obtained as follows:

$$\begin{aligned}
\sum_{k=1}^{\frac{N}{2}} \Psi_p(k) &= \frac{2}{N^2\sigma_w^2} \sum_{k=1}^{\frac{N}{2}} \sum_{u=1}^{k} |Y(u)|^2 \\
&= \frac{2}{N^2\sigma_w^2} |Y(1)|^2 && (k=1) \\
&+ \frac{2}{N^2\sigma_w^2} \Big(|Y(1)|^2 + |Y(2)|^2 \Big) && (k=2) \\
&\ldots \\
&+ \frac{2}{N^2\sigma_w^2} \Big(|Y(1)|^2 + |Y(2)|^2 \ldots |Y(\frac{N}{2})|^2 \Big) && (k=\frac{N}{2}) \\
&= \frac{2}{N^2\sigma_w^2} \sum_{k=1}^{\frac{N}{2}} \left(\frac{N}{2} - k + 1 \right) |Y(k)|^2 && (4.25)
\end{aligned}$$

Equation (4.25) shows the main difference between the proposed detection algorithm and the Energy Detector (ED), where $\left(\frac{N}{2}-k+1\right)$ acts as a weighting function on the samples in frequency domain.

4.4.1.1 False Alarm Probability of T_p

Under H_0, the test statistic T_p depends only on the noise $w(n)$. Using equation (4.25), T_p can be written as follows:

$$\begin{aligned} T_p &= \sum_{k=1}^{\frac{N}{2}} \left[\frac{2}{N^2\sigma_w^2} \left(\frac{N}{2} - k + 1 \right) |W(k)|^2 - D\left(1, \frac{N}{2}; k\right) \right] \\ &= \sum_{k=1}^{\frac{N}{2}} \left[\Psi_p(k) - D\left(1, \frac{N}{2}; k\right) \right] \end{aligned} \tag{4.26}$$

Being the Discrete Fourier transform of a white noise $w(n)$, $W(k)$ asymptotically follows a normal distribution since it is the sum of independent terms. It is known that two Gaussian variables are independent iff they are uncorrelated [58]. Let us consider the autocorrelation function of $W(k)$, $r_{WW}(m)$ for $m \neq 0$.

$$\begin{aligned} r_{WW}(m) &= E\left[W(k)W^*(k-m) \right] \\ &= \sum_{q,n=-\frac{N}{2}+1}^{\frac{N}{2}} E\left[w(q)w^*(n) \exp\left(-j2\pi \left(\frac{qk-(k-m)n}{N} \right) \right) \right] \end{aligned}$$

Since $w(n)$ is zero mean *i.i.d.*, $r_{WW}(m)$ becomes:

$$r_{WW}(m) = \sum_{n=-\frac{N}{2}+1}^{\frac{N}{2}} E[|w(n)|^2] e^{-j2\pi nm/N}$$

Since $m \in \mathbb{Z}^*$, we obtain:

$$r_{WW}(m) = \sigma_n^2 \sum_{n=-\frac{N}{2}+1}^{\frac{N}{2}} \exp\left(-j2\pi nm/N\right) = 0 \tag{4.27}$$

Then, $E[W(k)W^*(k-m)] = E[W(k)]E[W^*(k-m)] = 0$. Therefore $W(k)$ becomes *i.i.d.* Being the sum of independent terms and according to the Central Limit Theorem (CLT), the distribution of T_p tends towards $\mathcal{N}(\mu_0, V_0)$ under H_0. In this case, the probability of

False Alarm p_{fa}^{p} of T_p can be found as follows:

$$p_{fa}^{p} = Q\left(\frac{\lambda - \mu_0}{\sqrt{V_0}}\right) \tag{4.28}$$

Where $Q(.)$ is the Q-function [3], and λ is the threshold of comparison. As $E\left[|W(k)|^2\right] = N\sigma_w^2$ and based on equation (4.26), μ_0 can be evaluated as follows:

$$\begin{aligned}\mu_0 &= E[T_p] \\ &= \frac{2}{N^2\sigma_w^2}\sum_{k=1}^{\frac{N}{2}}\left(\frac{N}{2} - k + 1\right)E\left[|W(k)|^2\right] - \frac{N+2}{4} \\ &= 0\end{aligned} \tag{4.29}$$

In this case, the variance, V_0, of T_p becomes (see appendix (A)):

$$\begin{aligned}V_0 &= E[T_p^2] - \mu_0^2 = \\ &= E[T_p^2] = \frac{(N+2)(N+1)}{6N}\end{aligned} \tag{4.30}$$

4.4.1.2 Probability of Detection of T_p

Under H_1, $Y(k) = hS(k) + W(k)$, where $hS(k) = DFT\{hs(n)\}$ and $Y(k) = DFT\{y(n)\}$, then equation (4.25) becomes as follows:

$$\Psi_p(k) = \frac{2}{N^2\sigma_w^2}\sum_{k=1}^{\frac{N}{2}}\left(\frac{N}{2} - k + 1\right)\left|hS(k) + W(k)\right|^2 \tag{4.31}$$

Since $S(k)$ is deterministic and the terms of $W(k)$ are independent, the distribution of T_p under H_1 tends also towards $\mathcal{N}(\mu_1, V_1)$. In this case, the probability of detection p_d^p, of T_p can be found as follows:

$$p_d^p = Q\left(\frac{\lambda - \mu_1}{\sqrt{V_1}}\right) \tag{4.32}$$

μ_1 and V_1 should be evaluated in order to find p_d^p. Under H_1, $|Y(k)|^2$ becomes:

$$\begin{aligned}|Y(k)|^2 &= Y(k)Y^*(k) \\ &= |hS(k)|^2 + |W(k)|^2 + 2Re\{hS(k)W^*(k)\}\end{aligned} \tag{4.33}$$

[3] $Q(x) = \frac{1}{\sqrt{2\pi}}\int_x^{+\infty} e^{\frac{-t^2}{2}}dt$ [58]

where $Re\{X\}$ is the real part of X. The mean value of T_p under H_1 can be found by equation (4.16) as follows:

$$\begin{aligned}
\mu_1 = & \underbrace{\frac{2}{N^2\sigma_w^2} E\left[\sum_{k=1}^{\frac{N}{2}} \left(\left(\frac{N}{2}-k+1\right)|W(k)|^2 - D\left(1,\frac{N}{2};k\right)\right)\right]}_{=\mu_0=0,\ according\ to\ equation\ (4.29)} \\
& + \underbrace{\frac{2}{N^2\sigma_w^2} E\left[\sum_{k=1}^{\frac{N}{2}} \left(\frac{N}{2}-k+1\right)|hS(k)|^2\right]}_{S(k)\ is\ deterministic} \\
& + \underbrace{\frac{2}{N^2\sigma_w^2} E\left[\sum_{k=1}^{\frac{N}{2}} 2Re\{hS(k)W^*(k)\}\right]}_{=0,\ as\ S(k)\ is\ deterministic\ and\ W(k)\ is\ zero\ mean} \\
& = \frac{2\gamma}{N^2}\sum_{k=1}^{\frac{N}{2}} \left(\frac{N}{2}-k+1\right)|S(k)|^2 \\
& = b\gamma
\end{aligned} \tag{4.34}$$

Where $b = \frac{2}{N^2}\sum_{k=1}^{\frac{N}{2}}(\frac{N}{2}-k+1)|S(k)|^2$, and γ is the SNR as defined by equation (4.4). Under H_1, the variance V_1 is given by the following equation (see Appendix B):

$$\begin{aligned}
V_1 &= V_0 + \frac{8\gamma}{N^3}\sum_{k=1}^{\frac{N}{2}} \left(\frac{N}{2}-k+1\right)^2 |S(k)|^2 \\
&= V_0 + c\gamma
\end{aligned} \tag{4.35}$$

Where $c = \frac{8}{N^3}\sum_{k=1}^{\frac{N}{2}}(\frac{N}{2}-k+1)^2|S(k)|^2$.

T_a is based on a similar idea to T_p, but it covers the N frequency points instead of just positive ones ($\frac{N}{2}$ points). Since $W(k)$ is *i.i.d.* and $S(k)$ is deterministic, then by following similar steps of calculus for p_{fa}^p and p_d^p, the probability of False Alarm p_{fa}^a and the Probability of detection p_d^a of the detector T_a can be found as follows:

$$p_{fa}^a = Q\left(\frac{\lambda-\mu_0^a}{\sqrt{V_0^a}}\right) \tag{4.36}$$

$$p_d^a = Q\left(\frac{\lambda-\mu_1^a}{\sqrt{V_1^a}}\right) \tag{4.37}$$

Where $\mu_0^a = 0$; $V_0^a = \frac{N}{3} + \frac{1}{2} + \frac{1}{6N}$; $\mu_1^a = b_a\gamma$, where $b_a = \frac{1}{N^2}\sum_{k=1}^{N}(N-k+1)|S(k)|^2$, and $V_1^a = V_0^a + c_a\gamma$, where $c_a = \frac{2}{N^3}\sum_{k=1}^{N}(N-k+1)^2|S(k)|^2$.

4.4.2 Probabilities of T_{or}

T_{or} applies the OR-rule between the decisions of T_p and T_n, then T_{or} can be considered as a hard cooperative detector of these two detectors. Since T_p and T_n are independent and have the same statistics as defined previously, the probability of false alarm p_{fa}^{or}, and the probability of detection p_d^{or}, of T_{or} can be found as follows [20]:

$$p_{fa}^{or} = 1 - \left(1 - p_{fa}^{p}\right)^2 \tag{4.38}$$

$$p_d^{or} = 1 - \left(1 - p_d^{p}\right)^2 \tag{4.39}$$

4.4.3 Probabilities of T_{av}

T_{av} can be developed following similar steps to equation (4.26).

$$T_{av} = \frac{2}{N^2\sigma_w^2}\sum_{k=1}^{\frac{N}{2}}\left(\frac{N}{2} - k + 1\right)\frac{|Y(k)|^2 + |Y(-k+1)|^2}{2}\frac{N+2}{4} \tag{4.40}$$

Under H_0, $Y(k) = W(k)$, then T_{av} becomes the sum of independent terms. Based on CLT, T_{av} asymptotically follows $\mathcal{N}(\mu_0^{av}, V_0^{av})$ under H_0.
Under H_1, $Y(k) = hS(k) + W(k)$ and $S(k)$ is deterministic, so T_{av} is still following under H_1 a normal distribution: $\mathcal{N}(\mu_1^{av}, V_1^{av})$. The probability of false alarm, p_{fa}^{av}, and detection, p_d^{av}, of T_{av} are expressed as follows:

$$p_{fa}^{av} = Q\left(\frac{\lambda - \mu_0^{av}}{\sqrt{V_0^{av}}}\right) \tag{4.41}$$

$$p_d^{av} = Q\left(\frac{\lambda - \mu_1^{av}}{\sqrt{V_1^{av}}}\right) \tag{4.42}$$

Since $W(k)$ is *i.i.d.* and $P_s(k)$ is even, μ_0^{av},V_0^{av}, μ_1^{av}, V_1^{av} can be found by following similar steps to μ_0, V_0, μ_1 and V_1: $\mu_0^{av} = \mu_0$; $V_0^{av} = \frac{V_0}{2}$; $\mu_1^{av} = \mu_1$ and $V_1^{av} = \frac{V_1}{2}$.
The theoretical and the simulated ROC curves of proposed detectors are with good agreement as shown in figure (4.3). Simulations were done under following conditions: 16-QAM modulation, $\gamma = -12$ dB, $N = 1000$ samples and $N_s = 4$ sps. As shown in

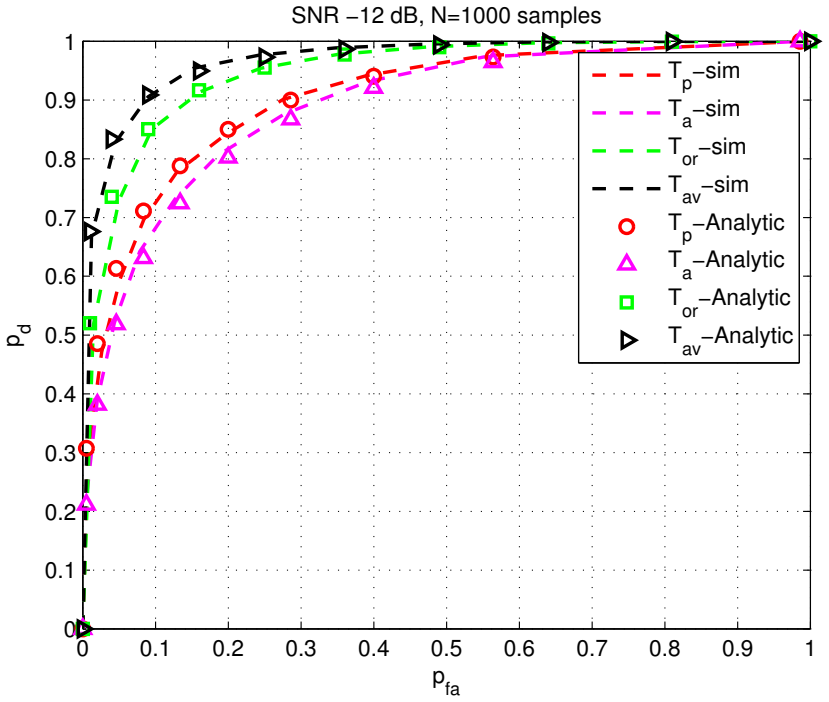


FIGURE 4.3: Analytic results Vs Simulation results under Gaussian channel

figure (4.3), T_{av} is the most efficient detector. For the simulations of section 4.6 under Gaussian channel, only T_{av} and T_p are compared to other well known detectors.

4.5 Probability of detection over Rayleigh Fading Channel

In this section, we derive the detection probability over the Rayleigh flat fading channel. The effect of the Rayleigh channel appears as fluctuation in the SNR, since the channel becomes a time variant. The false alarm probability remains the same since it is independent of the channel gain h. The distribution of the SNR, γ, in a Rayleigh channel is given by [58]:

$$f_\gamma(\gamma) = \frac{1}{\bar{\gamma}} \exp\left(-\frac{\gamma}{\bar{\gamma}}\right) \tag{4.43}$$

Where $\bar{\gamma}$ is the average SNR.
Over a Rayleigh channel, the probability of detection, p_{dr}, can be found as the average of the probability of detection, p_{dg}, under Gaussian channel with respect to $f_\gamma(\gamma)$.

$$p_{dr} = \int_0^{+\infty} p_{dg} f_\gamma(\gamma) d\gamma \tag{4.44}$$

Concerning the proposed detectors, T_p, T_a and T_{av}, detection probabilities over Rayleigh fading channel can be derived similarly, since the three detectors have a similar probability of detection: $p = Q(\frac{\lambda-\delta\gamma}{V_{H_0}+\beta\gamma})$, where δ, V_{H_0} and β are constants.
Hereinafter, we only derive p_{dr}^{p}, the detection probability of T_p over a Rayleigh channel. Once p_{dr}^{p} is derived, p_{dr}^{a} and p_{dr}^{av}, the probability of detection of T_a and T_{av}, can be easily expressed.
Using equations (4.32), (4.43) and (4.44), p_{dr}^{p} can be expressed as follows:

$$p_{dr}^{p} = \frac{1}{\bar{\gamma}} \int_{0}^{+\infty} Q\left(\frac{\lambda - \mu_1}{\sqrt{V_1}}\right) \exp\left(-\frac{\gamma}{\bar{\gamma}}\right) d\gamma \tag{4.45}$$

The above integral doesn't have an analytic solution. Therefore, the first order Taylor series, $g_1(\gamma)$, is used as an approximation of $g(\gamma) = Q\left(\frac{\lambda-\mu_1}{\sqrt{V_1}}\right) = \frac{\lambda-b\gamma}{\sqrt{V_0+c\gamma}}$, around $\gamma_0 = \lambda/b$ as follows (see Appendix (C)):

$$\begin{aligned} g_1(\gamma) &= g(\gamma_0) + g'(\gamma_0)(\gamma - \gamma_0) \\ &= g'(\gamma_0)(\gamma - \gamma_0) \end{aligned} \tag{4.46}$$

The approximation of p_{dr}^{p}, $\hat{p}_{dr}^{p}$ is given by :

$$\hat{p}_{dr}^{p} = \frac{1}{\bar{\gamma}} \int_{0}^{+\infty} Q\Big(\theta(\gamma - \gamma_0)\Big) \exp\left(-\frac{\gamma}{\bar{\gamma}}\right) d\gamma \tag{4.47}$$

With $\theta = g'(\gamma_0) = -\frac{b}{\sqrt{V_0+c\lambda/b}}$. According to [85], we can find:

$$\int \exp(qx) Q(px) dx = \frac{1}{q}\left[\exp(qx) Q(px) - \exp\left(\frac{q^2}{2p^2}\right) Q\left(px - \frac{q}{p}\right)\right] \tag{4.48}$$

Using equation (4.48), and the fact that $Q(-x) = 1 - Q(x)$, the integral of equation (4.47) becomes:

$$\hat{p}_{dr}^{p} = Q(-\theta\gamma_0) + \exp\left(\frac{1}{2\theta^2\bar{\gamma}^2} - \frac{\gamma_0}{\bar{\gamma}}\right) Q\left(\theta\gamma_0 - \frac{1}{\theta\bar{\gamma}}\right) \tag{4.49}$$

For the approximation $\hat{p}_{dr}^{a}$, of p_{dr}^{a}, it can be found by replacing the number of samples $N/2$ used in T_p by N used in T_a. Similarly to $\hat{p}_{dr}^{p}$,the approximation $\hat{p}_{dr}^{av}$ of p_{dr}^{av} can be derived as follows:

$$\hat{p}_{dr}^{av} = Q\left(-\theta_{av}\gamma_0\right) + \exp\left(\frac{1}{2\theta_{av}^2\bar{\gamma}^2} - \frac{\gamma_0}{\bar{\gamma}}\right) Q\left(\theta_{av}\gamma_0 - \frac{1}{\theta_{av}\bar{\gamma}}\right) \tag{4.50}$$

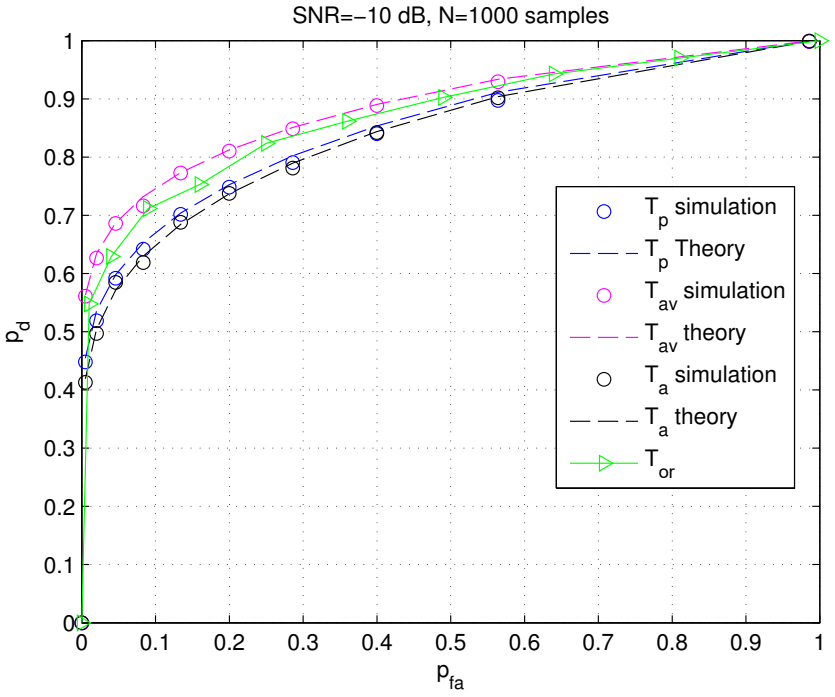


FIGURE 4.4: Simulations result Vs. Analysis result over Rayleigh fading channel, $N_s = 3$ sps

Where $\theta_{av} = -\frac{b}{\sqrt{V_{0av}+\frac{c\lambda}{2b}}}$.

γ_0 is not modified in the expression of $\hat{p}_{dr}^{av}$, since T_p and T_{av} have the same mean under H_1.

The detection probability of T_{or} under Gaussian channel is a non-linear combination of the probability of detection of T_p and T_n. Over a Rayleigh channel, the fading coefficient, h, is the same for T_p and T_n, p_{dr}^{or} of T_{or} becomes:

$$\begin{aligned} p_{dr}^{or} &= \frac{1}{\bar{\gamma}} \int_0^{\infty} (1-(1-p_d^p)^2) \exp\left(-\frac{\gamma}{\bar{\gamma}}\right) d\gamma \\ &= \frac{2}{\bar{\gamma}} \int_0^{\infty} Q\left(\frac{\lambda - b\gamma}{\sqrt{V_0 + c\gamma}}\right) \exp\left(-\frac{\gamma}{\bar{\gamma}}\right) d\gamma \\ &- \frac{1}{\bar{\gamma}} \int_0^{\infty} Q^2\left(\frac{\lambda - b\gamma}{\sqrt{V_0 + c\gamma}}\right) \exp\left(-\frac{\gamma}{\bar{\gamma}}\right) d\gamma \end{aligned} \tag{4.51}$$

As there is no analytic solution of equation (4.51), we solve it in a numerical way.

In figure (4.4), analysis results are very closed to simulation results. Since T_{av} and T_{or} have the best performance, they are compared to ED, ACD and CSD under Rayleigh channel.

4.6 Performance Evaluation

In this section, we compare the performance of our detectors to that of the Energy Detector (ED) [55], the Cyclostationary Detector (CSD) [44] and the Autocorrelation Detector (ACD) [47], under Gaussian and Rayleigh channels. The comparison will be done based on three criteria: the ROC curves, the required number of samples to reach ($p_{fa} = 0.1; p_d = 0.9$) and the computational complexity. Throughout the upcoming simulations, A 16-QAM baseband modulated PU signal is considered.

4.6.1 Performance analysis over Gaussian Channel

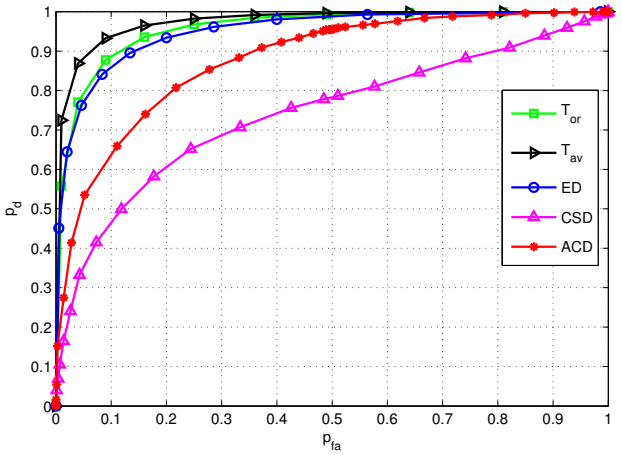
Figure (4.5) presents the ROC curves under a Gaussian channel of various numbers of samples per symbol N_s. Simulations are done using $N = 1500$ samples and $\gamma = -12$ dB. According to that figure, the performance increases with N_s. For the limiting case, *i.e.* when $N_s = 2$ sps, ACD and CSD show a poor performance relatively to T_{av}, T_{or} and ED, while T_{av} outperforms all other detectors. However, T_{av} and T_{or} outperform ED and CSD for different values of N_s. For $N_s = 8$ sps, ACD outperforms slightly T_{or} and it is closed to T_{av}.

Figure (4.6) shows the variation of the probability of detection with respect to SNR for a constant $p_{fa} = 0.1$. The number of samples is fixed $N = 1000$ samples and various values are assigned for N_s. T_{av} and T_{or} reach higher probabilities of detection than ED, CSD and ACD for similar SNR and different values of N_s for $N_s = 2$ and $N_s = 4$ sps. For $N_s = 8$ sps, ACD outperforms slightly T_{av} for the $SNR < -12$ dB. In addition, increasing N_s leads to enhancing the performance of T_{or}, T_{av}, CSD and ACD. For examples, T_{av} reaches $p_d = 0.9$ at SNR $\simeq -7$ dB for $N_s = 2$ sps, while the same probability of detection is reached for SNR $\simeq -9$ dB and SNR $\simeq -10$ dB at $N_s = 4$ sps and $N_s = 8$ sps respectively.

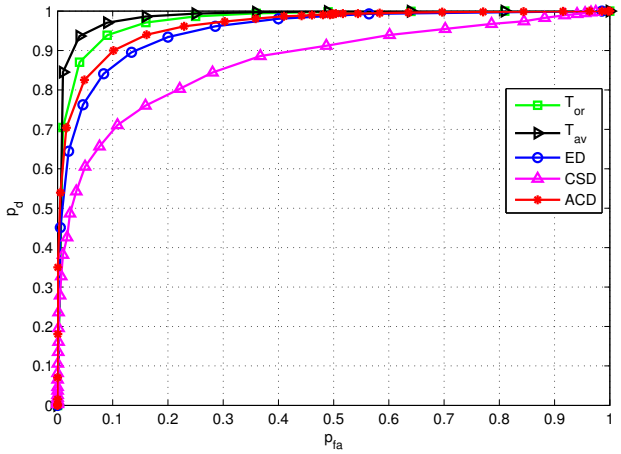
4.6.2 Performance analysis over Rayleigh Channel

Figure (4.7) shows the ROC curves under Raleigh Fading channel for $N_s = 4$ and 8 sps, with $N = 1000$ samples and an average SNR of -5 dB.

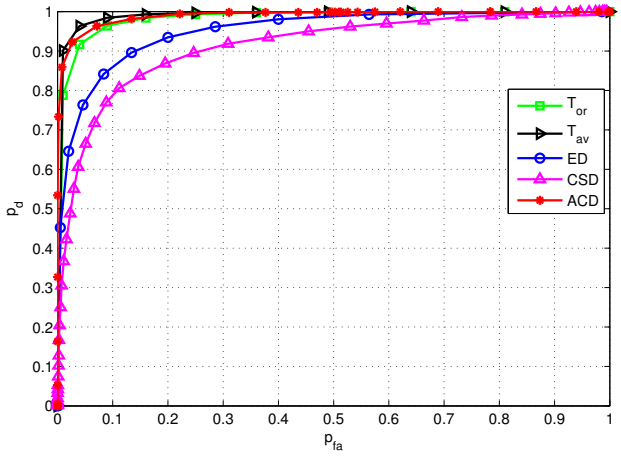
Over Rayleigh fading channel, T_{av} and T_{or} are still outperforming ED and CSD. The same fading suffered by the negative and the positive frequency parts of PSD affects the performance of our detectors. As shown in figure (4.7), the gap of performance among our detectors, ED and CSD becomes smaller comparing to a Gaussian channel.



(a) $N_s = 2$ sps

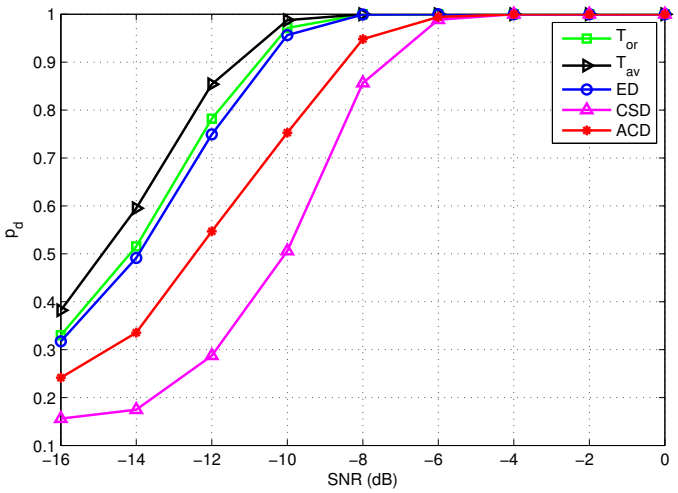


(b) $N_s = 4$ sps

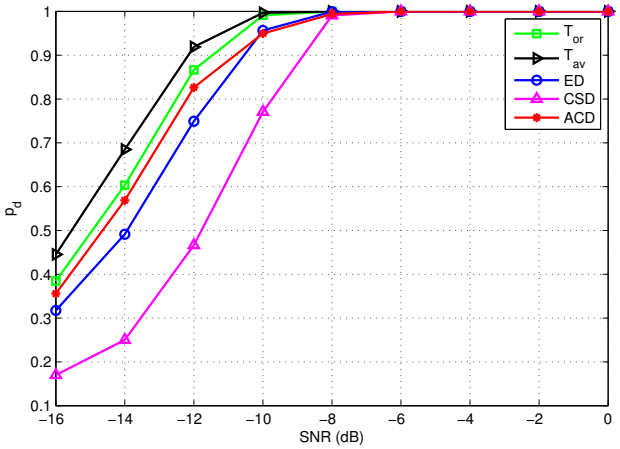


(c) $N_s = 8$ sps

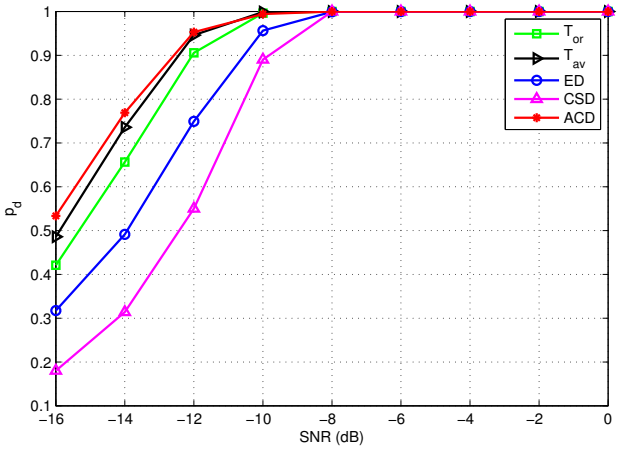
FIGURE 4.5: ROC curves of our proposed detectors comparing to ED and CSD for various N_s, SNR of $-12dB$ and $N = 1500$ samples.



(a) $N_s = 2$ sps

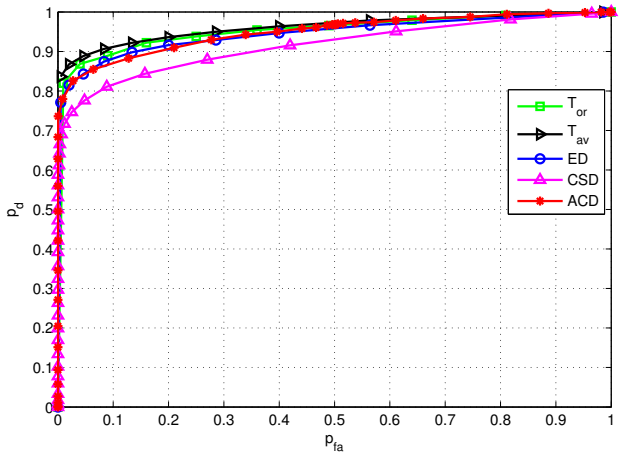


(b) $N_s = 4$ sps

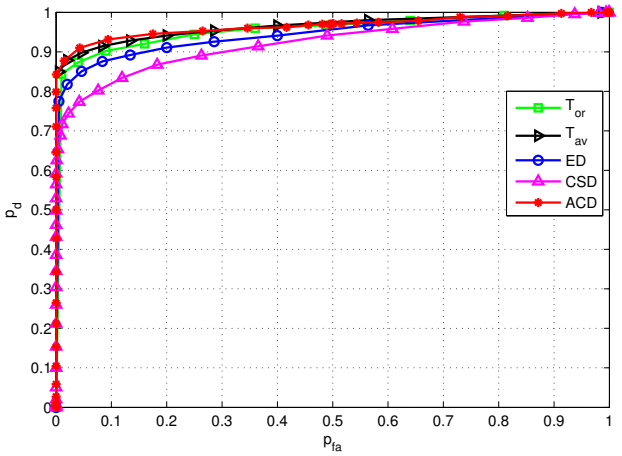


(c) $N_s = 8$ sps

FIGURE 4.6: Variation of the probability of detection in terms of SNR for $N = 1000$ samples, a constant $p_{fa} = 0.1$ and various values of N_s.



(a) $N_s = 4$ sps



(b) $N_s = 8$ sps

FIGURE 4.7: ROC curves over Rayleigh fading channel for $N_s = 4$ and 8 sps for N=1000 samples and average SNR $= -5$ dB.

Besides that, our proposed detectors outperform ACD for $N_s = 4$ sps, while ACD has approximately the same performance as T_{av} for $N_s = 8$ sps.

4.6.3 Complexity Analysis

According to equation (4.25), T_p needs $\frac{N}{2}$ operations to obtain $|Y(k)|^2$, and $\frac{N}{2}$ multiplication operations to evaluate the product $(\frac{N}{2} - k + 1)|Y(k)|^2$. Moreover, T_p performs N addition operations: $\frac{N}{2}$ operations to calculate $(\frac{N}{2} - k + 1)$, $\frac{N}{2} - 1$ operations to compute the overall sum and, at the end, one addition operation is required to subtract $\frac{N+2}{4}$. Furthermore, the evaluation of $Y(k)$ needs $Nlog_2(N)$ operations using the Fast Fourier Transform (FFT) algorithm. The overall number of operations needed by T_p is $\mathcal{C}(T_p)$:

$$\mathcal{C}(T_p) = \mathcal{O}(N(2 + log_2(N)) \tag{4.52}$$

To obtain the decision of T_{or}, we have to previously find T_p and T_n. Since those two test statistics have the same complexity, therefore, the complexity of T_{or} becomes the double of that of T_p except for the calculus of the FFT which should be evaluated once. Then the complexity of T_{or}, $\mathcal{C}(T_{or})$, becomes:

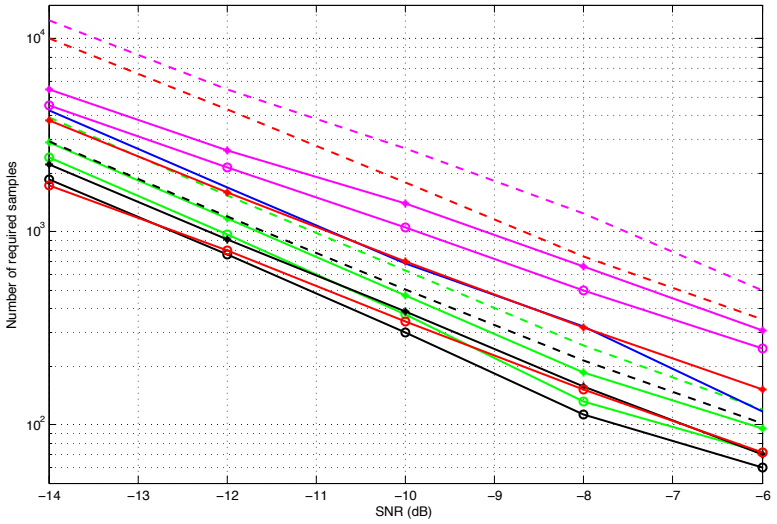
$$\mathcal{C}(T_{or}) = \mathcal{O}(N(4 + log_2(N)) \tag{4.53}$$

The complexity of T_{av} is similar to T_{or}:

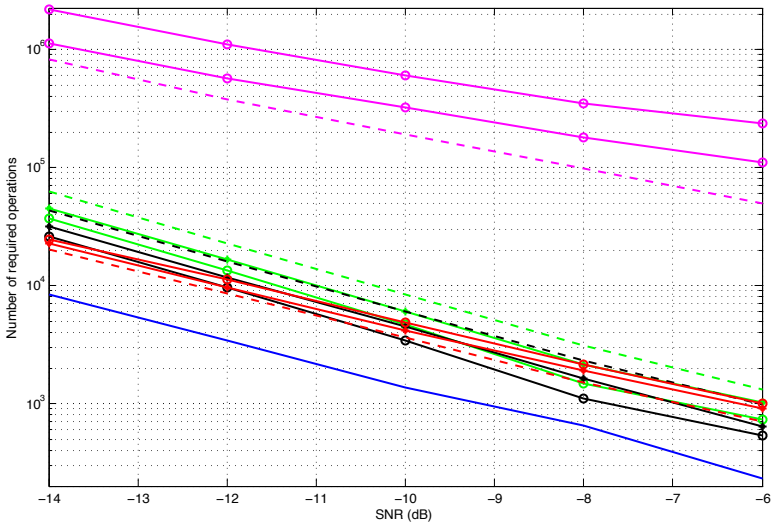
$$\mathcal{C}(T_{av}) = \mathcal{O}(N(3 + log_2(N))) \tag{4.54}$$

According to equations (4.53) and (4.54), the complexity of T_{or} and T_{av} are independent of the number of samples per symbol N_s, contrary to CSD and ACD where their complexities depend on N_s (as shown in equations (2.52) and (2.53)). As shown previously, increasing the oversampling rate leads to obtain a robust performance for T_{or}, T_{av}, CSD and ACD, while the performance of ED is not affected by the oversampling rate.

Figure (4.8) shows the number of samples and the complexity of the various detectors in terms SNR for a target $(p_{fa}; p_d) = (0.1; 0.9)$ under a Gaussian channel. As shown in figure (4.8(a)), T_{or} and T_{av} need a number of samples less than that of ED and CSD, in order to reach the target probabilities. In contrast, for $N_s = 8$ sps, ACD needs less observed samples than T_{av} when the SNR < -12 dB. However, for all the examined detector (except ED), the required number of samples decreases with an increasing N_s. Figure (4.8(b)) shows the number of performed operations corresponding to the number of required samples given in figure (4.8(a)). The complexity of T_{or} and T_{av} decreases inversely to N_s due to the fact that the number of required samples decreases with an increasing N_s. Contrariwise, the complexities of CSD and ACD grow with N_s even if the total number of samples decreases, this is because the complexities of CSD and ACD depend on N_s. On the other side, our proposed detectors are slightly more complicated than ED, and they have similar complexity to ACD. Consequently, our proposed detectors need a shorter observation window, while they are of moderate complexity relative to ED, CSD and ACD.



(a) Number of Samples



(b) Number of required operations



(c)

FIGURE 4.8: (a): The number of samples needed by the detectors in order to reach $(p_{fa}; p_d) = (0.1; 0.9)$ for various SNR and (b): the number of required operations performed by each detectors corresponding to the number of samples given in (a)

4.7 Robustness of our proposed detectors under Noise Uncertainty

This section deals with the Noise Uncertainty (NU) problem related to the estimation error of the noise variance. In fact, due to many factors (such as thermal noise, ambient interference, receiver non-linearity, *etc.*), the noise variance may be not estimated accurately. NU may prevent the detector from reaching a target (p_{fa}, p_d) even with a large observation time. According to equation (4.12), the noise variance should be pre-estimated in order to perform the normalization. That means our proposed detectors are sensitive to the estimation of the noise variance. In this section, the impact of the NU on the robustness of our proposed detectors is evaluated.

The estimated noise variance $\hat{\sigma}_w^2$ can be bounded as follows:

$$\hat{\sigma}_w^2 \in \left[\frac{1}{r}\sigma_w^2; r\sigma_w^2\right] \tag{4.55}$$

σ_w^2 is the nominal value of the noise variance and $r \geq 1$ stands for the NU factor. The distribution of $\hat{\sigma}_w^2$, $f_{\hat{\sigma}_w^2}(\hat{\sigma_w^2})$, is assumed to be uniform in a logarithmic scale.

$$f_{\hat{s}}(\hat{s}) = \begin{cases} \dfrac{1}{2\rho}, & s-\rho \leq \hat{s} \leq s+\rho \\ 0, & elsewhere \end{cases} \tag{4.56}$$

Where $s = 10\log_{10}(\sigma_w^2)$, $\hat{s} = 10\log_{10}(\hat{\sigma}_w^2)$ and $\rho = 10\log_{10}(r)$.

To show the effect of the noise uncertainty on the proposed detectors, we evaluate numerically the performance loss $\Delta p_d = p_d(0) - p_d(\rho)$ where $p_d(0)$ stands for the case where there is no NU, and $p_d(\rho)$ stands for probability of detection for the case where NU is equal to ρ dB. Figure (4.9) presents Δp_d of our detectors and ED for $p_{fa} = 0.1$, N=1000 samples, SNR of -10 dB and $N_s = 3$ sps. As shown in this figure, our detectors are less sensitive to the noise uncertainty than the energy detector for $p_{fa} = 0.1$. T_a is most affected detector by NU while T_p is the least one. However, T_{or} and T_{av} have a similar performance loss.

Spectrum Sensing based on Self Normalized CPSD :

As discussed previously, the normalization by the noise variance (equation (4.12)) leads to a possible noise uncertainty problem. In order to avoid this problem, a slightly modified model of the proposed detectors is introduced. Instead of normalizing the CPSD by the

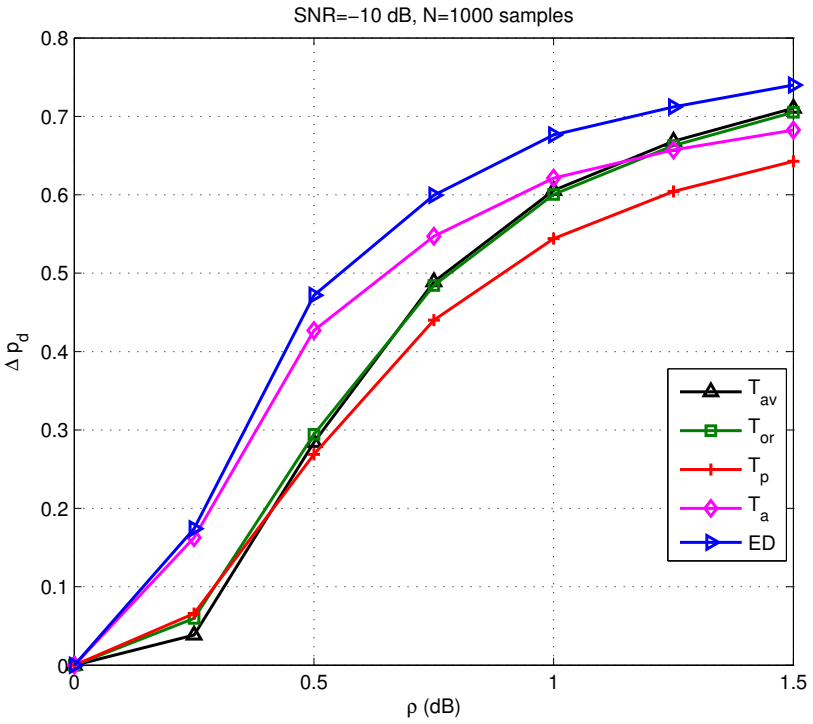


FIGURE 4.9: Performance loss of p_d in terms of noise uncertainty for $p_{fa} = 0.1$

mean value of the last term of $CP_w(k)$, the CPSD is normalized using the last term. The self normalized CPSD of the received signal, $y(n)$, is defined as follows:

$$\eta_y(k) = \frac{CP_y(k)}{CP_y(l)}; \quad v \leq k \leq l \tag{4.57}$$

For $[v; l] = [-\frac{N}{2} + 1; \frac{N}{2}]$, $CP_y(\frac{N}{2})$ is the estimated energy of the received signal. Using Parseval's theorem, $CP_y(\frac{N}{2})$ becomes:

$$\begin{aligned} CP_y\left(\frac{N}{2}\right) &= \frac{1}{N} \sum_{k=-\frac{N}{2}+1}^{\frac{N}{2}} |Y(k)|^2 \\ &= \sum_{n=1}^{N} |y(n)|^2 \end{aligned} \tag{4.58}$$

This normalization is equivalent to a scaling and does not change the shape form of the CPSD.

Without taking into account the relative position of $\eta_y(k)$ with respect to the reference straight line, the decision about the presence of the PU signal is made by comparing the $\eta_y(k)$ shape to the reference line shape. Figure (4.10) shows $\eta_y(k)$ under H_0 and H_1 and

a SNR = 0 dB for various values of N_s. We have under H_0 a shape looks like a straight line, but a curved shape under H_1. As shown in this figure, the difference between $\eta_y(k)$ and the straight line increases as N_s increases, which means the detection becomes more reliable with the increasing of N_s.
Similarly to the detectors T_p, T_a, T_{or} and T_{av}, we define the Self-Normalization detectors: T_p^s, T_a^s, T_{or}^s and T_{av}^s as follows respectively:

$$T_p^s = \sum_{k=1}^{\frac{N}{2}} \left| \eta_y(k) - D\left(1, \frac{N}{2}; k\right) \right| \tag{4.59}$$

$$T_a^s = \sum_{k=-\frac{N}{2}+1}^{\frac{N}{2}} \left| \eta_y(k) - D\left(-\frac{N}{2}+1, \frac{N}{2}; k\right) \right| \tag{4.60}$$

$$T_{or}^s = OR(d_{T_p^s}, d_{T_n^s}) \tag{4.61}$$

$$T_{av}^s = \sum_{k=1}^{\frac{N}{2}} \left| \eta_y^{av}(k) - D\left(1, \frac{N}{2}; k\right) \right| \tag{4.62}$$

Where $\eta_y^{av}(\nu)$ is given by:

$$\eta_y^{av}(k) = \frac{\sum_{u=1}^{k} P_y^{av}(u)}{\sum_{u=1}^{\frac{N}{2}} P_y^{av}(u)} \tag{4.63}$$

Figure (4.11) shows the performance of proposed detectors under a NU of 0, 0.75, and 1.5 dB with $N_s = 4$ sps, SNR of -10 dB and $N = 1000$ samples under a Gaussian channel. For a NU = 0 dB, T_{av}, T_{or} outperform T_{av}^s and T_{or}^s respectively. Beside that, when the NU grows, the performance of T_{av}^s, T_{or}^s is not affected, whereas the detectors T_{av}, T_{or} and ED suffer a performance degradation and become less robust than the self normalization detectors, as shown in figures (4.11(b)) and (4.11(c)). However, T_{av} and T_{or} have a superior performance relative to ED for different values of ρ.

4.8 Conclusion

In this chapter, we proposed Spectrum Sensing detectors based on the Cumulative Power Spectral Density (CPSD). The proposed detectors are based on the shape of the received signal CPSD.
The negative and the positive frequencies PSD one are exploited to perform Hard and soft schemes. These two schemes lead to enhance the detection performance. False alarm and detection probabilities are derived analytically under both Gaussian and Rayleigh

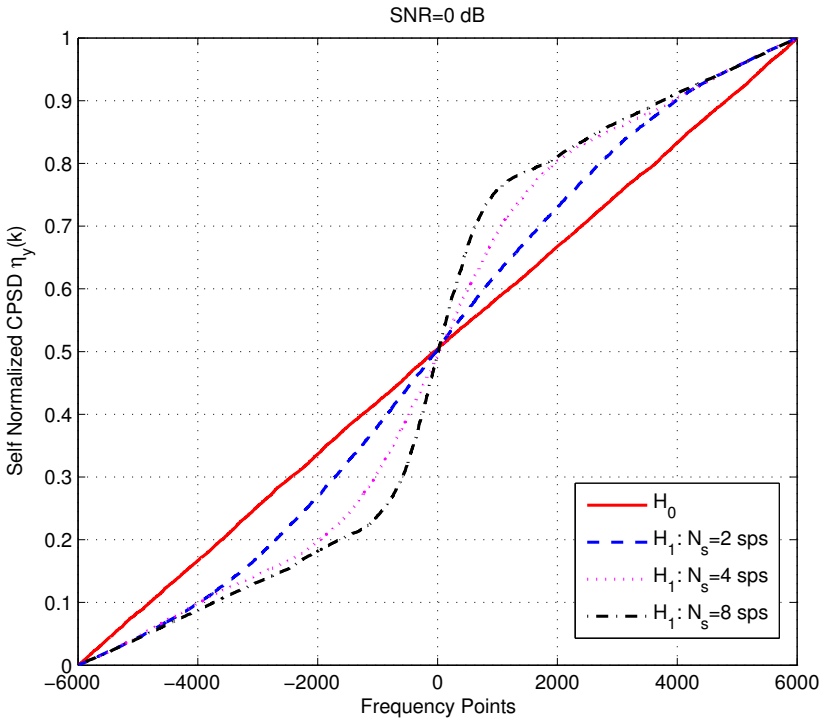
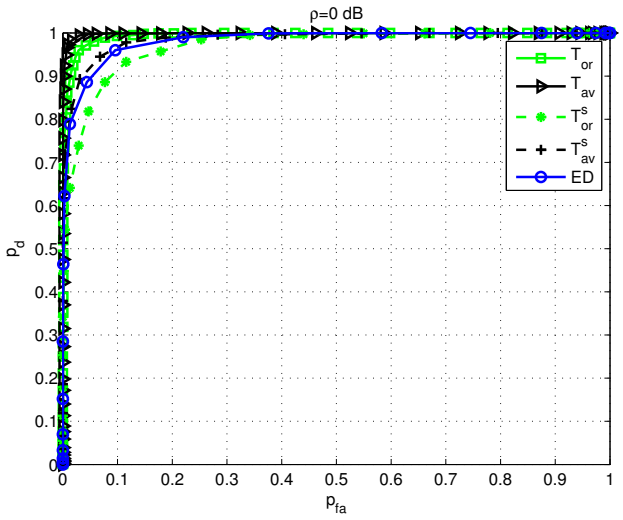


FIGURE 4.10: Self normalized CPSD under H_0 and H_1

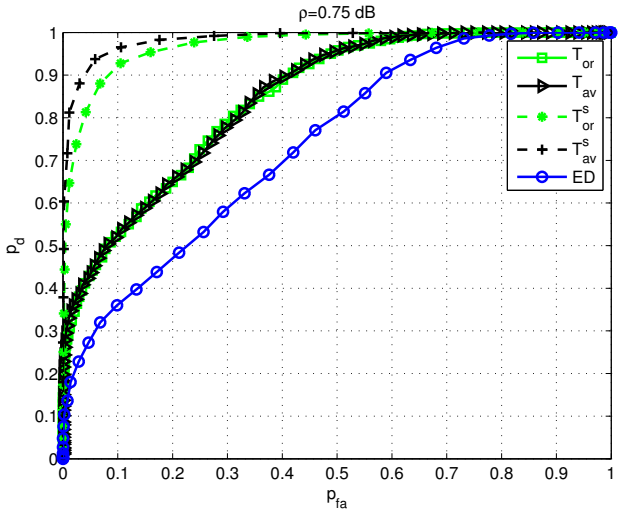
flat fading channels. Our simulation results corroborate the performance superiority of our detectors comparing to classic detectors such as the energy, the cyclostationary and the autocorrelation detectors.

In addition, simulation results show that the proposed detectors are less affected by the noise uncertainty than the energy detector. However, to avoid the impact of the noise uncertainty, the measured CPSD is normalized by the estimated energy of the received signal. By doing this, we make our detectors independent from the noise variance.

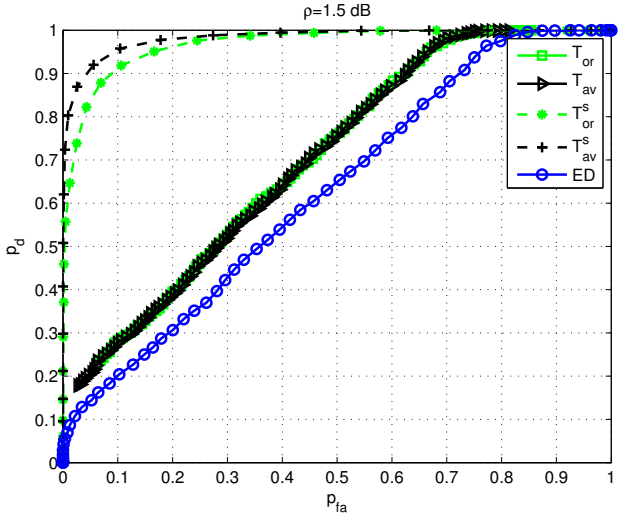
In a future work, the windowing effect of the PSD will be tested in the Spectrum Sensing context. Further, enhancing the PSD estimator performance and extending our algorithms to deal with Multiple Antennas Spectrum Sensing are the perspectives of this work continuity.



(a) $\rho = 0$ dB



(b) $\rho = 0.75$ dB



(c) $\rho = 1.5$ dB

FIGURE 4.11: ROC curves of the proposed schemes under various values of NU, N=1000 samples and SNR=-10 dB

Chapter 5

Full-Duplex Cognitive Radio

List of Acronyms

AC Auxiliary Chain

ADC Analogue to Digital Converter

CR Cognitive Radio

DFT Discrete Fourier Transform

ED Energy Detector

FD Full-Duplex

FD-CR Full-Duplex Cognitive Radio

FFT Fast Fourier Transform

GN Gaussian Noise

HD Half-Duplex

HD-CR Half-Duplex Cognitive Radio

HD-CR Half-Duplex Cognitive Radio

HIM Hardware Imperfections Mitigation

LNA Low-Noise Amplifier

LSE Least-Square Error

MAS Multi-Antenna System

NLD Non-Linear Distortion

OFDM Orthogonal Frequency Division Multiplex

PDR Probability of Detection Ratio

PN Phase Noise

PSD Power Spectral Density

PU Primary User

ROC Receiving Operating Characteristics

RSI Residual Self Interference

SI Self Interference

SIC Self Interference Cancellation

SNIR Signal to Noise and Interference Ratio

SNR Signal-to-Noise Ratio

SOAO Shared Oscillator between Auxiliary and Ordinary Chains

SoI Signal of Interest

SU Secondary User

TS Test Statistic

This chapter deals with Full-Duplex Cognitive Radio (FD-CR). FD-CR can eliminate the silence period of the Secondary User (SU) during the Spectrum Sensing. Thus, SU should be able to diagnose the channel status while it is transmitting. Consequently the channel throughput is enhanced. This throughput gain comes at the cost of a perfect cancelling of Self Interference (SI), which is the image of the SU signal at the receiving antenna. To achieve a robust SI Cancellation (SIC), many challenges should be addressed.

Similarly to the Full-Duplex transceiver, which is proposed to double the channel efficiency by simultaneously transmitting and receiving at the same band, the main challenge in FD functioning consists in minimizing the Residual Self Interference (RSI) which represents the SIC error and the receiver impairments (such as the oscillator Phase Noise

(PN), the Non-Linear Distortion (NLD) of the receiver Low-Noise Amplifier (LNA), the Analog to Digital Converter (ADC) noise *etc*).

This chapter addresses the above mentioned problems by analytically evaluating the impact of the additive RSI on the Spectrum Sensing performance. A model of the receiver of the FD system is also proposed, to mitigate both the PN and the NLD of LNA. Our new receiver model can totally omit PN. For the NLD, a new wire channel is added to connect the transmitting to the receiving chains. This channel is used only off-line to estimate the NLD coefficients without affecting greatly the throughput of the transceiver according to the fact that the NLD coefficients vary slowly with time. Therefore the time between two estimation operations can be relatively long. In order to test the overall efficiency of the proposed techniques, a performance analysis on the Full-Duplex Cognitive Radio (FD-CR) with all FD receiver impairments is presented. In Cognitive Network, SU should be aware of the Primary User (PU) activity. In FD-CR the RSI represents an important challenge for the SU to make a decision on the presence of PU. Minimizing RSI impacts positively both the detection performance and the CR throughput. Various simulations are carried out to illustrate the performance and the efficiency of our proposed FD receiver model. Our simulations show the superiority of the proposed FD model compared to recently proposed and classical models. [1], [2].

5.1 Introduction

Full-Duplex (FD) communication has recently gained a lot of attention due to its capability to double the channel efficiency. FD is not a new concept in the telecommunication field, but several problems such as receiver imperfections and channel estimation have limited the application of FD. The recent advances in both the Self-Interference Cancellation (SIC) and the Hardware Imperfections Mitigation (HIM) techniques make the FD applicable. Reducing the residual Self-Interference to the Noise Floor is the main challenge of any SIC and HIM techniques, in a classical FD transceiver.
To achieve an efficient SIC, passive suppression and active cancellation are both considered. The passive suppression can be related to many factors that can reduce the Self Interference (SI) in Radio-Frequency domain, such as the transmission direction, the absorption of the metals and the distance between the transmitting antenna, T_X, and the receiving antenna, R_X. On the other hand, the active cancellation reduces the Self-Interference (SI) by using a known copy of the transmitted signal. In general, the

[1] Part of this chapter was published in CrownCom 2016 [27] and as chapter in Springer Book [81]
[2] Part of this work was submitted to EURASIP Journal on Wireless Communication and Networking (EUARSIP JWCN) [82]

received signal at R_X contains the SI and the Signal of Interest (SoI). The main aim of the FD system is to eliminate completely SI in order to get purely SoI. Here, the problem is the very low power of SoI relative to SI due to the short distance between T_X and R_X and, generally, the long distance between the SoI transmitter and R_X. The estimation of channel coefficients between T_X and R_X becomes, in this case, an essential factor in the active cancellation process. Any error in the channel estimation can decrease the SIC gain.
Besides that, experimental results show that hardware imperfections such as the non-linearity of amplifiers and the oscillator Phase Noise (PN) are the main limiting performance factors [22, 86–88] since they affect the channel estimation process and add residuals to the received signal. These residuals are of considerable power relative to SoI since they are related to the SI power which is highly greater than the power of SoI. Therefore, the SIC should also consider the receiver imperfections.

To eliminate the PN effects, many works have been proposed [86, 89]. In [89], FD transceiver architecture is proposed to reduce the PN effects. The transmitting and receiving chains of the transceiver share the same oscillator to alleviate the PN. Sharing the same oscillator is feasible in such a situation since the two chains are collocated. In [86], a receiver Auxiliary Chain (AC) is introduced in the transceiver architecture. AC becomes a reference for Ordinary Chain (OC), which helps eliminating the hardware imperfections. However, in the proposed transceiver architecture, AC and OC share the same oscillator. Such an architecture leads to eliminate the principal frequency component of the PN. The work of [90] handles PN problem with separate oscillators and a negligible gain was obtained.

To estimate the channel and the NLD of LNA, an algorithm is proposed in [91] and developed in [86]. This algorithm requires two training symbol periods. During the first period, the channel coefficients are estimated in the presence of the NLD. The non-linearity of the amplifier can be found in the second period using the previously estimated channel coefficients. Of course, the estimated NLD parameters in the second phase depend on the estimated channel coefficients of the first phase. However, the estimation of the channel coefficients in the first phase depends on the unknown NLD parameters. To solve the previous dilemma, we propose hereinafter an estimation method which reduces the effect of LND on the channel estimation.

In FD-CR, SU is assumed to have two antennas T_X and R_X, the first one is for transmitting data whereas the second one stands for receiving data (see figure (5.1)). SU aims

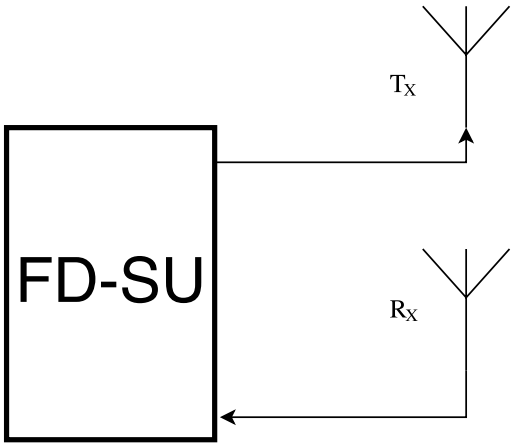


FIGURE 5.1: The model of SU in FD-CR

at eliminating the SI coming from T_X to R_X in order to perform an accurate Spectrum Sensing. This is similar to a classical SIC problem, where in the case of FD-CR, the RSI affects the Spectrum Sensing robustness.
To show the effect of RSI on the Spectrum Sensing in the context of FD-CR, analytic relationship between the detection, p_d, and the false alarm, p_{fa}, probabilities under HD and FD are derived. [23–26, 43, 56] deal with the application of FD in CR. In [23–25, 43], the RSI is modelled as a linear combination of the SU signal without considering hardware imperfections. In [24, 56] the Energy Detection (ED) is studied in FD mode and the probability of detection, (p_d), and false alarm, p_{fa}, are found analytically. However, these works did not develop any analytic relationship between the RSI, p_d and p_{fa} for both HD and FD mode.

Using the works of [86] a new FD transceiver architecture is proposed, where OC and AC are sharing the same oscillator to suppress completely the receiver PN. Notice that in [86] only the principal component of PN in frequency-domain is eliminated. Numerical results show the reliability of our proposed architecture in eliminating the PN effect. This fact ensures a reliable channel estimation, then an accurate SIC process is performed. Another hardware imperfection, the NLD of the LNA, is also considered. To well estimate the NLD coefficients, we propose a new circuit architecture that can work off-line. In this case, the data rate of the FD transceiver is not affected since the period between two successive operations of NLD coefficients estimations is relatively long thanks to the fact that these coefficients slowly change with time.

This chapter is organized as follows, in section (5.2), an overview on the OFDM receiver is presented by focusing on the circuit imperfections. In section (5.3), the effect of the additive distortion due to the SIC operation is analysed. A new architecture of the FD

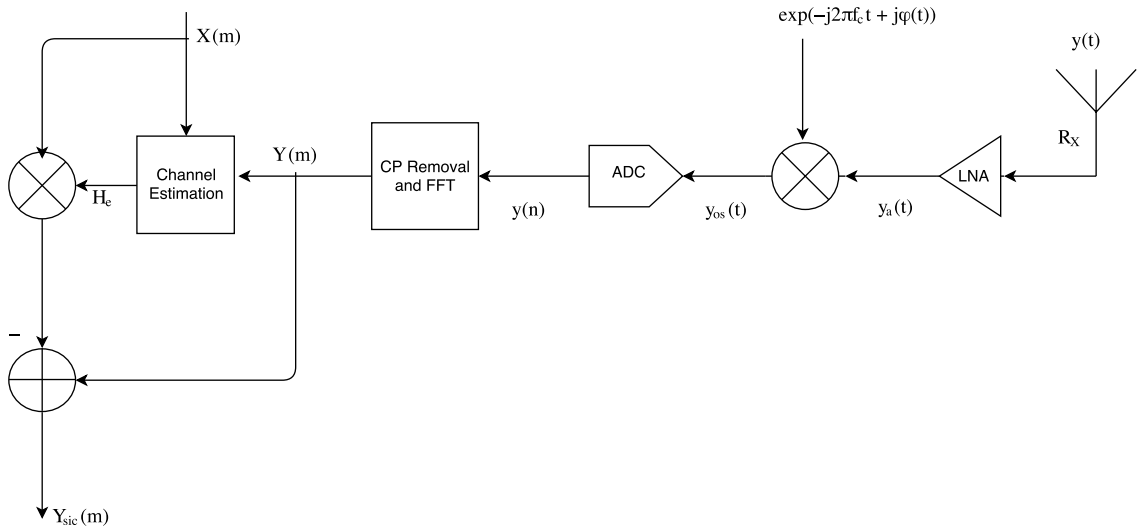


FIGURE 5.2: Classical FD OFDM receiver

transceiver is presented in section (5.4). This architecture aims at eliminating the PN effect of the oscillator in the receiver chain. Section (5.5) deals with NLD of the LNA by presenting a proposed architecture to reduce the distortion power. The efficiency of the proposed architecture is tested and examined by intensive simulations. In section (5.6), the proposed Full-Duplex Cognitive Radio architecture is presented to show its efficiency where the SIC is of high level. At the end, section (5.7) concludes the chapter.

5.2 System model and Receiver chain Imperfection Analysis

By assuming perfect filters, figure (5.2) presents the Ordinary Chain (OC) of an OFDM Receiver block diagram system. The received signal by the OC is a mixture of the Self-Interference (SI) signal and the Signal of Interest (SoI) (if it exists). The signal received at R_X is modelled as:

$$\begin{aligned} y(t) &= h(t) \otimes x(t) + \eta s(t) \\ &= h(t) * [x_t(t) \exp(j2\pi f_c t)] + \eta s(t) \end{aligned} \tag{5.1}$$

where $h(t)$ is the channel effect between T_X and R_X, f_c is the carrier frequency, $x(t)$ is the transmitted SI signal, $x_t(t)$ is the base-band SI, $s(t)$ is the SoI, involving the channel effects, η is the channel indicator ($\eta = 0$ if the SoI is absent, otherwise $\eta = 1$), and *otimes* stands for the convolution product.

In the following, SoI is assumed to be absent during the estimation period. As LNA introduces a NLD, the output $y_a(t)$ of LNA can be modelled in general form as a polynomial of odd degrees [92]:

$$y_a(t) = \sum_{i=0}^{\infty} a_{2i+1} y^{2i+1}(t) \tag{5.2}$$

The first coefficient a_1, stand for the linear output component of LNA. The other coefficients ($a_{2i+1},\ i \geq 1$) stand for the non-linear components contributing in NLD. Since the higher components are of negligible power, the LNA output is limited to the third order polynomial output [86, 91]. In this case, $y_a(t)$ can be simplified as:

$$\begin{aligned} y_a(t) &= a_1 y(t) + a_3 y^3(t) \\ &= a_1 \Big(h(t) \otimes x(t) \Big) + a_3 \Big(h(t) \otimes x(t) \Big)^3 \end{aligned} \tag{5.3}$$

After the amplification process, the received signal is down-converted to the base-band form using the oscillator. This oscillator introduces a Phase Noise (PN) $\phi(t)$:

$$y_{os}(t) = y_a(t) exp(-j2\pi f_c t) p(t) \tag{5.4}$$

where $p(t) = \exp(j\phi(t))$ is the multiplicative PN.
In the base-band, the Analog-to-Digital Converter (ADC) digitizes the received signal by introducing a uniform noise, $w_d(n)$ with a power inversely proportional to the number of used bits. Consequently, the received time-domain base-band signals at the output of OC becomes:

$$y(n) = \Big(a_1 h(n) \otimes x(n) + a_3 d(n) \Big) p(n) + w_d(n) + w(n) \tag{5.5}$$

where:

$$d(n) = \Big(h(n) \otimes x(n) \Big) \Big| h(n) \otimes x(n) \Big|^2 \tag{5.6}$$

and $w(n)$ is the Gaussian Noise (GN) in the OC, and it is related to the input signal power and to the Noise Figures of the blocks in the receiver chain.

After the CP removal and FFT operations, the frequency domain signal, $Y(m)$, of $y(n)$ is presented by:

$$Y(m) = (a_1 H(m) X(m) + a_3 D(m)) \otimes P(m) + W_d(m) + W(m) \tag{5.7}$$

$$\tag{5.8}$$

Where $P(m)$, $D(m)$, $W_d(m)$ and $W(m)$ are the Discrete Fourier Transforms (DFTs) of $p(n)$, $d(n)$, $w_d(n)$ and $w(n)$ respectively.
Since a copy of the SI signal, $X(m) = DFT\{x(n)\}$, is known for the receiver, the channel effect $H(m)$ can be estimated by $H_e(m)$ as follows:

$$H_e(m) = \frac{Y(m)}{X(m)} = \frac{\Big(a_1 H(m)X(m) + a_3 D(m)\Big) \otimes P(m) + W_d(m) + W(m)}{X(m)} \tag{5.9}$$

For an ideal receiver (*i.e.* $P(m) = \delta(m)$ ($\phi(n) = 0$), $a_3 = 0$ and $W_d(m) = 0$), $W(m)$ becomes the only limiting performance factor and its effect can be reduced using the averaging estimator of the channel:

$$H_e(m) = \frac{1}{N_t} \sum_{k=1}^{N_t} \frac{Y^k(m)}{X^k(m)} \tag{5.10}$$

Where N_t is the number of training symbols used to estimate the channel and $Y^k(m)$ (resp. $X^k(m)$) represents the kth symbol of $Y(m)$ (resp. $X(m)$).
However, once the channel estimation is done, the Self-Interference is regenerated in order to cancel its effect from the received signal and obtain the resulting signal $Y_{sic}(m)$:

$$Y_{sic}(m) = Y(m) - H_e(m)X(m) \tag{5.11}$$

The main challenge of a FD system is to evaluate accurately $H_e(m)$ in order to cancel the Self-Interference effect. As shown in Equation (5.10), this can be done by eliminating the receiver imperfections, where the NLD of LNA and the oscillator PN play the main role in such a limitation.
In order to help the OC in eliminating these imperfections, an Auxiliary Chain (AC) is associated to OC. Acting as reference for OC, AC is connected via a wire to the transmitted chain, so that the channel effect is omitted.

5.3 The RSI effect on the Spectrum Sensing

By only focusing on the additive receiver distortion (*i.e.* the NLD of LNA, GN and ADC noise), the received signal after the SIC in frequency-domain can be given by:

$$Y_{sic}(m) = R(m) + W(m) + \eta S(m) \tag{5.12}$$

where $R(m)$ represents the total RSI due to the channel estimation error and the NLD of LNA. In order to decide the existence of the PU, the Energy Detector (ED) compares the received signal energy, T_{ED}, to a predefined threshold, λ.

$$T_{ED} = \frac{1}{N}\sum_{m=1}^{N} |Y_{sic}(m)|^2 \underset{H_0}{\overset{H_1}{\gtrless}} \lambda \tag{5.13}$$

By assuming the $i.i.d$ property of $R(m)$, $W(m)$ and $X(m)$, the distribution of T should asymptotically follow a normal distribution for a large number of samples, N, according to the Central Limit Theorem. Consequently, the probabilities of False Alarm, p_{fa}^F, and the Detection, p_d^F, under the FD mode can be obtained as follows (See Appendix (D)):

$$p_{fa}^F = Q\left(\frac{\lambda - \mu_0}{\sqrt{V_0}}\right) = Q\left(\frac{\lambda - (\sigma_w^2 + \sigma_d^2)}{\frac{1}{\sqrt{N}}(\sigma_w^2 + \sigma_d^2)}\right) \tag{5.14}$$

$$p_d^F = Q\left(\frac{\lambda - \mu_1}{\sqrt{V_1}}\right) = Q\left(\frac{\lambda - (\sigma_w^2 + \sigma_d^2 + \sigma_s^2)}{\frac{1}{\sqrt{N}}(\sigma_w^2 + \sigma_d^2 + \sigma_s^2)}\right) \tag{5.15}$$

Where μ_i and V_i are the mean and the variance of T_{ED} under H_i respectively, $i \in \{0; 1\}$, $\sigma_d^2 = E[|R(m)|^2]$ represents the RSI power, $\sigma_w^2 = E[|W(m)|^2]$ and $\sigma_s^2 = E[|S(m)|^2]$. The SNR, γ_s, is defined as:

$$\gamma_s = \frac{\sigma_s^2}{\sigma_w^2} \tag{5.16}$$

If the SIC is perfectly achieved, *i.e.* $\sigma_d^2 = 0$, p_{fa}^F and p_d^F take their expressions under the HD mode. Therefore, ROC curves represent under HD mode the asymptotes of ROC curves under FD mode.

Figure (5.3) shows the required number of samples to reach $p_d = 0.9$ and $p_{fa} = 0.1$ under the HD and FD modes for different values of SNR. In FD mode, we set $\sigma_d^2 = \sigma_w^2$ as the target values of σ_d^2 in digital communication. Figure (5.3) shows that the number of required samples slightly increases under the FD modes. For example, when $\gamma_s = -5$ dB, then 85 samples are enough to reach the target $(p_d; p_{fa})$ under the HD mode but under FD mode, around 300 samples are needed.

Let us define the Probability of Detection Ratio (PDR), δ, for the same probability of false alarm under FD and HD modes, as follows:

$$\delta = \frac{p_d^F}{p_d^H} \; with \; p_{fa}^F = p_{fa}^H = \alpha \tag{5.17}$$

Where p_d^H and p_{fa}^H are the probabilities of detection and false alarm under HD respectively, $0 \leq \alpha \leq 1$ and $0 \leq \delta \leq 1$. With an excellent SIC, the ROC can mostly reach in FD the same performance as HD. In order to show the effect of RSI on δ, let us define

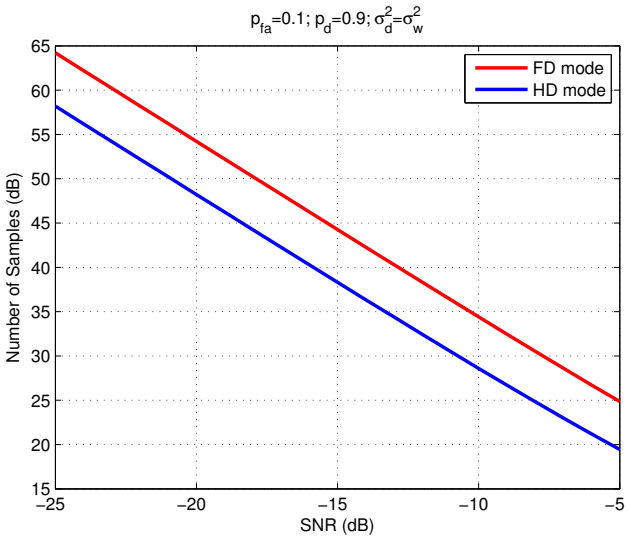


FIGURE 5.3: The number of samples required to reach $p_d = 0.9$ and $p_{fa} = 0.1$ with respect to SNR (dB)

the RSI to noise ratio γ_d as follows:

$$\gamma_d = \frac{\sigma_d^2}{\sigma_w^2} \tag{5.18}$$

Using (5.14) and (5.17), the threshold, λ, can be expressed as follows:

$$\lambda = \left(\frac{1}{\sqrt{N}} Q^{-1}(\alpha) + 1\right)(\sigma_w^2 + \sigma_d^2) \tag{5.19}$$

By replacing (5.19) in (5.15), γ_d can be expressed as follows:

$$\gamma_d = \frac{(1+\gamma_s)Q^{-1}(\delta p_d^H) - Q^{-1}(\alpha) + \sqrt{N}\gamma_s}{Q^{-1}(\alpha) - Q^{-1}(\delta p_d^H)} \tag{5.20}$$

If $\delta = 1$, then γ_d becomes zero which means that the SIC is perfectly achieved. Figure (5.4) shows the curves of γ_d for various values of PDR, δ, with respect to the SNR, γ_s, for $P_d^H = 0.9$ and $\alpha = 0.1$. This figure shows that as δ increases γ_d decreases. To enhance the PDR, the selected SIC technique should mitigate at most the SI. In fact, for $\gamma_s = -5$ and a permitted loss of 1% (*i.e.* $\delta = 0.99$), γ_d is about -15 dB

5.4 Phase Noise Analysis

In this section, a new receiver architecture to mitigate the PN effect is presented. Our proposed architecture is inspired from the one proposed in [86], SOAO (Shared Oscillator between AC and OC), where the same oscillator is shared between AC and OC (figure (5.5)).

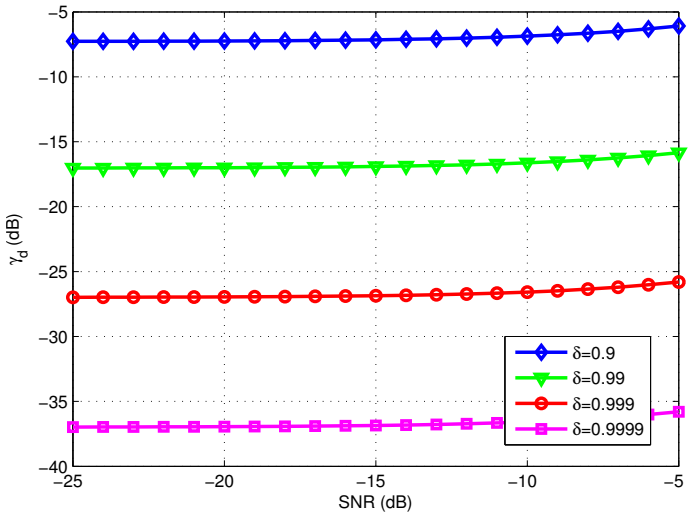


FIGURE 5.4: Evolution of γ_d with respect to the SNR γ_s, for various values of PDR δ, $(p_{fa}^H \ ; \ p_d^H) = (0.1 \ ; \ 0.9)$

In the following, a brief analysis of the SOAO architecture is given. Thanks to the same oscillator between OC and AC, the output $y_{os}^{AC}(t)$ of the oscillator at AC has the same PN as that of OC oscillator output, $y_{os}(t)$. $y_{os}^{AC}(t)$, can be modelled by:

$$y_{os}^{AC}(t) = x_t(t)p(t) \tag{5.21}$$

$x_t(t)$ is the time base-band model of $x(t)$. After converting the signal to the base-band, $y_{os}^{AC}(t)$ is digitized using an ADC, then the CP removal and FFT operations are applied in order to obtain the frequency-domain signal $Y_{aux}(m)$ used in the channel estimation process. Following the same process at OC, assuming the absence of SoI, and neglecting all the imperfections and noises other the PN at both AC and OC, $Y_{aux}(m)$ and $Y(m)$ becomes:

$$Y_{aux}(m) = X(m) \otimes P(m) \tag{5.22}$$

$$Y(m) = [H(m)X(m)] \otimes P(m) \tag{5.23}$$

The channel can be estimated by the following simple ratio:

$$\begin{aligned} H_e(m) &= \frac{Y(m)}{Y_{aux}(m)} = \frac{[H(m)X(m)] \otimes P(m)}{X(m) \otimes J(m)} \\ &= \frac{\sum_{k=1}^{N} H(k)X(k)P(m-k))}{\sum_{k=1}^{N} X(k)P(m-k)} \\ &= H(m) + \frac{\sum_{k=1}^{N} (H(k) - H(m))X(k)P(m-k)}{\sum_{k=1}^{N} X(k)P(m-k))} \end{aligned} \tag{5.24}$$

It is clear from equation (5.24) that the channel estimation depends on the PN bandwidth

TABLE 5.1: Simulations Parameters

Signal Bandwidth	20 MHz
Number FFT-points	64
QAM-Mapping	64
CP length	16
Number of Guard-Band point	11
Channel order	10
Power of the Non-LoS channel components	-20 dBc
Number of OFDM Symbols (N_s)	25
Number of training symbols, N_t, for channel estimation	4
Received SI power	-10 dBm

and power, in addition to the non-LoS components of the channel. $H(m)$ corresponds to the Line-of-Site (LoS) components of the channel, whereas the other components $H(k)$ ($k \neq m$) represent the Non-LoS ones. In fact, due to the convolution operation between PN and the SI signal in frequency-domain, the non-LoS components of the channel affect greatly the channel estimation of the LoS components. Note that the error in the channel estimation affects the SIC process since the SI has a very high power compared to SoI, and it can dominate the circuit impairments. Accordingly, reducing PN before estimating the channel is of high importance for the SI canceller. This was our first motivation to introduce a new receiver chain in the FD transceiver.

5.4.1 Proposed Architecture for PN suppressing

Figure (5.6) presents our proposed architecture to suppress the PN, OC and AC share the same oscillator as SOAO, so that PNs in OC and AC are the same. Since $x_t(t)$ is known to the receiver, the conjugate, $p^*(t)$, of $p(t)$ can be found as follows:

$$p^*(t) = \frac{y_{os}^{AC}(t)}{x_t(t)} \tag{5.25}$$

Due to the fact that the receiver's and the transmitter's circuits are collocated, $x_t(t)$ can be easily linked to the phase noise estimation block. In addition, the two inputs (*i.e.* $y_{os}^{AC}(t)$ and $x_t(t)$) can be synchronized using a tapped delay line. In our analysis, we assume that the synchronization is perfectly done.
Back to equation (5.25), once $p^*(t)$ is evaluated, then it is multiplied by $y_{os}(t)$ to eliminate the PN effect as shown in figure (5.6).

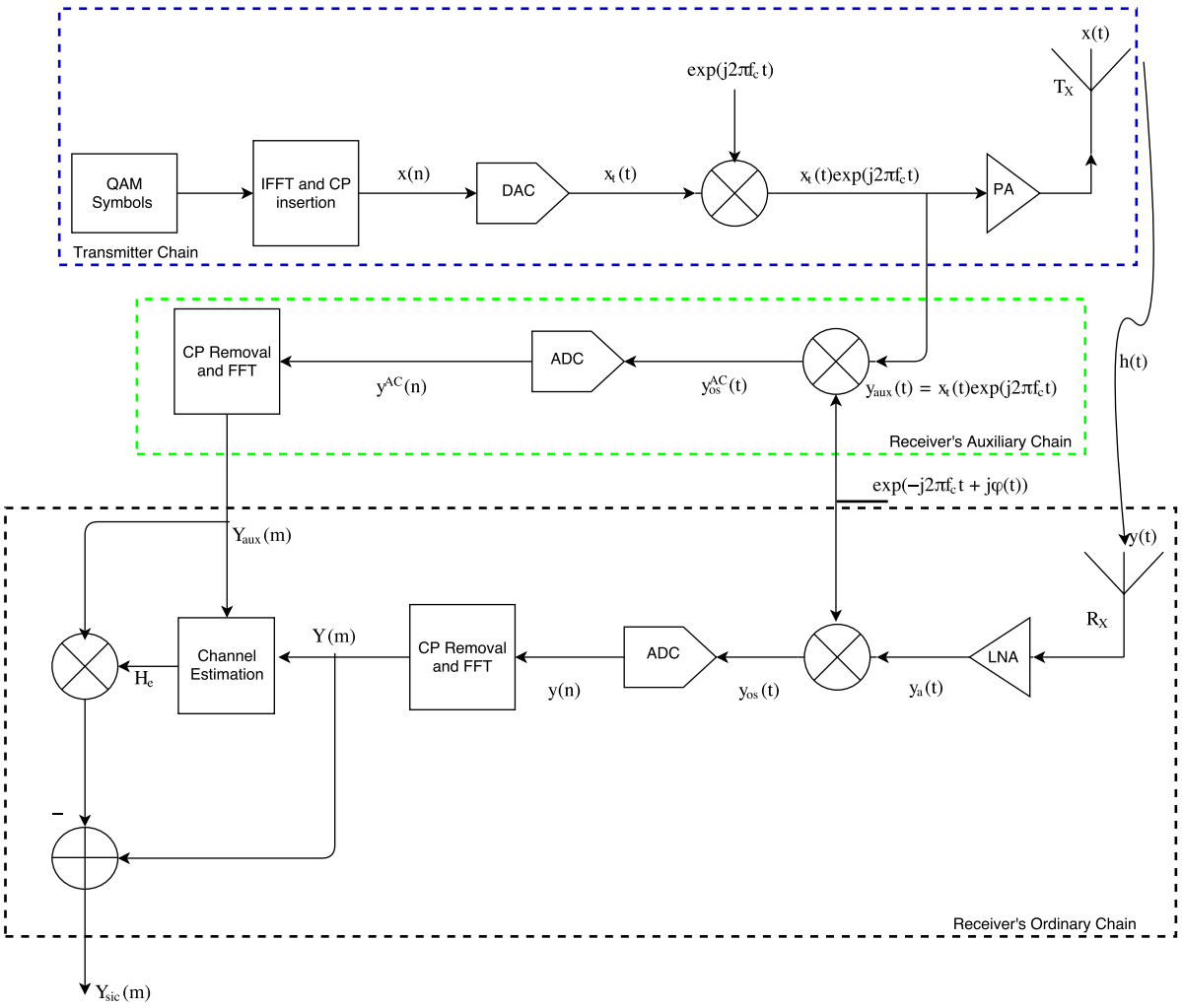


FIGURE 5.5: Receiver architecture for a FD OFDM to reduce Phase Noise [86]

Unlike the architectures presented in [89] and [86], the proposed solution is not affected by the PN noise power neither its bandwidth. Consequently, the channel estimation is done without any residual caused by the Non-LoS components of the channel due to the convolution with the PN as in equation (5.24).

5.4.2 Numerical Analysis

Figure (5.7) shows the Monte-Carlo simulations on the effect of the Non-LoS channel component power to the RSI power. It compares the RSI power resulted after using our PN suppressor to that of the classical SIC and SOAO [86]. These results are obtained by simulating an OFDM signal with 64 sub-carriers, a cyclic prefix length of 16 points and a 64-QAM mapping with a 53 useful OFDM points in each OFDM symbol, (as considered in the 802.11g standard [93]). The remaining simulation parameters are presented in

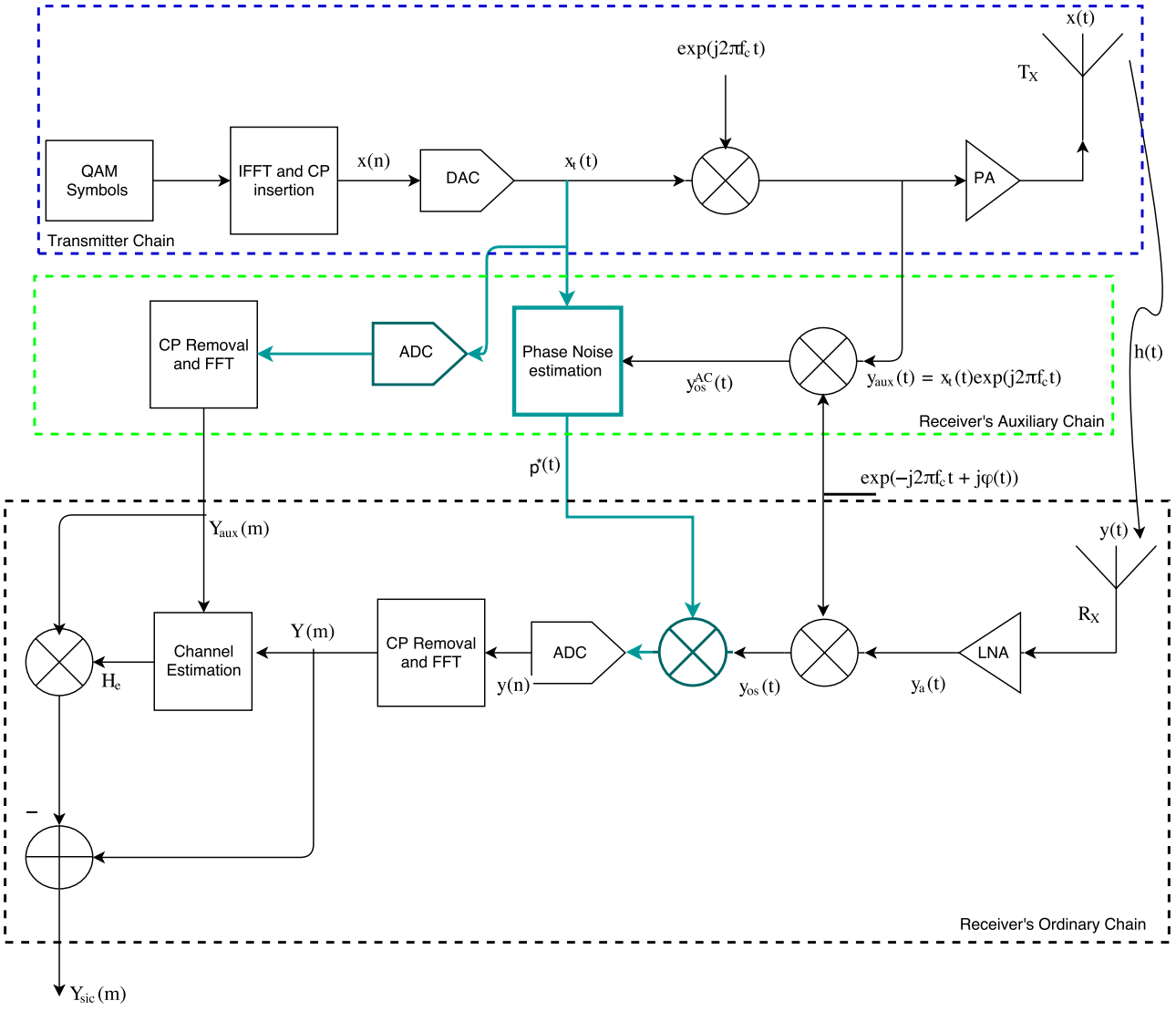


FIGURE 5.6: Proposed FD OFDM receiver architecture to suppress the Phase Noise effect, the conjugate of PN is estimated at AC, then it is multiplied by the output of the OC oscillator in order to suppress its effect.

table (5.1). The power and the frequency bandwidth of PN are set to -91 dBc/Hz and 20 KHz respectively, as the typical values of the transceiver NI 5644R [94].

Figure (5.7) shows the Non-LoS channel components effect on the RSI power when PN is the only considered imperfection. The classical SIC architecture (SIC is performed without PN Suppression (PNS)), SOAO and the proposed architecture. As shown in this figure, the proposed PN suppressor is not affected by the Non-LoS components power, while the classical SI canceller is slightly affected, and SOAO canceller exhibits a performance degradation with the increasing of the power of the Non-LoS components (about a 10 dB loss was observed for an increase of 10 dB in the Non-LoS channel components power.

In addition to the PN bandwidth, the PN power is considered as a performance limiting

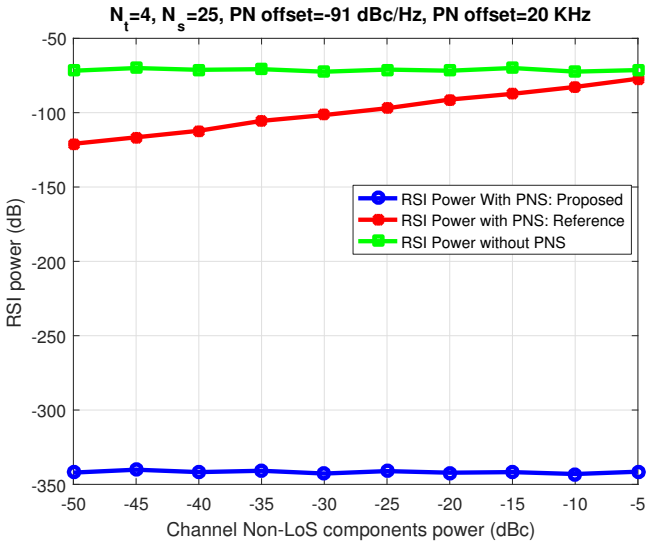


FIGURE 5.7: Effect of the Non-LoS components power on the RSI power

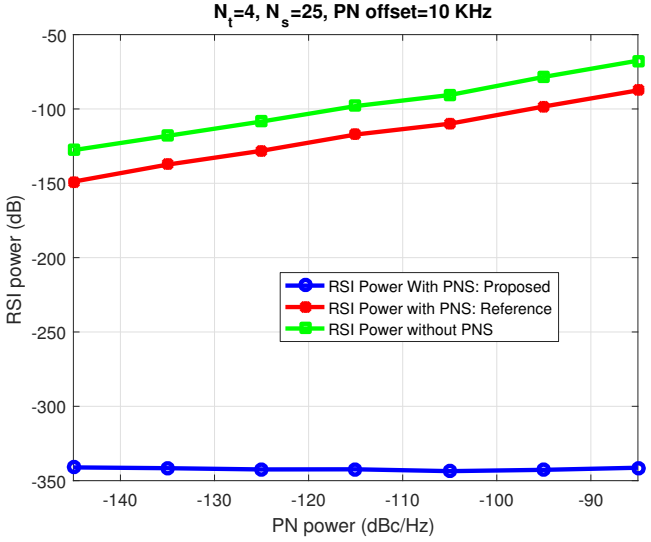


FIGURE 5.8: PN power effect on the RSI power. PN offset is fixed to 10 KHz

factor. In figure (5.8), RSI power is obtained in terms of the PN power for a fixed PN bandwidth (BW) to 10 KHz. Our algorithm keeps an almost zero RSI power. On the other hand, the RSI power corresponding to classical and SOAO cancellers increases with the PN power.

To show the effect of the PN frequency offset on the SIC performance, figure (5.9) presents the variation of RSI power for a PN power of -90 dBc/Hz and various values of PN frequency offsets. As shown in this figure, SIC residual increases with the frequency offset for the classical and SOAO SIC cancellers, while the proposed PN suppressor cancels almost totally the SI for all the considered values of the PN offsets.

Figures (5.7), (5.8) and (5.9) show that the performance of our proposed PN suppressor is not affected by the PN specifications neither by the Non-LoS of the channel since the

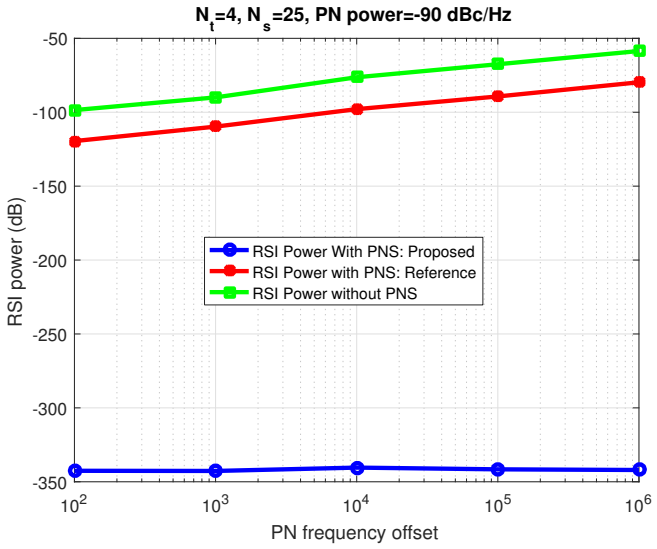


FIGURE 5.9: Effect of the PN offset on the RSI power. PN power is fixed to -90 dBc/Hz

PN is totally suppressed before estimating the channel, unlike the classical SI and SOAO suppressors.

In the following, we discuss the performance of the proposed PN suppressor (figure (5.6)) when the Gaussian Noise (GN) is present. $N_t = 4$, $N_s = 25$ are assigned in addition to a PN power of -91 dBc/Hz and PN BW of 20 KHz. The RSI power corresponding to our proposed architecture increases with the GN power as shown in figure (5.10), unlike the classical and SOAO ones. The latter two suppressors keep a constant RSI while the noise power is lower than a certain value. This is because the PN power (which is constant in this simulation) dominates the GN power before this values. After that, the RSI increases linearly (in dB scale) with the GN power. This limitation is caused by the channel estimation affected by GN, in other terms, if the channel is estimated perfectly, then RSI approaches zero for the proposed PN suppressor.

Figure (5.11) tests the capability of the classical, SOAO and the proposed suppressors to reach the GN level power in terms of the number of training symbols. Thus, this is the capability of how much the algorithm can cancel the SI in order to obtain the GN, this case refers to the perfect SIC. The GN power is fixed to -105 dB as a typical value in NI 5644R [94], and the other parameters are the same as in the previous simulations. As shown in figure (5.11), the total power of $Y_{sic}(m)$ decreases with the increase of N_t, and reaches 6 dB (resp. 4 dB) for $N_t = 4$ (resp. $N_t = 10$) comparing to the noise floor respectively. As also shown in this figure, our proposed receiver model reduces the RSI by 18 dB than SOAO and 40 dB than the classical models.

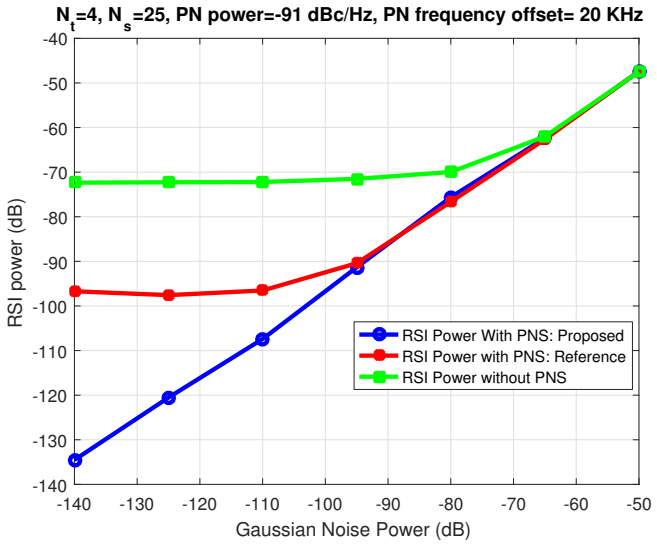


FIGURE 5.10: Effect of the Gaussian Noise on the RSI power

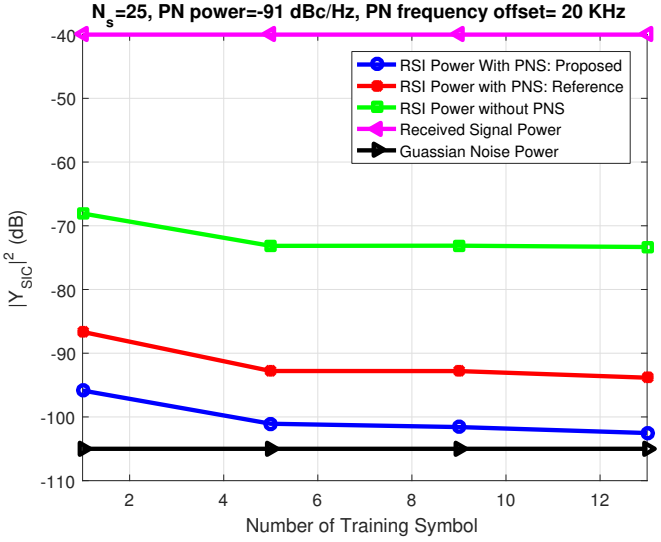


FIGURE 5.11: The variation of the RSI power in terms of the number of training symbols

5.5 The Non-Linear Distortion of the Low Noise Amplifier

The NLD of LNA is an important SIC performance limiting factor [22, 86–88, 91] in real world applications. According to equation (5.6), the distortion $D(m)$ contains the SI signal, the channel effect $H(m)$ and the non-linearity coefficient a_3. In this case, a_3 becomes hard to estimate even if the SI signal is known because the channel effect is unknown. This problem becomes more complicated in the presence of PN. On the other hand, NLD is considered as a limiting performance factor since it prevents a robust channel estimation process. In addition, even with a perfect channel estimation, NLD can dominate the SoI when the latter reaches R_X with a low power. Based on the above discussion, the suppression of NLD becomes a main aim for the FD system.

In [27], we introduced a Least Square Error (LSE) estimator to estimate the NLD coefficient. Even though this algorithm shows a good performance, the estimation process needs the estimation of high order cumulants of the received signal (order 2, 4 and 6) in RF domain (2.4 GHz for a WiFi signal). This fact may introduce a non-linearity in the electronic components used in the estimation process, which causes corruption to the estimation results.

A new receiver architecture is proposed here, associated with a Least Square (LS) algorithm that can be used to estimate the NLD of the LNA in digital frequency domain. The new receiver architecture introduces a new wire channel between the transmitter and the receiver. This wire channel may only be used when the NLD coefficients are needed. Figure (5.12) shows the block-diagram presented to overcome the channel effect. Since the LNA characteristics are changing slowly, because they are related to the circuit age and the temperature [86], then the estimation process will be repeated once every several transmitted frames. As shown in figure (5.12), when the switch is on (1), this means that the channel is working on ordinary conditions, where the channel between T_X and R_X is wireless. In such a situation, the NLD is hard to be identified due to the channel effect on the SI signal. To avoid such effect, the transmitter and the receiver may communicate a training sequence using a wire. In this case, the power splitter should control the power transmitted to the OC in order to avoid any saturation in the circuit.

LSE estimation :

Since the PN is totally suppressed using the architecture of (5.6), the received signal after the CP removal and the FFT operations is presented in frequency domain by:

$$Y(m) = a_1 X(m) + a_3 D_2(m) + W(m) \tag{5.26}$$

where $D_2(m) = DFT\{x(n)|x(n)|^2\}$. The quantization noise is neglected, since it is dominated by the GN. By applying the LS estimator on $Y(m)$, the following cost function $\mathcal{L}$ should be minimized with respect to u_1 and u_3, which are the estimations of a_1 and a_3 respectively.

$$\mathcal{L} = E\left[\Big(Y(m) - (u_1 X(m) + u_3 D_2(m))\Big) \Big(Y(m) - (u_1 X(m) + u_3 D_2(m))\Big)^*\right] \tag{5.27}$$

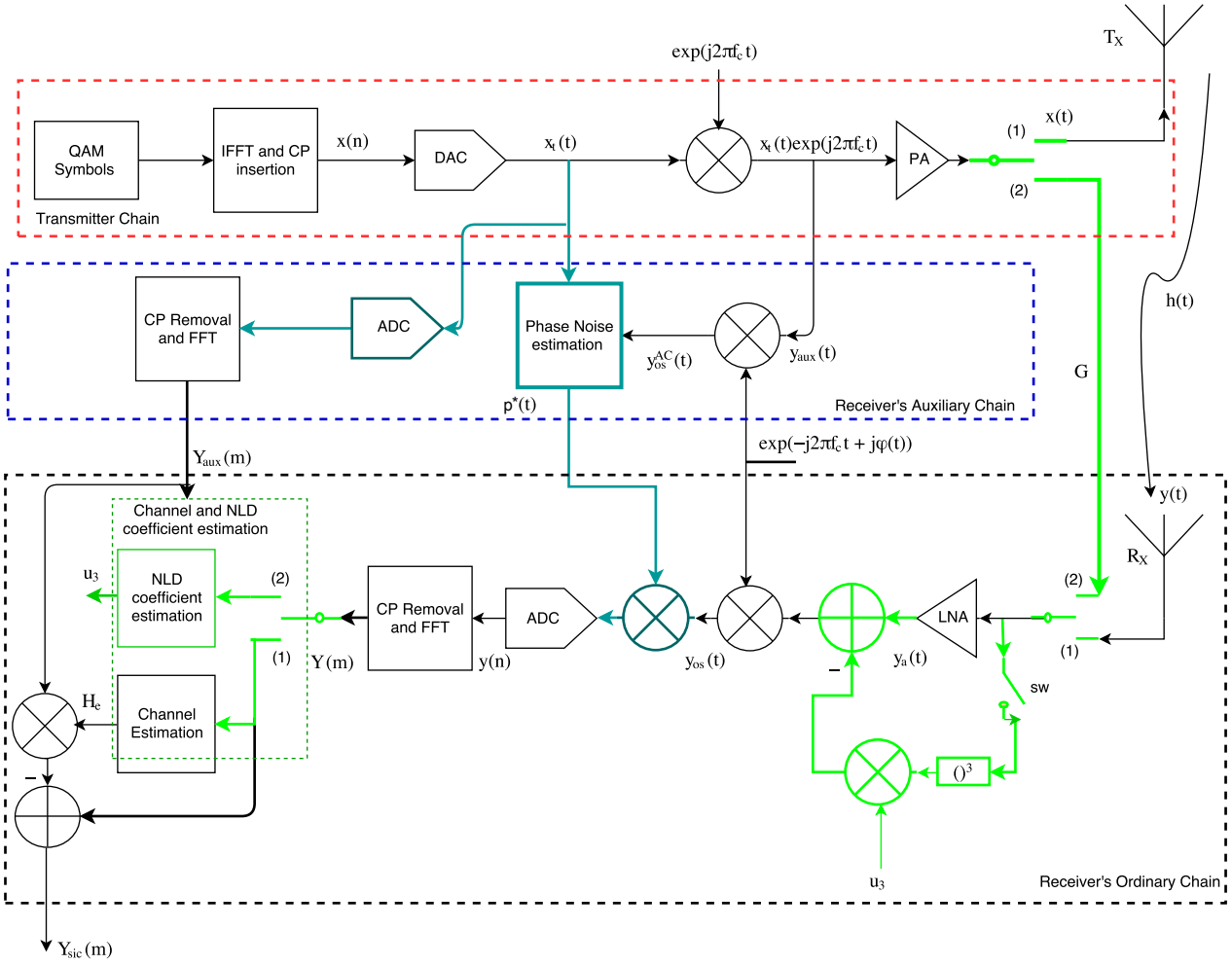


FIGURE 5.12: FD architecture capable to eliminate the receiver PN and to reduce the NLD of the receiver LNA. When the switches are on (2), the NLD coefficients are estimated by avoiding the wireless channel. When the switches are on (1), the transceiver works in ordinary conditions, and the circuit associated to LNA alleviates the NLD at the output of LNA

According to equation (5.27), GN is a performance limiting factor. Accordingly, the minimization of $\mathcal{L}$ leads to the following:

$$\begin{bmatrix} u_1 \\ u_3 \end{bmatrix} = U^{-1}V \tag{5.28}$$

where:

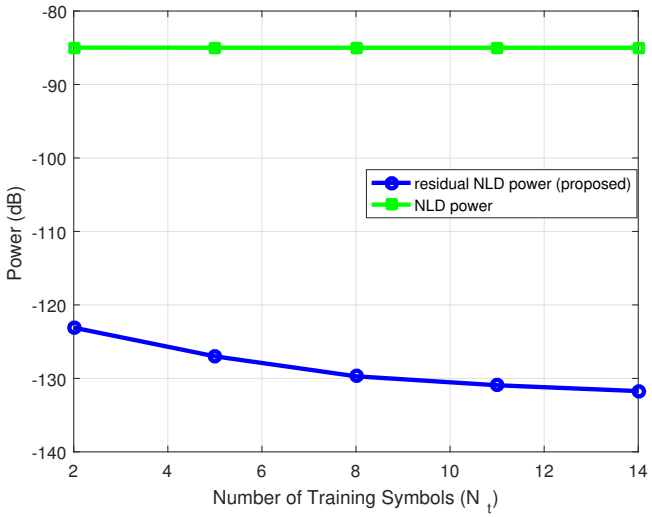


FIGURE 5.13: The power of the residual NLD in terms of the number of training symbols. NLD power is fixed to -45 dBc (*i.e.* -85 dB for a 0 dB gain of the LNA)

$$U = \begin{bmatrix} E\left[|X(m)|^2\right] & E\left[Re\{X(m)D_2^c(m)\}\right] \\ \left[Re\{X(m)D_2^c(m)\}\right] & E\left[|D_2(m)|^2\right] \end{bmatrix}; \tag{5.29}$$

$$V = \begin{bmatrix} E\left[Re\{X^c(m)Y(m)\}\right] \\ E\left[Re\{D_2^c(m)Y^c(m)\}\right] \end{bmatrix} \tag{5.30}$$

Where $Re\{.\}$ stand for the real part. By solving the above system, the NLD coefficient is estimated, then the NLD is regenerated and subtracted from $y_a(t)$ at the output of the LNA as shown in the figure (5.12).

To show the efficiency of the proposed NLD suppressor, figure (5.13) shows the reduction of the NLD power after applying our proposed suppressor. The SI power at R_X is fixed to -40 dB and the NLD is 45 dB under the linear amplified component. The GN power is fixed to -105 dB. As shown, the NLD reduction increases with the increase of the number of training symbols, N_t^{nld}, of NLD used in the NLD coefficient estimation phase. For $N_t^{nld} = 2$, the NLD power is reduced by 38 dB, making the NLD power at -123 dB, which means that it becomes under the GN floor by 18 dB. Such a value of NLD is enough to avoid any influence on the channel estimation process neither on the power of Y_{SIC}.

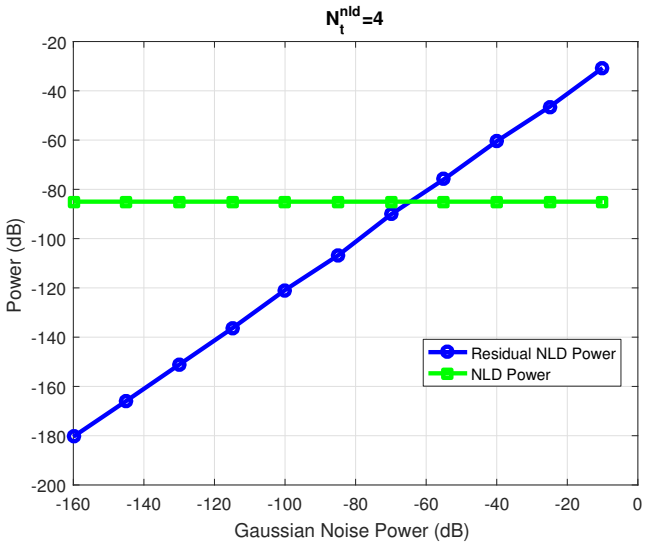


FIGURE 5.14: The effect of the GN power on the residual NLD power using LSE estimator

The effect of the GN power on the NLD coefficient estimation is shown in figure (5.14). The NLD power and N_t^{nld} are fixed to -45 dBc and 4 respectively. NLD coefficient is very sensitive to the GN power, where the results in figure (5.14) show that the residual of the NLD has the same power as NLD when the noise power become -65 dB. However, in real applications, when the NLD is lower than the noise floor, we can neglect it as its effect on the channel estimation becomes negligible. In NI 5664R, at a received power of -30 dB, the noise power is about -105 dB, the NLD power is about -56 dBc, *i.e.* -86 dB under the linear amplified component if the amplification gain is 0 dB. This means that the NLD power is 20 dB over the noise floor. In this case, the NLD has to be eliminated in order to omit its effects on the SIC process.

Figure (5.15) presents the RSI power of $Y_{sic}(m)$ after applying our proposed suppressor (figure (5.12)) as well as the results of the classical SIC one. The parameters of the table (5.1) are respected in addition to the setting of the NLD of LNA, where N_t^{nld} and the NLD power are fixed to 4 and -45 dBc respectively. As shown in figure (5.15), for all the considered values of the NLD power, the RSI is reduced to -100 dB, which is the same value as that presented in figure (5.11) for $N_t = 4$, where the NLD is not considered. This fact means that our proposed suppressor almost eliminates the NLD power. On the other hand, the RSI corresponding to the classical SIC is increased with the NLD power. For a NLD power greater than -40 dBc, the RSI exhibits an important increasing, this is because the NLD power dominates other imperfections such as PN and GN.

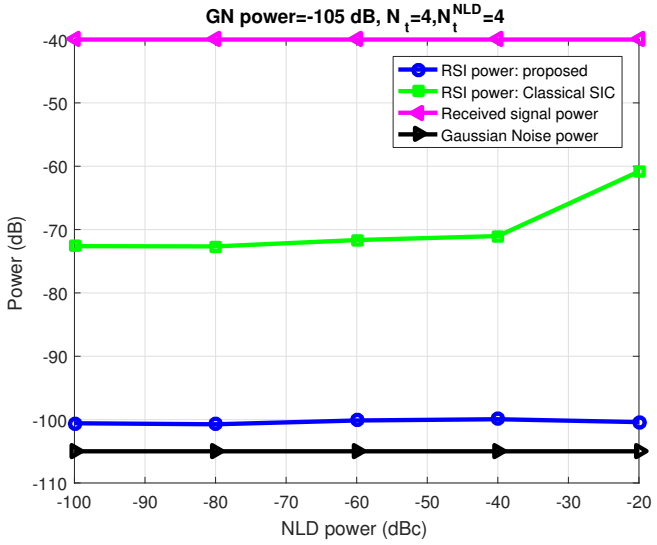


FIGURE 5.15: The power of the residual SIC power in terms of the NLD power

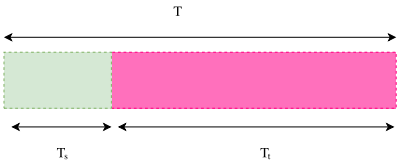


FIGURE 5.16: Activity period of SU under HD functioning is divide into Sensing sub-period (T_s) and Transmission sub-period (T_t).

5.6 Full-Duplex Cognitive Radio

In this section, the efficiency of the proposed receiver model (figure (5.12)) is tested in the Cognitive Radio (CR) context by focusing on the Spectrum Sensing performance and the throughput of the Secondary User (SU). In classical CR systems, the activity period, T, of SU is divided into two sub-periods: the sensing sub-period, T_s, and the transmission one, T_t, with $T_s + T_t = T$ (figure (5.16)).

As long as T_s decreases, the detection reliability decreases but the SU throughput increases. Increasing the SU throughput is obtained at the cost of non-reliable detection process which leads to cause a harmful interference to PU when the SU misses the detection of the active PU. However, in FD-CR the problem of T_s is solved by a simultaneous transmission and sensing. Note that the throughput of the SU in HD-CR can be given by [95]

$$\begin{aligned} R(T_s,\lambda) = &\frac{T_t}{T} C_0 \Big(1 - p_{fa}(T_s,\lambda)\Big) P(H0) \\ &+ \frac{T_t}{T} C_1 \Big(1 - p_d(T_s,\lambda)\Big) P(H1) \end{aligned} \tag{5.31}$$

TABLE 5.2: SNR and SNIR definitions

γ_r^s	SNR of the Secondary transmitted signal at the Secondary receiver
γ_r^p	SNR of the Primary transmitted signal at the Secondary receiver
γ_s	SNR of the Primary transmitted signal at the Secondary transmitter (as defined in equation (5.16))
ζ_r^s	SNIR of the Secondary transmitted signal at the Secondary receiver

C_0 (resp. C_1) is the throughput of SU when it operates under H_0 (resp. (H_1)). C_0 and C_1 are given by [3]:

$$C_0 = log_2(1 + \gamma_r^s) \tag{5.32}$$

$$C_1 = log_2(1 + \zeta_r^s) \tag{5.33}$$

with γ_r^s and ζ_r^s are defined as given in table (5.2) (In this case, PU signal is considered as interference).
Regarding FD-CR, there is no sub-period allocated for the spectrum sensing (*i.e.* $T_s = 0$). Note that C_0 and C_1 as they are related to Secondary receiver, which is assumed to use Half-Duplex communication.

For the forthcoming simulations, the channel between the PU base station and the SU antennas is modelled as Rayleigh, the PN power is set to -91 dBc/Hz, the NLD power is -55 dBc, $N_t^{nld} = 4$.

Figure 5.17 shows the ROC curves of ED under HD, FD with classical architecture, and FD with our proposed one. The SNR of PU at the SU, γ_s, is set to -5 dB, $N_s = 30$ and the other modulation parameters are given in table (5.1). The ROC curves exhibit a performance loss with the going from HD to FD. However, our proposed architecture compensates greatly this loss. For example, at a $p_{fa} = 0.1$, the classical architecture results in $p_d = 0.23$, whereas our proposed one leads to $p_d = 0.86$. Therefore an important gain in the detection rate is obtained relative to the classical SIC.

To show the effect of the SNR of PU at the sensing robustness, figure (5.18) presents p_d in terms of γ_s for $p_{fa} = 0.1$, $N_s = 40$ and $N_t = 10$ are considered. Due to the high number of symbols in the detection, spectrum sensing under HD is almost one for the

[3]The expressions of C_0 and C_1 are given by assuming that SU and PU signals are statistically independent, white and Gaussian. The last assumption can be considered for OFDM signals due to the IFFT process which performs the sum of independent QAM symbols, then OFDM signal approaches Gaussian signal according to Limit Central Theorem

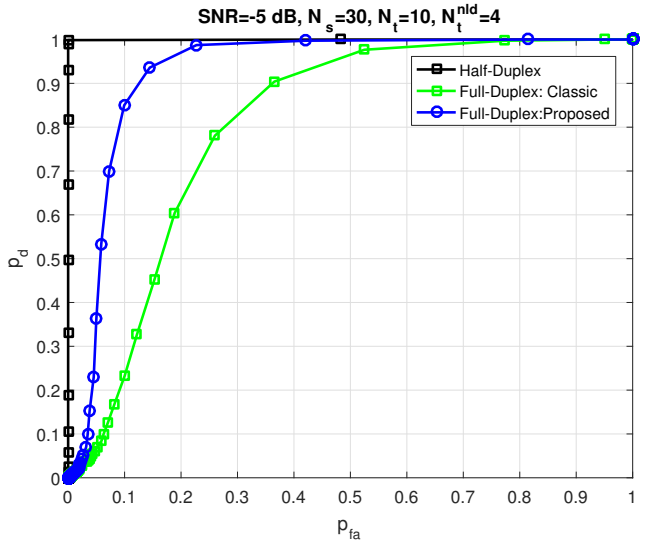


FIGURE 5.17: Model of a Network where Secondary Transmitter and Secondary Receiver co-exists with a PU

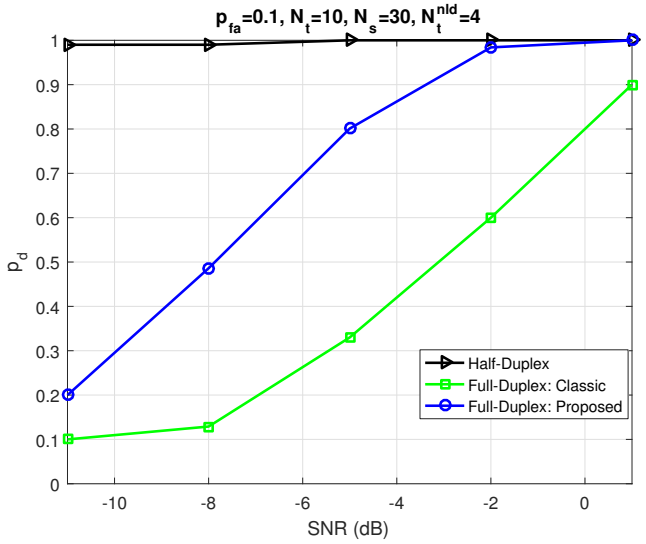


FIGURE 5.18: Model of a Network where Secondary Transmitter and Secondary Receiver co-exists with a PU

tested SNR. Regarding FD mode, the performance is enhanced as the SNR increases. At $\gamma_s = -2$ dB, p_d corresponding to our architecture is very close to one, whereas the a p_d of 0.6 corresponds to the classical SIC. The main limiting performance factor here is the RSI which is inversely proportional to the number of training symbols. In figure (5.19), the results show the effect of N_t on the detection process. $\gamma_s = -5$ dB, $N_s = 25$ and $p_{fa} = 0.1$ are considered. p_d corresponding to our proposed SIC architecture increases clearly with N_t. This fact can be explained by the reduction of RSI for the accurately estimated channel.

The throughput benefits from using FD is discussed in figure (5.20). In order to make

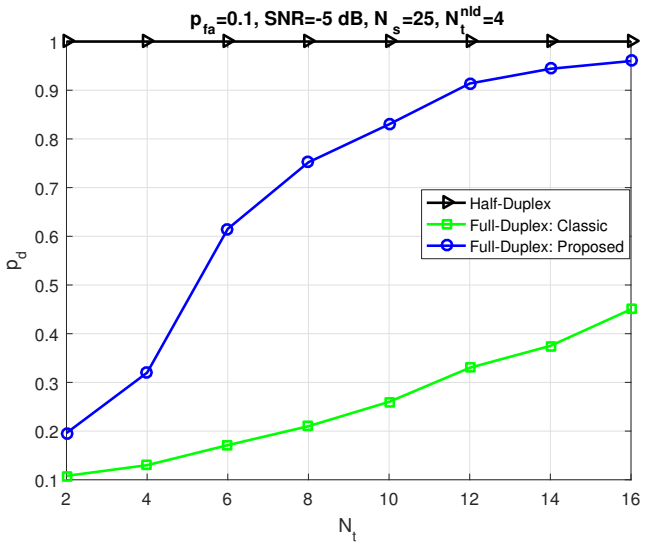


FIGURE 5.19: Variation of p_d in terms of N_t

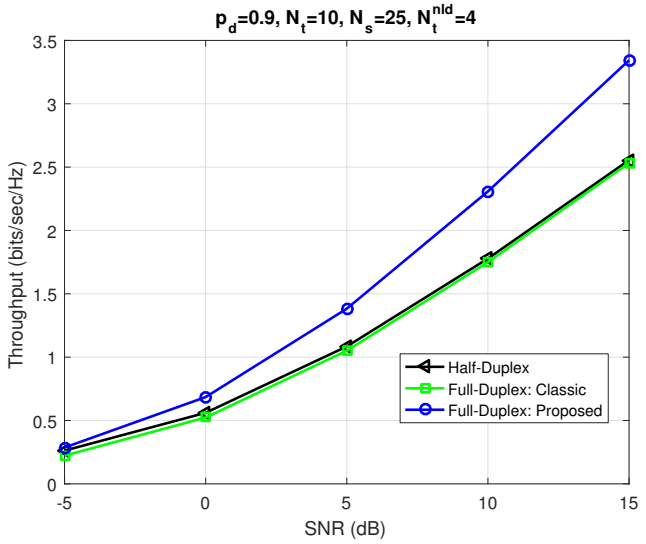


FIGURE 5.20: Variation of p_d in terms of N_t

a fair comparison among HD, classical FD and the proposed FD CR, we assume that $p_d = 0.9$ under the three modes (HD, FD with classical SIC model, FD with proposed SIC model (figure (5.12))) [4]. This is because p_d is the corresponding parameter responsible for the interference from SU to PU. The Signal to Noise and Interference Ratio (SNIR) of PU at the secondary receiver is fixed to 0 dB under all the modes, $N_t = 12$ and $N_s = 25$ are assigned. We assume that $P(H_0) = 0.25$, consequently $P(H_1) = 0.75$ and the ratio $\frac{T_t}{T} = \frac{2}{3}$ for HD activity. Figure (5.20) shows the throughput of the considered CR functioning, where the proposed SIC for FD-CR enhances importantly the CR throughput. On the other hand, the throughput corresponding to the classical SIC is slightly under the HD throughput, therefore no benefits is obtained by using it for FD-CR.

[4] p_{fa} is practically zero for the HD mode, and it is 0.335 for the classical SIC and 0.12 for the proposed SIC (results obtained by simulations)

5.7 Conclusion

In this chapter, Full-Duplex Cognitive Radio (FD-CR) is addressed. Main receiver imperfections, acting as limiting performance factors such as the Phase Noise and the Non-Linear Distortion, have been analysed. A new transceiver architecture for a Full-Duplex (FD) system is proposed in order to suppress the hardware imperfections of the receiver in a FD system. A total phase noise suppression is achieved by the proposed architecture, in addition to a high reduction of the Non-Linear Distortion of the Low-Noise Amplifier. Such an elimination of the hardware imperfections leads to enhance the channel estimation performance, and to reduce the Residual Self Interference. This fact shows an enhancement in the detection rate and the throughput for the FD-CR.

Chapter 6

General Conclusion and Future Works

This manuscript deals with the Spectrum Sensing challenge in Interweave Cognitive Radio System. The aim of the Spectrum Sensing is to detect the Primary User (PU) signal at low SNR within a short sensing period. Reliable detection leads to protect PU from possible interference which could be generated by the Secondary User (SU), and can provide SU with the spectrum opportunity. The sensing duration, even short, affects the SU throughput. For that reason, this type of CR is called Half-Duplex (HD-CR). Full-Duplex Cognitive Radio has been recently proposed in order to cancel this silence period, by allowing SU to be active during the Spectrum Sensing period. This can be done by performing the Self-Interference Cancellation (SIC). In our work, both systems, HD-CR and FD-CR have been considered.

6.1 Contributions

In this thesis, we developed new Spectrum Sensing algorithms dealing with HD-CR based on the Cyclostationary features Detection (CSD) and the Power Spectral Density (PSD) of the PU signal. Besides that, a new receiver architecture is proposed to overcome some SIC limiting performance factors affecting the reliability of FD-CR. The new contributions can be summarized as follows:

- New CSD Spectrum Sensing algorithm based on the Canonical Correlation theory is proposed for HD-CR. The Test Statistic (TS) is found in this algorithm using the Cyclic Correlation Significance Test (CCST). This algorithm detects the common cyclic features among the delayed versions of the received signal. When the channel

is only occupied by the stationary noise, then there is no common cyclic features. Our simulation results show the robustness of this detector with respect to the Noise Uncertainty (NU). Further, our algorithm outperforms classical CSD algorithms with Single-Antenna System (SAS) or Multi-Antenna System (MAS).

- A second proposed algorithm is based on the Cumulative Power Spectral Density (CPSD) of the received signal. This algorithm can detect the presence of a non white signal in the channel based on the fact that its PSD is not flat contrary to the white noise. Non flat PSD results in a curved CPSD, whereas the flat PSD results in a linear shape. By distinguishing between linear (noise only) and curved (signal plus noise) CPSD leads to examine the channel status. Analytical study is provided by deriving the False Alarm (p_{fa}) and Detection (p_d) probabilities of the proposed detectors under Gaussian and Rayleigh channels. Numerical results corroborate the superiority of the performance of the proposed detectors comparing to classical ones such as Energy Detector, CSD or Autocorrelation detector. In addition, the proposed detectors can overcome the Noise Uncertainty limitation.

- In FD-CR, we derive the relation of the impact of the Residual Self-Interference (RSI) on p_d and p_{fa} in FD functioning relative to HD. Using an analytic study, we can evaluate the required RSI level in FD to achieve a target (p_{fa}, p_d) with respect to HD.

- One of the main limiting performance factors in FD is the Phase Noise (PN), which is a main contributor of the RSI. We proposed a new receiver model to eliminate PN. Our numerical results show that PN was totally suppressed and RSI was minimized significantly.

- Another limiting performance factor is the Non-Linear Distortion (NLD) of the Low-Noise Amplifier (LNA). In order to reduce its effect, we also proposed a new FD receiver architecture model. A new wire channel is added between the transmitting chain and the receiving one in order to estimate the NLD coefficients. This operation is done off-line in order to avoid the effect of the wireless channel. As the NLD coefficients are varying slowly, then the time between two successive estimations can be relatively long, therefore the FD transceiver throughput is not greatly affected. We carried out intensive simulations to prove the efficiency of this new architecture..

- Our new architecture model combining the proposed PN and NLD suppressors for FD receiver chain is examined in the FD-CR. We analysed and discussed the influence of the RSI on the Spectrum Sensing performance and consequently on the throughput of SU. We found that FD leads to enhance the SU throughput only

where the SIC is efficient, otherwise, it can affect the throughput. Our proposed architecture enhances the throughput of the SU contrary to the classical FD one, which has a negative impact on the SU throughput.

6.2 Future Works

Cognitive Radio is still an attractive research domain, and it gains more and more the attention of the communication community. Many perspectives can be addressed as continuity of our work.

- An analytic study of our proposed cyclostationary algorithm based on the Canonical Correlation Theory will be the next step of the work presented in this manuscript. Such a study helps the Secondary User to fulfil the detection requirement.
- Regarding our proposed detector based on CPSD, windowing methods can significantly enhance the estimation of PSD. In the next phase of this work, a study on the effect of the windowing method on the Spectrum Sensing performance will be considered.
- The new model of the FD receiver considers only the receiver impairments. As a short term perspective, the performance of the new proposed model will be discussed in the presence of both transmitter and receiver imperfections in order to show the overall SIC level.
- For FD-CR, in order to overcome the RSI problem that is caused by the short distance between the transmitting and the receiving antennas and a non perfect SIC, a system of distributed antennas can be used to perform the Spectrum Sensing. In this case, the problem of the high power of SU signal power relative to PU signal can be solved due to the spatial diversity of the receiving antennas. Here, the number of detected signals will play the main role in order to examine the availability of the channel instead of cancelling the SU copy received in the mixture in establish the Spectrum Sensing. Blind Source Separation techniques can be good candidates as they do not require pre-information about the SU signal neither the PU signal. Even these techniques have been proposed in the context of Spectrum Sensing for Cognitive Radio, their related contributions in such context are very limited, hence, new horizons can be opened.
- Spatial False Alarm (SFA) is a detection problem that has been recently addressed. It happens when a PU which is outside of the SU operating cell is detected. Here,

distinguishing between PUs inside and outside SU operating cell becomes mandatory in order to do not loss the available channel opportunity. Here, the Spectrum Sensing and source localization can be jointly performed in order to diagnose the channel status.

- For Underlay CR, SU can occupy sub-carriers not used by an OFDM PU signal. Using OFDM by SU can affect the Quality of Service of PU signal due to the interference caused by the side lobes. To solve this problem, Filter-Bank Multicarrier (FBMC) modulation can be considered to be used by SU, due to its capability to reduce considerably the power of the side lobes, which alleviates its impact on the primary transmission. Many challenges face FBMC, such as its complexity and low flexibility for the Multi-Input Multi-Ouput (MIMO) CR systems. Such a problem is an actual research field.

- With the going to 5G where CR will be a emerging module, MIMO systems will be more and more used. In such a context, the study of FD-CR for MIMO system becomes of high importance in order to show its applicability under the RSI problems circumstances.

- The transmitting antennas designed for 5G are not omnidirectional, and their transmission are of tight beam-width. This fact makes the Spatial Diversity Multiple Access (SDMA) communication possible. Here, instead of sensing the PU signal presence, the angle of arrival of this signal should be sensed. Such a sensing will open new research horizons and offers new dimensions to the spectrum opportunity.

Appendix A

Variance of T_p under H_0

As $\mu_0 = E[T_p] = 0$, using equation (4.26), the variance V_0 can be written as follows:

$$
\begin{aligned}
V_0 &= E[T_p^2] \\
&= \frac{4}{N^4\sigma_w^4} E\left[\left(\sum_{k=1}^{\frac{N}{2}}(\frac{N}{2}-k+1)|W(k)|^2\right)^2\right] + \underbrace{\left(\sum_{k=1}^{\frac{N}{2}} R\left(1,\frac{N}{2};k\right)\right)^2}_{=\frac{(N+2)^2}{16}} \\
&\quad - \frac{4}{N^2\sigma_w^2}\underbrace{\sum_{k=1}^{\frac{N}{2}} R\left(1,\frac{N}{2};k\right)}_{=\frac{N+2}{4}}\underbrace{E\left[\sum_{k=1}^{\frac{N}{2}}\left(\frac{N}{2}-k+1\right)|W(k)|^2\right]}_{=\frac{N(N+2)N\sigma_w^2}{8}} \\
&= \frac{4}{N^4\sigma_w^4} E\left[\left(\sum_{k=1}^{\frac{N}{2}}\left(\frac{N}{2}-k+1\right)|W(k)|^2\right)^2\right] - \frac{(N+2)^2}{16}
\end{aligned}
\tag{A.1}
$$

The term $\frac{4}{N^4\sigma_w^4} E\left[\left(\sum_{k=1}^{\frac{N}{2}}\left(\frac{N}{2}-k+1\right)|W(k)|^2\right)^2\right]$ can be simplified as follows:

$$\begin{aligned}
&\frac{4}{N^4\sigma_w^4}E\left[\left(\sum_{k=1}^{\frac{N}{2}}\left(\frac{N}{2}-k+1\right)|W(k)|^2\right)^2\right] \\
&=\frac{4}{N^4\sigma_w^4}E\left[\sum_{k_1\neq k_2=1}^{\frac{N}{2}}\left(\frac{N}{2}-k_1+1\right)|W(k_1)|^2\left(\frac{N}{2}-k_2+1\right)|W(k_2)|^2\right] \\
&+\frac{4}{N^4\sigma_w^4}E\left[\sum_{k=1}^{\frac{N}{2}}\left(\frac{N}{2}-k+1\right)^2|W(k)|^4\right] \qquad \text{(A.2)}
\end{aligned}$$

Since $W(k)$ is Gaussian and *i.i.d.* then:
1) The kurtosis of $W(k)$ is zero:

$$kurt(W(k)) = E[|W(k)|^4] - E[W^2(k)]^2 - 2E^2[|W(k)|^2] = 0$$

Since $E[W^2(k)] = 0$ because $W(k)$ is circular symmetric Gaussian, then

$$E[|W(k)|^4] = 2E[|W(k)|^2]^2 = 2N^2\sigma_w^4 \qquad \text{(A.3)}$$

2) For $k_1 \neq k_2$:

$$E[|W(k_1)|^2|W(k_2)|^2] = E[|W(k_1)|^2]E[|W(k_2)|^2] = N^2\sigma_w^4 \qquad \text{(A.4)}$$

Using equations (A.3) and (A.4), the equation (A.2) becomes:

$$\frac{4}{N^4\sigma_w^4}E\left[\left(\sum_{k=1}^{\frac{N}{2}}(\frac{N}{2}-k+1)|W(k)|^2\right)^2\right] = \frac{N^2}{16}+\frac{5N}{12}+\frac{3}{4}+\frac{1}{3N} \qquad \text{(A.5)}$$

Back to equation (A.1), V_0 becomes:

$$\begin{aligned}
V_0 &= \frac{N^2}{16}+\frac{5N}{12}+\frac{3}{4}+\frac{1}{3N}-\frac{(\frac{N}{2}+1)^2}{4} \\
&= \frac{N}{6}+\frac{1}{2}+\frac{1}{3N} \qquad \text{(A.6)}
\end{aligned}$$

Appendix B

Variance of T_p under H_1

The calculation of equation (B.1) in the next page stands for finding the variance, V_1, of T_p under H_1. In equation (B.1), the part $A_2 = 0$ because:

$$
\begin{aligned}
V_1 &= E\left[\left(\sum_{k=1}^{\frac{N}{2}}\left[\frac{2(\frac{N}{2}-k+1)}{N^2\sigma_w^2}\left(|hS(k)|^2+|W(k)|^2+2Re\{hS(k)W^*(k)\}\right)-R\left(1,\frac{N}{2};k\right)\right]\right)^2\right]-\mu_1^2 \\
&= \underbrace{E\left[\left(\sum_{k=1}^{\frac{N}{2}}\left[\frac{2(\frac{N}{2}-k+1)}{N^2\sigma_w^2}|W(k)|^2-D\left(1,\frac{N}{2};k\right)\right]\right)^2\right]}_{=V_0}+E\left[\left(\sum_{k=1}^{\frac{N}{2}}\frac{2(\frac{N}{2}-k+1)}{N^2\sigma_w^2}\left(|hS(k)|^2+2Re\{hS(k)W^*(k)\}\right)\right)^2\right] \\
&+\underbrace{2E\left[\left(\sum_{k=1}^{\frac{N}{2}}\frac{2(\frac{N}{2}-k+1)}{N^2\sigma_w^2}\left(|hS(k)|^2+2Re\{hS(k)W^*(k)\}\right)\right)\left(\sum_{k=1}^{\frac{N}{2}}\left[\frac{2(\frac{N}{2}-k+1)}{N^2\sigma_w^2}|W(k)|^2-D\left(1,\frac{N}{2};k\right)\right]\right)\right]}_{A_2=0}-\mu_1^2 \\
&= V_0+\frac{4}{N^4\sigma_w^4}E\left[\left(\sum_{k=1}^{\frac{N}{2}}\left(\frac{N}{2}-k+1\right)\left(|hS(k)|^2+2Re\{hS(k)W^*(k)\}\right)\right)^2\right]-\mu_1^2 \\
&= V_0+\underbrace{\frac{4}{N^4\sigma_w^4}E\left[\left(\sum_{k=1}^{\frac{N}{2}}\left(\frac{N}{2}-k+1\right)|hS(k)|^2\right)^2\right]}_{=\mu_1^2;\ since\ s(n)\ is\ deterministic}+\frac{4}{N^4\sigma_w^4}E\left[\left(\sum_{k=1}^{\frac{N}{2}}\left(\frac{N}{2}-k+1\right)\left(2Re\{hS(k)W^*(k)\}\right)\right)^2\right] \\
&+\underbrace{\frac{8}{N^4\sigma_w^4}E\left[\left(\sum_{k=1}^{\frac{N}{2}}\left(\frac{N}{2}-k+1\right)\left(2Re\{hS(k)W^*(k)\}\right)\right)\left(\sum_{k=1}^{\frac{N}{2}}\left(\frac{N}{2}-k+1\right)|hS(k)|^2\right)\right]}_{=0;\ since\ s(n)\ is\ deterministic\ and\ E[W_q(k)]=E[W_p(k)]=0}-\mu_1^2 \\
&= V_0+\frac{4}{N^4\sigma_w^4}E\left[\left(\sum_{k=1}^{\frac{N}{2}}\left(\frac{N}{2}-k+1\right)\left(2Re\{hS(k)W^*(k)\}\right)\right)^2\right] \qquad \text{(B.1)}
\end{aligned}
$$

$$
\begin{aligned}
A_2 &= 2E\left[\left(\sum_{k=1}^{\frac{N}{2}}\frac{2(\frac{N}{2}-k+1)}{N^2\sigma_w^2}|hS(k)|^2\right)\left(\sum_{k=1}^{\frac{N}{2}}\frac{2(\frac{N}{2}-k+1)}{N^2\sigma_w^2}|W(k)|^2 - D\left(1,\frac{N}{2};k\right)\right)\right] \\
&+ 2E\left[\left(\sum_{k=1}^{\frac{N}{2}}\frac{2(\frac{N}{2}-k+1)}{N^2\sigma_w^2}Re\{hS(k)W^*(k)\}\right)\left(\sum_{k=1}^{\frac{N}{2}}\frac{2(\frac{N}{2}-k+1)}{N^2\sigma_w^2}|W(k)|^2 - D\left(1,\frac{N}{2};k\right)\right)\right] \\
&= 2\sum_{k=1}^{\frac{N}{2}}\frac{2(\frac{N}{2}-k+1)}{N^2\sigma_w^2}|S(k)|^2\underbrace{E\left[\sum_{k=1}^{\frac{N}{2}}\frac{2(\frac{N}{2}-k+1)}{N^2\sigma_w^2}|W(k)|^2 - D\left(1,\frac{N}{2};k\right)\right]}_{=\mu_0=0} \\
&+ 2E\left[\left(\sum_{k=1}^{\frac{N}{2}}\frac{2(\frac{N}{2}-k+1)}{N^2\sigma_w^2}\left[h_pS_p(k)W_p(k)+h_pS_q(k)W_q(k)+h_qS_p(k)W_q(k)-h_qS_q(k)W_qp(k)\right]\right)\right. \\
&\left.\left(\sum_{k=1}^{\frac{N}{2}}\left[\frac{2(\frac{N}{2}-k+1)}{N^2\sigma_w^2}\left(W_q^2(k)+W_p^2(k)\right) - D\left(1,\frac{N}{2};k\right)\right]\right)\right]
\end{aligned}
\tag{B.2}
$$

Since $W_p(k)$ and $W_q(k)$ are independent and $E[W_p(k_1)W_p^2(k_2)] = E[W_q^2(k_1)W_q(k_2)] = 0\ \forall k_1$ and k_2, since $W_q(k)$ and $W_p(k)$ are Gaussian, then equation (B.2) becomes zeros.

Using the *i.i.d.* and the circular properties of $W(k)$ and the fact that $s(n)$ is deterministic, equation (B.1) becomes:

$$
\begin{aligned}
V_1 &= V_0 + \frac{16}{N^4\sigma_w^4}E\left[\left(\sum_{k=1}^{\frac{N}{2}}\left(\frac{N}{2}-k+1\right)Re\{hS(k)W^*(k)\}\right)^2\right] \\
&= V_0 + \frac{16}{N^4\sigma_w^4}\sum_{k=1}^{\frac{N}{2}}\frac{1}{2}\left(\frac{N}{2}-k+1\right)^2E\left[\left|hS(k)W(k)\right|^2\right] \\
&= V_0 + \frac{8\gamma}{N^3}\sum_{k=1}^{\frac{N}{2}}\left(\frac{N}{2}-k+1\right)^2|S(k)|^2
\end{aligned}
\tag{B.3}
$$

Appendix C

Approximation of the Detection Probability

The approximation of the Q-function using a first-order Taylor series was proposed in [47] without justification. Here we show by simulation the effectiveness of this approximation. The Taylor series of a function $f(t)$ around t_0 can be developped as follows:

$$f(t) = \sum_{n=0}^{\infty} f^{(n)}(t_0) \frac{(t-t_0)^n}{n!} \tag{C.1}$$

Where $f^{(n)}(t_0)$ is the nth order derivative of $f(t)$ at t_0.
According to Equation (4.45), we aim at simplifying $p_d^p = Q(\frac{\lambda - b\gamma}{\sqrt{V_0 + c\gamma}})$ in order to find the analytic probability of detection under Rayleigh channel. Let us define $g(\gamma) = \frac{\lambda - b\gamma}{\sqrt{V_0 + c\gamma}}$. The first $g_1(\gamma)$ and the second order, $g_2(\gamma)$, Taylor series approximations of $g(\gamma)$ around γ_0 can be found as follows:

$$g_1(\gamma) = g(\gamma_0) + g'(\gamma_0)(\gamma - \gamma_0) \tag{C.2}$$

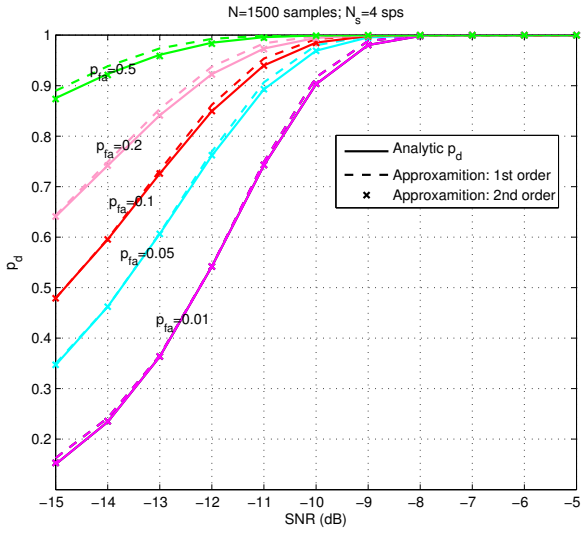
$$g_2(\gamma) = g(\gamma_0) + g'(\gamma_0)(\gamma - \gamma_0) + g''(\gamma_0)\frac{(\gamma - \gamma_0)^2}{2} \tag{C.3}$$

Let $\gamma_0 = \lambda/b$ as $g(\gamma_0) = 0$, and then $Q(g(\gamma_0)) = 0.5$, which is the middle point of the Q-function. Accordingly, $g'(\gamma_0)$ and $g''(\gamma_0)$ can derived as follows:

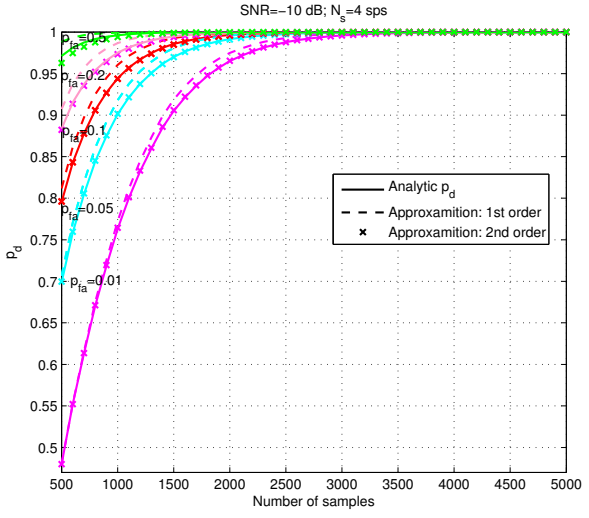
$$g'(\gamma_0) = -\frac{b}{\sqrt{V_0 + c\lambda/b}} \tag{C.4}$$

$$g''(\gamma_0) = \frac{c\left(c\lambda(1 + 3/b) + 4bV_0\right)}{4(V_0 + c\lambda/b)^{5/2}} \tag{C.5}$$

Figures (C.1(a)) and (C.1(b)) present a comparison between $p_d^p = Q(g(\gamma))$ and its approximations $Q(g_1(\gamma))$ and $Q(g_2(\gamma))$ under different conditions. Figure (C.1(a)) shows the variation of p_d^p and its approximations in terms of SNR for different p_{fa}. The number of samples is fixed to 1500 and $N_s = 4$ sps, while figure (C.1(b)) shows under SNR of 10 dB and $N_s = 4$ sps, the variation of p_d^p and its approximations in terms of N for different p_{fa}. As shown in figures (C.1(a)) and (C.1(b)), the analytic and the approximated curves are closed to each others under the various conditions. As expected, $g_2(\gamma)$ leads to a more robust approximation, since $Q(g_2(\gamma))$ is almost colinear with $Q(g(\gamma))$. Even though, $g_1(\gamma)$ results are very closed to exact ones. Therefore $g_1(\gamma)$ is used to approximate the detection probability under Rayleigh fading channel.



(a)



(b)

FIGURE C.1: (a): The probability of detection p_d^p and its approximation in terms of SNR for different p_{fa}, $N = 1500$ samples and $N_s = 4$ sps, (b): The probability of detection p_d^p and its approximation in terms of the number of samples N, for different p_{fa}, SNR$=-10$ dB samples and $N_s = 4$ sps

Appendix D

Probability of Detection and Probability of False Alarm under Full-Duplex mode

As by our assumption $D(m)$, $W(m)$ and $X(m)$, are Gaussian *i.i.d.*, then $Y_{sic}(m)$ is also Gaussian and *i.i.d.*. Therefore the Test Statistic, T_{ED}, of equation (5.13) follows a normal distribution according to the Central Limit Theorem (CLT) for a large N. Under H_0 (*i.e.* PU's sugnal $S(m)$ does not exist), the mean, μ_0, and the variance, V_0 of T can be obtained as follows:

$$\mu_0 = E[T] = E\left[\frac{1}{N}\sum_{m=1}^{N}|D(m)+W(m)|^2\right] = \sigma_d^2 + \sigma_w^2 \tag{D.1}$$

$$\begin{aligned} V_0 &= E[T^2] - E^2[T] = \frac{1}{N^2}E\left[\left(\sum_{m=1}^{N}|Y_{sic}(m)|^2\right)^2\right] - (\sigma_w^2+\sigma_d^2)^2 \\ &= \frac{1}{N^2}E\left[\sum_{m_1=m_2=1}^{N}|Y_{sic}(m_1)|^4\right] \\ &\quad + \frac{1}{N^2}E\left[\sum_{m_1\neq m_2=1}^{N}|Y_{sic}(m_1)|^2 Y_{sic}(m_2)|^2\right] - (\sigma_w^2+\sigma_d^2)^2 \\ &= \frac{1}{N^2}\sum_{m=1}^{N}E\left[|Y_{sic}(m)|^4\right] - \frac{1}{N}(\sigma_w^2+\sigma_d^2)^2 \end{aligned} \tag{D.2}$$

Since $Y_{sic}(m)$ is Gaussian, then its kurtosis, $kurt(Y_{sic}(m))$, is zero.

$$kurt(Y_{sic}(m)) = E[|Y_{sic}(m)|^4] - E[Y_{sic}^2(m)] - 2E^2[|Y_{sic}(m)|^2] = 0 \tag{D.3}$$

Assuming that the real and the imaginary parts of $Y_{sic}(m)$ are independent and of the same variance then $E[Y_{sic}^2(m)]$ becomes zero. Therefore:

$$E[|Y_{sic}(m)|^4] = 2E^2[|Y_{sic}(m)|]^2 = 2(\sigma_w^2 + \sigma_d^2)^2 \tag{D.4}$$

Back to equation (D.2), the variance, V_0 becomes:

$$V_0 = \frac{1}{N}(\sigma_w^2 + \sigma_d^2)^2 \tag{D.5}$$

By following the same procedure, μ_1 and V_1 can be obtained as follows under H_1 ($X(m)$ exists):

$$\mu_1 = \sigma_w^2 + \sigma_d^2 + \sigma_s^2 \tag{D.6}$$

$$V_1 = \frac{1}{N}(\sigma_w^2 + \sigma_d^2 + \sigma_s^2)^2 \tag{D.7}$$

Once the mean and the variance of TS, which has normal distribution under both H_0 and H_1, are found, the expressions of False Alarm and Detection Probabilities can be derived using the $Q-$ function.

Bibliography

[1] M. Wyglinski, M. Nekovee, and Y. Hou. Cognitive radio communications and networks principles and practice. Elsevier, 2010.

[2] H. Kaushal and G. Kaddoum. Optical communication in space: Challenges and mitigation techniques. *IEEE Communications Surveys Tutorials*, PP(99):1–1, 2016.

[3] A. Mansour, R. Mesleh, and M. Abaza. New challenges in wireless and free space optical communications. *Optics and Lasers in Engineering*, 2015(1), May 2016. URL http://dx.doi.org/10.1016/j.optlaseng.2016.03.027.

[4] M. N. O. Sadiku and S.M. Musa. Free space optical communications: An overview. *European Scientific Journal edition*, 12(9):55 – 68, February 2016.

[5] B. Wang and K. J. R. Liu. Advances in cognitive radio networks: A survey. *IEEE Journal of Selected Topics in Signal Processing*, 5(1):5–23, Februrary 2011.

[6] E.D.N. 02-135 Spectrum Policy Task Force Report. Federal Communication Commission, Washington, DC, 2002.

[7] P. Leaves, K. Moessner, R. Tafazolli, D. Grandblaise, D. Bourse, R. Tonjes, and M. Breveglieri. Dynamic spectrum allocation in composite reconfigurable wireless networks. *IEEE Communications Magazine*, 42(5):71–81, May 2004.

[8] I. F. Akyildiz, W. Y. Lee, M. C. Vuran, and S. Mohanty. Next generation/dynamic spectrum access/cognitive radio wireless networks: A survey. *Computer Networks (Elsevier)*, 50(13):2127–2159, May 2006.

[9] J. Mitolal. Cognitive radio: Making software radios more personal. 6(4):13 – 18, August 1999.

[10] J. Mitola. Software radio architecture: a mathematical perspective. *IEEE Journal on Selected Areas on Communications*, 17(4):514–538, April 1999.

[11] Ian F. Akyildiz, Won-Yeol Lee, Mehmet C. Vuran, , and Shantidev Mohanty. A survey on spectrum management in cognitive radio networks. *IEEE Communications Magazine*, 46(4):40 – 48, May 2008.

[12] Establishement of interference temperature metric to quantify and manage interference and to expand available unlicensed operation in certain fixed mobile and satellite frequency bands. *Federal Comminication Commission*, FCC Doc. ET Docket 03-289 2003.

[13] H. Arslan and E. M. Sahin. *UWB-Based Cognitive Radio Networks*. Springer US, 2007.

[14] A. Goldsmith and I. Marié. *Capacity of Cognitive Radio Networks*. Cambridge University Press, Boston, MA, 2012.

[15] M. Song, C. Xin, Y. Zhao, and X. Cheng. Dynamic spectrum access: From cognitive radio to network radio. *IEEE Journal on Wireless Communication*, 50(1):23 – 29, February 2012.

[16] A. Goldsmith. Breaking spectrum gridlock with cognitive radios: An information theoretic perspective. *IEEE Proceedings*, 97(5):894–914, May 2009.

[17] M. Costa. Writing on dirty paper. *IEEE Transactions on Information Theory*, 29 (3):439 – 441, May 1983.

[18] C. Xin. Network coding relayed dynamic spectrum access. *Proceedings of ACM Workshop in Cognitive Radio Networks (CoRoNet)*, pages 31 – 36, New York, NY, USA 2010.

[19] T. Yucek and H. Arslan. A survey of spectrum sensing algorithms for cognitive radio applications. *IEEE Communication Surveys & Tutorials*, 11(1):116 – 130, First Quarter 2009.

[20] I. F. Akyildiz, B. F. Lo, and R. Balakrishnan. Cooperative spectrum sensing in cognitive radio networks: A survey. 4(4):40 – 62, 2011.

[21] E. Everett, A. Sahai, and A. Sabharwal. Passive self-interference suppression for full-duplex infrastructure nodes. *IEEE Transactions on Wireless Communication*, 13(2):680 – 694, Fevruary 2014.

[22] E. Ahmed, A. M. Eltawil, and A. Sabharwal. Rate gain region and design tradeoffs for full-duplex wireless communications. *IEEE Transaction on Wireless Communications*, 12(7):3556–3565, July 2013.

[23] J. Heo, H. Ju, Sungsoo Park, E. Kim, and D. Hong. Simultaneous sensing and transmission in cognitive radio. *IEEE Transaction on Wireless Communications*, 13 (4):149 – 160, April 2014.

[24] T. Riihonen and R. Wichman. Energy detection in full-duplex cognitive radios under residual self-interference. *9th International Conference on Cognitive Radio Oriented Wireless Networks (CROWNCOM)*, pages 57 – 60, July 2014.

[25] W. Afifi and M. Krunz. Incorporating self-interference suppression for full-duplex operation in opportunistic spectrum access systems. *IEEE Transaction on Wireless Communications*, 14(4):2180 – 2191, April 2015.

[26] W. Cheng, X. Zhang, and Hailin Zhang. Full-duplex spectrum-sensing and mac-protocol for multichannel nontime-slotted cognitive radio networks. *IEEE Journal on Selected Areas in Communications*, 33(5):820 – 831, May 2015.

[27] A. Nasser, A. Mansour, K. C. Yao, H. Charara, and M. Chaitou. Spectrum sensing for full-duplex cognitive radio systems. *11th International Conference on Cognitive Radio Oriented Wireless Networks (CROWNCOM)*, Grenobel, May 2016.

[28] D. Cabric, S. Mishra, and R. Brodersen. Implementation issues in spectrum sensing for cognitive radios. *Proceedings of Asilomar Conference on Signals, Systems, and Computers*, 1:772–776, June 2004.

[29] A. Ghasemi and E. Sousa. Collaborative spectrum sensing for opportunistic access in fading environments. *Proceeding of IEEE DySPAN*, pages 131–136, June 2004.

[30] S. Mishra, A. Sahai, and R. Brodersen. Collaborative spectrum sensing for opportunistic access in fading environments. *Proceeding of IEEE Iinternational Conference on Communication*, 4:1658–1663, June 2006.

[31] M. T. Masonta, M. Mzyece, and N. Ntlatlapa. Spectrum decision in cognitive radio networks: A survey. *IEEE Communications Surveys & Tutorials*, 15(3):1088 – 1107, Third Quarter 2013.

[32] W.-Y. Lee and I. F. Akyildiz. Optimal spectrum sensing framework for cognitive radio networks. *IEEE Transaction on Wireless Communications*, 7(10):3845 – 3857, September 2008.

[33] Y. Yuan, P. Bahl, R. Chandra, T. Moscibroda, and Y. Wu. Allocating dynamic time-spectrum blocks in cognitive radio networks. *Proceedings ACM International Symposium on Mobile ad hoc Networking and Computing Wireless Communications and Networking Conference*, Quebec, Canada, September 2007.

[34] V. Pla, J. R. Vidal, J. Martinez-Bauset, and L. Guijarro. Modeling and characterization of spectrum white spaces for underlay cognitive radio networks. *Proceedings IEEE International Conference on Communications (ICC)*, Cape Town, South Africa, May 2010.

[35] D. Xu, E. Jung, and X. Liu. Optimal bandwidth selection in multichannel cognitive radio networks: How much is too much. *Proceedings IEEE International Symposium for New Frontiers in DySPAN*, pages 230–239, October, Chicago, Illinois, USA 2008.

[36] S. Singh G. Wu and T. Chiueh. Implementation of dynamic channel switching on ieee 802.11-based wireless mesh networks. In *Proceeedings International Wireless Internet Conference (WICON)*, Hawaii, USA November, 2016.

[37] Part 22 IEEE Std 802.22. Cognitive wireless ran medium access control (mac) and physical layer (phy) specifications: Policies and procedures for operation in the tv bands. *IEEE Computer Society*, July, New York, USA 2011.

[38] T. Li, W. Mow, V. Lau, M. Siu, R. S. Cheng, and R. D. Murch. Robust joint interference detection and decoding for ofdm-based cognitive radio systems with unknown interference. *IEEE Journal on Selected Areas in Communications*, 25(3): 566 – 575, April 2007.

[39] A. Rabbachin, T. Q. S. Quek, H. Shin, and M. Z. Win. Cognitive network interference. *IEEE Journal on Selected Areas in Communications*, 29(2):480 – 493, February 2011.

[40] Ivan Christian, Sangman Moh, Ilyong Chung, and Jinyi Lee. Spectrum mobility in cognitive radio networks. *IEEE Communications Magazine*, 50(6):114 – 121, June 2012.

[41] L.-C. Wang and C.-W. Wang. Spectrum handoff for cognitive radio networks: Reactive-sensing or proactive-sensing? *Proceedings IEEE International Conferenve on Performance,Computing and Communication (IPCCC)*, pages 343 – 348., December,Austin, Texas, USA 2008.

[42] L. Yang, L. Cao, and H. Zheng. Proactive channel access in dynamic spectrum networks. *Physical Communication (Elsevier)*, 1(2):103 – 111, June 2008.

[43] W. Afifi and M. Krunz. Adaptive transmission-reception-sensing strategy for cognitive radios with full-duplex capabilities. In *International Symposium on Dynamic Spectrum Access Networks (DYSPAN)*, pages 149 – 160, 2014.

[44] A. Dandawate and G. Giannakis. Statistical tests for presence of cyclostationarity. *IEEE Transaction on Signal Processing*, 42(9):2355 – 2369, September 1994.

[45] M. Derakhshani, T. Le-Ngoc, and M. Nasiri-Kenari. Efficient cooperative cyclostationary spectrum sensing in cognitive radios at low snr regimes. *IEEE Transaction on Wireless Communications*, 10(11):3754 – 3764, November 2011.

[46] Y. Zhu, J. Liu, Z. Feng, and P. Zhang. Sensing performance of efficient cyclostationary detector with multiple antennas in multipath fading and lognormal shadowing environments. *Journal of Communications and Networks*, 16(2):162 – 171, April 2014.

[47] M. Naraghi-Poor and T. Ikuma. Autocorrelation-based spectrum sensing for cognitive radio. *IEEE Trans. on Vehicular Technology*, 59(2):718 – 733, February 2010.

[48] Y. Zeng and Y.-C. Liang. Eigenvalue-based spectrum sensing algorithms for cognitive radio. *IEEE Transactions on Communications*, 57(6):1784–1793, June 2009.

[49] G. Zhang, X. Wang, Y.-C. Liang, and J. Liu. Fast and robust spectrum sensing via kolmogorov-smirnov test. *IEEE Transaction on Communications*, 58(12):3410–3416, December 2010.

[50] D. Teguig, V. Le Nir, and B. Scheers. Spectrum sensing method based on the likelihood ratio goodness of fit test. *IEEE Electronic Letters*, 51(3):253–255, February 2015.

[51] S. Suresh, S. Prakriya, and M. R. Bhatnagar. Kurtosis based spectrum sensing in cognitive radio. *Physical Communication (Elsevier)*, 3(3):230–239, September 2012.

[52] A. Nasser, A. Mansour, K. C. Yao, H. Charara, and M. Chaitou. Efficient spectrum sensing approaches based on waveform detection. pages 13–17, April 2014.

[53] D. Cabric, A. Tkachenko, and R. W. Brodersen. Spectrum sensing measurements of pilot, energy, and collaborative detection. *Military Communications Conference (MILCOM)*, pages 1 – 7, October 2006, Washington, DC.

[54] Draft Standard for Wireless Regional Area Networks. IEEE 802.22 WRAN, March, 2008.

[55] F. Digham, M.-S. Alouini, and K. Simon. On the energy detection of unknown signals over fading channels. *IEEE Transaction on Communications*, 55(1):21 – 24, January 2007.

[56] W. Cheng, X. Zhang, , and H. Zhang. Full duplex spectrum sensing in non-time-slotted cognitive radio networks. In *The IEEE Military Communications Conference (Milcom)*, pages 1029 – 1034, 2011.

[57] S. Atapattu, C. Tellambura, and Hai Jiang. Energy detection for spectrum sensing in cognitive radio. Springer, 2014.

[58] M. Barkat. In *Signal Detection and estimation*. Artech House, 2005.

[59] Qian Wang and Qian Ge. International conference on blind estimation algorithm of parameters in pn sequence for dsss-bpsk signals. In *Wavelet Active Media Technology and Information Processing (ICWAMTIP)*, pages 371–376, December 2012.

[60] S. M. Kay. Robust detection by autoregressive spectrum analysis. *IEEE Transaction on Acoustics, Speech and Signal Processing*, ASSP-30(2):256–269, April 1982.

[61] L. Pakula and S. M. Kay. Detection performance of the circular correlation coefficient receiver. *IEEE Transaction on Acoustics, Speech and Signal Processing*, ASSP-34(3):399–404, June 1986.

[62] S. Singh G. Wu and T. Chiueh. Covariance based signal detections for cognitive radio. In *IEEE DySPAN*, April, 2007.

[63] Antonio Napolitano. Cyclostationarity: Limits and generalizations. *Signal Processing*, 120:232–347, March 2016. doi: 10.1016/j.sigpro.2015.09.011.

[64] Antonio Napolitano. Cyclostationarity: New trends and applications. *Signal Processing*, 120, 2016. doi: 10.1016/j.sigpro.2015.09.011.

[65] Cyclostationarity: Half a century of research. *Signal Processing*, 86(4):639 – 697, March 2006.

[66] P. Urriza, E. Rebeiz, and D. Cabric. Multiple antenna cyclostationary spectrum sensing based on the cyclic correlation significance test. *IEEE Journal on Selected Areas in Communications*, 31(11):2185–2195, November 2013.

[67] A. Mansour and C. Jutten. What should we say about the kurtosis. *IEEE Signal Processing Letters*, 6(12):321–322, December 1999.

[68] A. Nasser, A. Mansour, K. C. Yao, H. Charara, and M. Chaitou. Spectrum sensing based on cumulative power spectral density. *EURASIP Journal on Advances in Signal Processing*, Under Review .

[69] Z. Khalaf, A. Nafkha, and J. Palicot. Blind spectrum detector for cognitive radio using compressed sensing. *IEEE GLOBECOM*, December 2011, Houton, Texas, USA.

[70] R. Tandra and A. Sahai. Snr walls for signal detection. *IEEE Journal of Selected Topics in Signal Processing*, 2(1):4–17, February 2008.

[71] S. S. Ivrigh, S. M. S. Sadough, and S. A. Ghorashi. A blind source separation technique for spectrum sensing in cognitive radio networks based on kurtosis metric. pages 333–337, October 2011.

[72] N. Tafaghodi Khajavi, S. Sadeghi, and S. M. S. Sadough. An improved blind spectrum sensing technique for cognitive radio systems. pages 13–17, December 2010.

[73] C. H. Lee and W. Wolf. Blind signal separation for cognitive radio. *Journal of signal Processing systems*, 63(1):67–81, August 2009.

[74] A. Mansour and M. Kawamoto. Ica papers classified according to their applications and performances. *IEICE Tansactions on Fundamentals*, E86-A(1), March 2003.

[75] D. Ramírez, J. Vía, I. Santamaría, R. López-Valcarce, and L. L. Scharf. Multi-antenna spectrum sensing: Detection of spatial correlation among time-series with unknown spectra. pages 2954–2957, March 2010.

[76] S. Schell and W. Gardner. Detection of the number of cyclostationary signals in unknown interference and noise. *24th Asilomar Conference on Signals, Systems and Computers*, 6, November 1990.

[77] A. Nasser, A. Mansour, K.-C. Yao, Mohamad Chaitou, and H. Charara. Spatial and time diversities for canonical correlation significance test in spectrum sensing. In *24th European Signal Processing Conference (EUSIPCO)*, pages 1232–1236, August 2016.

[78] A. Nasser, A. Mansour, K. C. Yao, H. Abdallah, M. Chaitou, and H. Charara. Spectrum sesning enhancement using principal component analysis. In *16th IEEE International Symposium on Signal Proessing and Information Theory (ISSPIT)*, December 2016.

[79] D. N. Lawley. Tests of significance in canonical analysis. *Biometrika*, 46(1):59–65, June 1959.

[80] W.Chen, J .P. Rei1ly, and K. M. Wong. Detection of the number of signals in noise with banded covariance. *IEEE Proceedings - matrices, Radar, Sonar and Navigation*, 143(5):289–294, October 1996.

[81] A. Nasser, A. Mansour, K. C. Yao, and H. Abdallah. *Spectrum Sensing for Half and Full-Duplex Cognitive Radio*, pages 15–50. Springer, 2017. ISBN 978-981-10-2254-8. doi: 10.1007/978-981-10-2254-8_2. URL http://dx.doi.org/10.1007/978-981-10-2254-8_2.

[82] A. Nasser, A. Mansour, K. C. Yao, H. Charara, M. Chaitou, and H. Abdallah. Receiver impairements mitigations and self interference cancellation for full-duplex transceiver with cognitive radio application. *EURASIP Journal on on Networking and Communication*, Submitted .

[83] C. Iouna, A. Mansour, A. Quinquiz, and E. Radoi. In *Digital Signal Processing using MATLAB*. Wiley, 2014.

[84] R. Gallager. In *Stochastic Processes:Theory for Applications*. Cambridge University Press, 2013.

[85] M. Abramowitz and I.A. Stegun. In *Handbook of Mathematical Functions With Formulas, Graphs, and Mathmatical Tables*. Dover Publications, 1972.

[86] Elsayed Ahmed and Ahmed M. Eltawil. All-digital self-interference cancellation technique for full-duplex systems. *IEEE Transaction on Wireless Communications*, 14(7):291–294, July 2015.

[87] A. Sahai, G. Patel, C. Dick, , and A. Sabharwal. On the impact of phase noise on active cancelation in wireless full-duplex. *IEEE Transaction on Vehicular Technology*, 62(9):3494–4510, November 2013.

[88] D. W. Bliss, T. M. Hancock, and P. Schniter. Hardware phenomenological effects on cochannel full-duplex mimo relay performance. In *Asilomar Conference on Signals, Systems and Computers*, pages 34 – 39, 2012.

[89] V. Syrjala, M. Valkama, L. Anttila, T. Riihonen, and D. Korpi. Analysis of oscillator phase-noise effects on self-interference cancellation in full-duplex ofdm radio transceivers. *IEEE Transactions on Wireless Communications*, 13(6):2977–2990, June 2014.

[90] E. Ahmed and A. M. Eltawil. On phase noise suppression in full-duplex systems. *IEEE Transactions on Wireless Communications*, 14(3):1237–1251, March 2015.

[91] E. Ahmed, A. M. Eltawil, and A. Sabharwal. Self-interference cancellation with nonlinear distortion suppression for full-duplex systems. volume II, page 1199 – 1203. Proceeding Asilomar Conference on Signals, Systems and Compututer, 2013.

[92] T. Schenk. Rf imperfections in high-rate wireless systems, impact and digital compensation. New York, NY, USA: Springer-Verlag 2008.

[93] T. Paul and T. Ogunfrunmiri. Wireless lan comes of age: Understanding the ieee 802.11n amendment. *IEEE Circuits and Systems Magazine*, 8(1):28–54, First 2008.

[94] NI 5644R. User manual and specifications. *Nat. Instrum., Austin, TX, USA*, Available: http://www.ni.com/datasheet/pdf/en/ds-422 .

[95] Y. C. Liang, Y. Zeng, E. C. Y. Peh, and A. T. Hoang. Sensing-throughput tradeoff for cognitive radio networks. *IEEE Transactions on Wireless Communications*, 7 (4):1326–1337, April 2008.

« Détection de Spectre pour les systèmes Half et Full-Duplex Radio Intelligente Entrelacée

Résumé : En raison de la demande croissante de services de communication sans fil et de la limitation des ressources de spectre, la radio cognitive (CR) a été initialement proposée pour résoudre la pénurie de spectre. CR divise les systèmes transmetteurs-récepteurs de communication en deux catégories : les Utilisateurs Principaux (PU) et les Utilisateurs Secondaires (SU). PU a le droit légal d'utiliser la bande spectrale, tandis que SU est un utilisateur opportuniste qui peut transmettre sur cette bande chaque fois qu'elle est vacante afin d'éviter toute interférence avec le signal de PU. De ce fait, la détection des activités de PU devient une priorité principale pour toute CR. Le Spectrum Sensing devient ainsi une partie importante d'un système CR, qui surveille les transmissions de PU. En effet, le Spectrum Sensing joue un rôle essentiel dans le mécanisme du fonctionnement du CR en localisant les canaux disponibles et, d'autre part, en protègeant les canaux occupés des interférences de la transmission SU. En fait, Spectrum Sensing a gagné beaucoup d'attention au cours de la dernière décennie, et de nombreux algorithmes sont proposés. Concernant la fiabilité de la performance, plusieurs défis comme le faible rapport signal sur bruit, l'incertitude de bruit (NU), la durée de détection du spectre, etc.
Cette thèse aborde les défis de la détection du spectre et apporte quelques solutions. De nouveaux détecteurs basés sur la détection des caractéristiques cyclo-stationnaires et la densité spectrale de puissance (PSD) du signal de PU sont présentés. Un algorithme de test de signification de corrélation canonique (CCST) est proposé pour effectuer une détection cyclo-stationnaire. CCST peut détecter la présence des caractéristiques cycliques communes parmi les versions retardées du signal reçu. Ce test peut révéler la présence d'un signal cyclo-stationnaire dans le signal de mélange reçu. Une autre méthode de détection basée sur la PSD cumulative est proposée. En supposant que le bruit est blanc (sa PSD est plate), la PSD cumulative s'approche d'une droite. Cette forme devient non linéaire pour les signaux de télécommunication. Distinguer la forme cumulative PSD peut donc conduire à diagnostiquer l'état du canal.
La radio cognitive Full-Duplex (FD-CR) a également été étudiée dans ce manuscrit, où plusieurs défis sont analysés en proposant de nouvelles contributions. Le fonctionnement FD permet au CR d'éviter la période de silence pendant la détection du spectre. Dans le système CR classique, le SU cesse de transmettre pendant la détection du spectre afin de ne pas affecter la fiabilité de détection. Dans FD-CR, SU peut éliminer la réflexion de son signal transmis et en même temps réaliser le Spectrum Sensing. En raison de certaines limitations, le résidu de l'auto-interférence ne peut pas être complètement annulé, alors la crédibilité de la détection du spectre est fortement affectée. Afin de réduire la puissance résiduelle, une nouvelle architecture de récepteur SU est élaborée pour atténuer les imperfections du circuit (comme le bruit de phase et la distorsion non linéaire de l'amplificateur à faible bruit du récepteur). La nouvelle architecture montre sa robustesse en assurant une détection fiable et en améliorant le débit de SU.

Mots Clés : Radio Intelligente Entrelacée, Détection de Spectre, Half-Duplex, Full-Duplex, Corrélation Cyclique, Densité Spectrale de Puissance Cumulée, Annulation de l'Auto-Interférence, Atténuation des Imperfection de Hardware

«Spectrum Sensing for Half and Full-Duplex Interweave Cognitive Radio Systems»

Abstract: Due to the increasing demand of wireless communication services and the limitation in the spectrum resources, Cognitive Radio (CR) has been initially proposed in order to solve the spectrum scarcity. CR divides the communication transceiver into two categories: the Primary (PU) or the Secondary (SU) Users. PU has the legal right to use the spectrum bandwidth, while SU is an opportunistic user that can transmit on that bandwidth whenever it is vacant in order to avoid any interference to the signal of PU. Hence the detection of PU becomes a main priority for CR systems. The Spectrum Sensing is the part of the CR system, which monitors the PU activities. Spectrum Sensing plays an essential role in the mechanism of the CR functioning. It provides CR with the available channel in order to access them, and on the other hand, it protects occupied channels from the interference of the SU transmission. In fact, Spectrum Sensing has gained a lot of attention in the last decade, and numerous algorithms are proposed to perform it. Concerning the reliability of the performance, several challenges have been addressed, such as the low Signal to Noise Ratio (SNR), the Noise Uncertainty (NU), the Spectrum Sensing duration, etc. This dissertation addresses the Spectrum Sensing challenges and some solutions are proposed. New detectors based on Cyclo-Stationary Features detection and the Power Spectral Density (PSD) of the PU are presented. Canonical Correlation Significance Test (CCST) algorithm is proposed to perform cyclo-stationary detection. CCST can detect the presence of the common cyclic features among the delayed versions of the received signal. This test can reveal the presence of a cyclo-stationary signal in the received mixture signal. Another detection method based on the cumulative PSD is proposed. By assuming the whiteness of the noise (its PSD is at), the cumulative PSD approaches a straight line. This shape becomes non-linear when a telecommunication signal is present in the received mixture. Distinguishing the Cumulative PSD shape may lead to diagnose the channel status.

Full-Duplex Cognitive Radio (FD-CR) has been also studied in this manuscript, where several challenges are analyzed by proposing a new contribution. FD functioning permits CR to avoid the silence period during the Spectrum Sensing. In classical CR system, SU stops transmitting during the Spectrum Sensing in order to do not affect the detection reliability. In FD-CR, SU can eliminate the reflection of its transmitted signal and at the same time achieving the Spectrum Sensing. Due to some limitations, the residual of the Self Interference cannot be completely cancelled, then the Spectrum Sensing credibility
is highly affected. In order to reduce the residual power, a new SU receiver architecture is worked out to mitigate the hardware imperfections (such as the Phase Noise and the Non-Linear Distortion of the receiver Low-Noise Amplifier). The new architecture shows its robustness by ensuring a reliable detection and enhancing the throughput of SU.

Keywords : Interweave Cognitive Radio, Spectrum Sensing, Half-Duplex, Full-Duplex, Canonical Correlation Significance Test, Cumulative Power Spectral Density, Self-Interference Cancellation, Hardware Imperfection Mitigation